The Effect of Temperature on the Fischer – Tropsch Selectivity and Further Mechanistic Insights

Thesis submitted for the Masters in Applied Science degree at the Department of Chemical Engineering, University of Cape Town.

by

Jack Vincent Fletcher

Supervisor: Prof. Eric van Steen, UCT

Cape Town

2009

Acknowledgements

I would like to thank the following people and organisations for their help and support throughout this study:

Prof. Eric van Steen, for his patience, assistance and guidance as my supervisor.

Sasol Technology, Research and Development Division for permitting me to undertake this project and for their financial support.

The Low Temperature and High Temperature Iron Fischer-Tropsch groups for allowing me the use of their reactor and equipment.

My parents, brother and fiancée for their immeasurable love, understanding and support.

I would also like to thank my colleagues at Sasol Technology for all their support and motivation, especially Khosi Mthembu, Rina van der Westhuizen, Toine Cents, Tracy Bromfield, Philip Gibson, Thelma Grobler, Renier Crous and Tania Crous

Synopsis

Concern's that the world's energy supply will not be able to keep pace with rising energy demands, have surfaced periodically for much of the petrochemical industry's nearly 150 year history, but each time the industry has responded with technological advances and innovations to satisfy the global energy needs. Future advances will most likely include the enhanced recovery of conventional oil, the production of extra-heavy oil / tar sands and the utilization of alternative energy production technologies (technologies other than crude oil refining).

The Fischer-Tropsch Synthesis (FTS) discovered in 1923 by Fischer and Tropsch, is one of these alternative fuel production technologies and can briefly be defined as the means used to convert synthesis gas containing hydrogen and carbon monoxide over a group VIII metal catalyst to hydrocarbon products and water.

Given the vast product spectrum possible for the FTS (paraffins, olefins, alcohols, carbonyls, acids and aromatics), a great deal of controversy still exists as to the chemical identity of the monomeric building block and the propagation of the hydrocarbon chain on the catalyst surface [van Dijk., 2001]. Several mechanisms have been published with the four most popular (alkyl, alkenyl, enol and CO-insertion), recently reviewed by Claeys and van Steen (2004). It must however, be appreciated that given the complexity of the FT reaction it is generally accepted that more than one mechanism may operate on the catalyst surface at any one time. Furthermore, process parameters such as temperature, total pressure, partial pressure, hydrogen to carbon monoxide ratio, space velocity and residence time all have an influence on the FT product selectivity. Because of this it becomes exceptionally complicated to determine the effects of just one parameter while taking the effects of the additional parameters into account.

The main aim of this thesis was therefore, to determine the catalyst activity and product selectivity in the absence of mass transport limitations as a function of reactor temperature while keeping the reactor partial pressures, catalyst and catalyst activation procedure constant. The partial pressures of the kinetically relevant components were kept constant, by changing the space velocity to obtain similar levels of conversion. Since the operation of differential or continuously stirred tank reactors (CSTR) such as slurry reactors is simplified by the fact that the reactants and products are completely mixed (i.e. there are no concentration gradients in the reactor) a CSTR reactor is used.

The analyses of the organic products are achieved by standard one-dimensional and the relatively new, comprehensive gas chromatographic (GC) separation techniques. The comprehensive GC technique allows for the routine analysis of complex organic mixtures making it possible to separate and quantitatively determine both the major and minor products of the Fischer-Tropsch Synthesis.

The extent of diffusion limitations (external and internal) were determined since any variation of partial pressures will impact on reaction rates and contribute to shifts with regard to product selectivity [Steynberg[a]., 2004]. After evaluation of the internal and external mass transport limitations it was shown that for this catalyst applied under the reaction conditions of this thesis, mass transport limitations do not occur to any significant extent. The apparent activation energy and pre-exponential factors for both the water-gas shift (WGS) and low temperature Fischer-Tropsch (LTFT) reactions were calculated by non-linear regression. The values for activation energy are 94 kJ/mol and 63.5 kJ/mol respectively.

Overall the chain growth probability in the range C_8 to C_{14} decreases with increasing temperature from 0.91 at 220°C to 0.87 at 270°C. This is in line with literature [Donnelly *et al.,* 1989], but realistically the decrease in chain growth probability is quite small considering the 50°C variation in temperature. Interestingly, the chain growth probability in the range C_3 to C_7 is observed to increase from 0.63 at 220°C to 0.75 at 270°C, with the rate of increase slowing at higher temperatures. Furthermore, the predicted chain growth probability of the C_3 to C_7 olefin and paraffin fractions suggest that primary olefin

formation will be favored over primary paraffin formation and that the ratio of olefins to paraffins of the same carbon number will increase with increasing temperature.

The chain length dependent desorption model of Botes (2008) was fitted to the experimental C_3 to C_8 hydrocarbon fraction from experiments at five different reaction temperatures via non-linear regression (fitting of T_O, T_P and K). The results of the fitting procedure show K to be independent of temperature i.e. temperature does not seem to have much effect on the observed rate of decrease in olefin to paraffin ratio with increasing carbon number. As with the chain growth probability in the range C_3 to C_7, the fitted value of T_O (relates the competition between desorption to form an olefin vs. further chain growth) decreases with increasing temperature and then levels off around 260℃, while T_P (relates the competition between hydrogenation to form a paraffin vs. further chain growth) continues to decrease with increasing temperature. The decreasing nature of T_O and T_P with increasing temperature are opposite to what is expected from literature and may be related to the secondary reactions of ethene.

Based on the results of this thesis, it is expected that the ratio of linear olefin selectivity relative to the linear paraffin selectivity of the same carbon number in the C_3+ fraction will increase with increasing temperature due to an increased rate of desorption (as an olefin) vs. hydrogenation for the primarily formed surface species. The make - up of the olefin fraction (internal olefin vs. α-olefin) varying, due to the differences in the residence time of the surface species.

Table of Contents

List of Figures

List of Tables

Chapter 1

Introduction

1.1 Background and Industrial Relevance

Concern's that the world's energy supply will not be able to keep pace with rising energy demands have surfaced periodically for much of the petrochemical industry's nearly 150 year history, but each time the industry has responded with technological advances and innovations to satisfy the global energy needs. Stuart McGill, Senior Vice President of ExxonMobil forecasts that the global energy demand will increase at 1.7% a year (on average) through 2030 [The Lamp, 2005]. This increase in energy demand will have to be met by the enhanced recovery of conventional oil, the production of extra-heavy oil and tar sands and the utilization of alternative energy production technologies (technologies other than crude oil refining).

The conversion of gas to liquids (GTL) and coal to liquids (CTL) via Fisher-Tropsch Synthesis (FTS) is an alternative fuel production technology that is increasingly becoming more attractive. The reasons for this are strategic and economic as FT technology can be utilised by countries with an abundance of coal or natural gas and a shortage of crude oil. Some of the countries that fall into his category are China the U.S.A., Australia, India, South Korea and South Africa [Eisberg, 2005; Robinson, 2003; Steynberg[a], 2004; Asian Tribune 2003].

From an economic point of view the future expansion of GTL will depend on the price of crude oil as GTL will not be viable at crude oil prices under $20 per barrel [Steynberg[a], 2004]. CTL via FT will also depend on the price of crude oil and in most cases CTL will not be viable at crude oil prices under $60 per barrel, the increased cost mostly due to the high cost of coal gasification. An example of a strategic point of view is China which will certainly require the utilisation of its large coal reserves to solve its burgeoning demand for fuels. In the US, the Energy Bill, recently signed by President George Bush should also give the process the necessary jump start as loans are guaranteed for the construction of commercial scale CTL plants [Eisberg., 2005].

The Fischer-Tropsch Synthesis (FTS) can briefly be defined as the means used to convert synthesis gas containing hydrogen and carbon monoxide over a group VIII metal catalyst to hydrocarbon products and water. The synthesis gas can in general be derived from any carbonaceous (carbon containing) source. Preferably the feedstock should contain hydrogen increasing the FT efficiency [Steynberg[a], 2004].

The Fischer-Tropsch reaction:

$$CO + 2H_2 \rightarrow -CH_2 - + H_2O \quad \Delta H_{rxn.}(250°C) = -142 kJ/mol CO\ converted$$

The water produced in the Fischer-Tropsch reaction can be consumed in the water gas shift (WGS) reaction yielding carbon dioxide and hydrogen.

$$CO + H_2O \rightarrow CO_2 + H_2 \quad \Delta H_{rxn.}(250°C) = -41 kJ/mol CO_2\ formed$$

The Fischer-Tropsch synthesis is thus a highly exothermic reaction, and the combination of the Fischer-Tropsch synthesis with the water gas shift reaction increases the overall heat generated even more. Thus, heat removal in this process is a technological challenge.

1.2 History of Fischer-Tropsch Synthesis

In 1923 Fischer and Tropsch discovered that by reaction of hydrogen and carbon monoxide over an alkalised iron catalyst at high pressures a highly oxygenated liquid product was produced [Anderson, 1984]. Leading up to the 2nd World War Germany realised that they would require a large source of fuel, the potential of FTS was realised and hence the Germans greatly increased their efforts into FT research, in 1936 four FT plants were commissioned, with a total capacity of 200 000 tons per year. By the end of the 2nd World War there was a total of nine FT plants in Germany with a potential capacity of 700 000 tons per year [Dry, 1981]. After the 2nd World War research into FTS continued in the U.S.A. but later almost stopped entirely due to the discovery of the huge oil fields in the Middle East. In 1955 Sasol 1 was commissioned in South Africa, this was specifically due to trade embargoes imposed on the South African Government concerning the importation of crude oil because of their apartheid policy. The oil crisis of 1973 spurred new interest in FT research by the rest of the world and soon afterwards 2 more FT plants, Sasol 2 (1980) and 3 (1982) were commissioned in Secunda South Africa. All three Sasol plants are still fully operational but the original reactors have been replaced by the latest more efficient and selective reactors.

1.3 Aims and Scope

The major aim of this thesis is to understand the effect of temperature on Fischer-Tropsch selectivity with keeping the reactor partial pressures of the kinetically relevant components constant utilizing a precipitated iron catalyst in a gradientless slurry reactor.

The following key questions will be investigated:

- Can the conditions in the reactor be varied so that only temperature is changed but the partial pressures of the kinetically relevant components are kept constant?
- To what degree is the primary product selectivity affected by temperature?

- To what degree are secondary reactions affected by temperature?
- Can the selectivity results as a function of temperature be explained from the current understanding of the Fischer-Tropsch synthesis?

Chapter 2

Literature Review

The Fischer-Tropsch Synthesis (FTS) can briefly be defined as the means used to convert synthesis gas containing hydrogen and carbon monoxide over a group VIII metal catalyst to hydrocarbon products and water. The synthesis gas can in general be derived from any carbonaceous (carbon containing) source [Steynberg[a], 2004]. Consequently the FTS can be considered an alternative to crude oil for the production of both liquid fuels (gasoline and diesel) and chemicals (in particular, 1-olefins) [Dry, 1999].

Of the group VIII metals iron, cobalt, nickel and ruthenium are the most active catalysts for the FTS. Over these metals synthesis gas is converted to aliphatic (long chain) hydrocarbons in a “one step reaction” (reaction intermediates are not desorbed from the catalyst surface [Schulz, 1999]). Of these metals only iron and cobalt are utilized commercially as FT catalysts. Nickel is too hydrogenating, resulting in high methane yields and at lower temperatures volatile nickel carbonyls are formed. The low availability and high cost of ruthenium also eliminates its application for industrial use in FTS [Dry, 2004].

The most common feeds used to prepare synthesis gas for FTS are coal, which is rich in carbon, and natural gas, which is rich in methane. Other feedstock examples are coal bed methane, heavy oils, bitumen, and petroleum coke. In general the feedstock will become more desirable as the hydrogen content increases, since this will increase the efficiency with which it can be converted to hydrocarbon products [Aasberg-Peterson *et al.*, 2004, Steynberg[a], 2004]. The process of converting coal to synthesis gas is known as gasification. For the coal derived synthesis gas to be suitable for FTS the coal is gasified with steam and oxygen. The process for converting natural gas to synthesis gas

is called methane reforming and, as with gasification, the feedstock usually reacts with steam and oxygen to produce synthesis gas and carbon dioxide [Steynberg[a], 2004].

In commercial practice there are two modes of FT operation. The low temperature (200-240℃) Fischer-Tropsch process (LTFT) with either iron or cobalt catalysts, utilized for high molecular mass linear wax production, and the high temperature (300-350℃) process (HTFT) with iron-based catalysts, utilized for the production of gasoline and linear low molecular mass olefins [Dry, 2002 and 1999]. It was shown by Vosloo *et al.* (2004) that cobalt catalysts are more suitable for natural gas based processes whilst iron catalysts can be used for both natural gas and coal derived synthesis gas processes.

2.1 Stoichiometry and Usage Ratio

The amount of hydrogen consumed relative to the amount of carbon monoxide consumed in the FT reactor is called the usage ratio. Since the cost of synthesis gas is high, as much as possible must be converted to hydrocarbon products. In order to obtain a high overall conversion of synthesis gas, the hydrogen to carbon monoxide ratio in the feed must match the usage ratio [Dry, 2002].

The chemical reactions taking place in a FT reactor can be simplified into the stoichiometric equations:

Methanation

$$CO + 3H_2 \longrightarrow CH_4 + H_2O \qquad (2.1)$$

Olefins / CH_2 units

$$nCO + 2nH_2 \longrightarrow \left(-CH_2-\right)_n + nH_2O \qquad (2.2)$$

Alcohols

$$nCO + 2nH_2 \longrightarrow C_nH_{2n+2}O + \left(n-1\right)H_2O \qquad (2.3)$$

Water gas shift (WGS)

$$CO + H_2O \longleftrightarrow CO_2 + H_2 \quad (2.4)$$

For cobalt-based FT catalysts the extent of the water gas shift (WGS) reaction (2.4) is negligible and can be treated as a one way reaction producing a small amount of carbon dioxide. For cobalt catalysts, the usage ratio is determined primarily by the FT reaction (2.2) and is typically found to be between 2.06 and 2.16. The variation is due the small changes in FT product selectivity (selectivity toward paraffins) and the extent of the WGS reaction [Dry, 2002, 2004].

For the iron-based LTFT process the usage ratio is typically about 1.7. The main contribution is from the WGS reaction which readily occurs on iron-based FT catalysts. For the HTFT process the WGS reaction is rapid and goes to equilibrium allowing carbon dioxide to be converted to FT products via the reverse WGS reaction (2.6) followed by the FT reaction (2.2) [Dry, 2002]. When there is a net formation of carbon dioxide the role of WGS is best explained by examining the effect of the WGS reaction (2.4) on the FT reaction (2.2).

$$2CO + H_2 \longrightarrow -CH_2 - + CO_2 \quad (2.5)$$

Considering the reverse WGS reaction:

$$CO_2 + H_2 \longleftrightarrow CO + H_2O \quad (2.6)$$

Adding the reverse WGS reaction to reaction 2.2:

$$CO_2 + 3H_2 \longrightarrow -CH_2 - + 2H_2O \quad (2.7)$$

Therefore, for iron-based FT catalysts at high temperatures (300 - 350℃) two hydrogen molecules are consumed by one carbon monoxide molecule and three hydrogen molecules are consumed by each carbon dioxide molecule in order to form a "-CH_2-" product [Dry, 2004]. To maximize the carbon efficiency at HTFT conditions the following Ribblett ratio is used:

$$Ribblett\ ratio = \frac{H_2}{\left(2CO + 3CO_2\right)} \tag{2.8}$$

Thus if the Ribblett ratio is equal to one (all the reactants are in stoichiometric balance), all the hydrogen, carbon monoxide and carbon dioxide can in principle be converted to FT products.

As the FTS produces a wide variety of products the usage ratio will depend on the overall product selectivity as the value for the usage ratio is purely due to the stoichiometry of the reactions in question.

Table 2.1 Usage ratio of FT reactions [Dry, 2004]

FT product	Reactions	H_2 to CO usage ratio
CH_4	$CO + 3H_2 \longrightarrow CH_4 + H_2O$	3
C_2H_6	$2CO + 5H_2 \longrightarrow C_2H_6 + 2H_2O$	2.5
Paraffins	$nCO + \left(2n+1\right)H_2 \longrightarrow C_nH_{(2n+2)} + nH_2O$	(2n+1)/n
Olefins	$nCO + 2nH_2 \longrightarrow C_nH_{2n} + nH_2O$	2
Alcohols	$nCO + 2nH_2 \longrightarrow C_nH_{(2n+1)}OH + \left(n-1\right)H_2O$	2

For paraffins the usage ratio will decrease with increasing chain length, this is because the ratio of hydrogen to carbon in the product decreases with the addition of each -CH_2- unit. A paraffin with infinite -CH_2- units will have a usage ratio of two.

2.2 Synthesis Gas Preparation for Fischer-Tropsch Synthesis

The technology used to prepare synthesis gas for FTS can be separated into two main categories, coal gasification and natural gas (methane) reforming. When compared, the conversion of natural gas is preferred to coal for synthesis gas production. This is because the cost of natural gas reforming is lower and more efficient than coal

gasification [Dry, 2002]. The conversion of coal to synthesis gas is however worthwhile if the coal price is low enough and if both electricity and high value hydrocarbon products are co-produced with liquid fuels [Steynberg[a], 2004, Dry, 2002]. Countries with large coal reserves and limited natural gas reserves such as the U.S.A., China and India will certainly require the utilisation of coal gasification followed by FTS to solve their growing demands for fuels. In the U.S.A. the Energy Bill, recently signed by President George Bush, should also give CTL (coal to liquids) the necessary jump start as loans are guaranteed for the construction of commercial scale CTL plants [Eisberg, 2005].

2.2.1 Natural gas reforming

The lowest cost routes to synthesis gas so far, are based on natural gas as feedstock [Wilhelm *et al.*, 2001]. The principle technologies for producing synthesis gas from natural gas are steam methane reforming (SMR), two-step reforming, autothermal reforming (ATR), partial oxidation (POX) and heat exchange reforming. Their respective advantages and disadvantages are summarized in table 2.2.

For steam methane reforming, methane and steam are catalytically and endothermically converted to hydrogen and carbon monoxide. An alternative approach is partial oxidation, which is an exothermic non-catalytic reaction of methane and oxygen to produce a synthesis gas mixture. Even so, neither steam methane reforming nor partial oxidation produce a synthesis gas with the required hydrogen to carbon monoxide ratio for GTL application [Wilhelm, 2001]. The present choice of reforming technology for a large-scale FT plant based on natural gas is autothermal reforming (ATR), as it has a naturally favorable hydrogen to carbon monoxide ratio and becomes cheaper than steam (and CO_2) reforming because of a improved economy of scale for oxygen plants than for the tubular reformer [Rostrup-Nielsen, 2002]. ATR combines partial oxidation and catalytic steam reforming in one reactor. Future improvements for ATR may be related to the reduction in cost of oxygen manufacture and better integration of the oxygen plant and synthesis gas unit.

Table 2.2 Comparison of synthesis gas generation technologies [Wilhelm *et al.,* 2001]

Technology	Advantages	Disadvantages
Steam methane reforming (SMR)	• Extensive industrial experience • Oxygen not required • Low operating temperature requirement • Good for hydrogen production requirements	• H_2/CO ratio higher than required • High air emissions
Heat exchange reforming	• Compact size • Flexibility for additional capacity	• Limited commercial experience
Two-step reforming	• Produces high purity synthesis gas • Synthesis gas methane content can be tailored	• Increased process complexity • Usually requires oxygen
Autothermal reforming (ATR)	• Natural H_2/CO ratio is favorable • Low methane slip • Synthesis gas methane content can be tailored	• Limited commercial experience • Usually requires oxygen
Partial oxidation (POX)	• Feedstock desulphurization not required • No catalyst required • Low methane slip	• Very high operating temperatures • Usually requires oxygen • Synthesis gas methane content is low

Table 2.3 Techniques for adjusting H_2/CO ratios [Wilhelm *et al.,* 2001]

	Decreases ratio	Increases ratio
Recycle CO_2	X	
Import CO_2	X	
Remove H_2 via membrane	X	
Remove CO_2		X
Increase steam		X
Add shift converter		X

2.2.2 Coal Gasification

Gasification is a versatile process which can be used to convert a variety of solid or liquid carbonaceous feedstocks into synthesis gas [Aasberg-Petersen *et al.*, 2004]. When coal is gasified to produce synthesis gas and then converted to liquid hydrocarbons (fuels and chemicals) via the FT process it is referred to as CTL. A variety of gasifier technologies exist but all commercially applied gasification technologies can be classified into one of three generic groups according to the type of gasifier bed used [Aasberg-Petersen *et al.*, 2004]:

- Fixed bed or moving bed, for example the Sasol-Lurgi gasifier. Coal flows counter-current with the steam and oxidant and the highest temperatures are at the bottom of the gasifier.
- Fluidised bed gasifiers, such as the Kellogg-Rust-Westinghouse (KRW) gasifier. Coal, steam and oxidant are well mixed giving a uniform temperature distribution over the gasifier.
- Entrained flow gasifiers, like the Texaco and Shell gasifiers. These are plug flow reactors where the coal and reactants move co-currently through the reaction zone which is at a high uniform temperature.

When selecting a gasification technology the following factors must be taken into account:

- Feedstock characteristics (ash composition, ash melting properties, ash viscosity, particle size distribution, caking properties, etc.)

- Quality requirements for clean gas (synthesis gas composition)
- Quality of waste products
- Site-specific conditions
- Environmental legislation

Table 2.4 Operating parameters for generic types of gasifiers [Aasberg-Petersen *et al.*, 2004]

	Fixed Bed	**Fluidised Bed**	**Entrained Bed**
Preferred Feedstock	Lignite, reactive bituminous coal, wastes	Lignite, bituminous coal, cokes, biomass, wastes	Lignite, reactive bituminous coal, pet cokes
Coal feed size (mm)	6-75	< 6	< 0.1
Ash content	No limit	No limit	<25%
Exit gas temperature (°C)	420-650	920-1050	± 1200
Ash conditions	Dry/Slagging	Dry/agglomerating	Slagging
Key distinguishing characteristic	Hydrocarbon liquids in raw gas	Char recycle	Large amount of heat energy in the raw gas
Key technical issue	Utilisation of coal fines	Increased carbon conversion	Raw gas cooling
Technology supplier	Sasol-Lurgi	KRW	Texaco

Electrical power together with fuels and high value chemicals can be co-produced in a CTL process thus making it more competitive with the cheaper reforming technologies. The power is generated from the combustion of synthesis gas in the integrated gasification combined cycle (IGCC) [Neathery *et al.*, 1999].

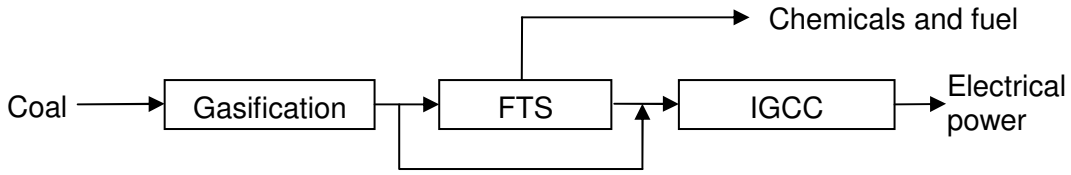

Figure 2.1 Co-production of Fischer-Tropsch Products and Electrical Power [Gray *et al*., 1997].

2.3 Industrial Application of Fischer-Tropsch Technology

Since Fischer-Tropsch end products (chemicals and fuels) have to directly compete with those produced from crude oil, the price of crude is one of the key factors determining whether or not a FT plant should be constructed. This is because the world's current chemical and fuel production is predominantly based on petroleum crude oil [Dry, 2002, 2003]. Other factors which may influence the industrial application of a FT process include the strategic needs of the particular country and, or the local economics. It is also important to note that the presently known reserves of natural gas and coal exceed those of crude oil by a factor of approximately 1.5 and 25, respectively, thus making FTS an important technology in the longer term for the petrochemical industry.

The current commercial application of FT technology is geared for the production of valuable linear alpha olefins and fuels (LPG, gasoline, kerosene, and diesel). Since the FT product consists predominantly of linear hydrocarbons the production of high quality diesel (cetane number of 75 vs. the required 45) is of particular interest. Given its availability the current feedstock of choice is natural gas (methane) over coal. Not only is the capital cost of a methane conversion plant about 30% less, it is also more efficient. This is due to the higher hydrogen content of methane as compared to coal. Hence less carbon is converted to carbon dioxide in the production of the synthesis gas when methane is used as feedstock [Dry, 2002].

2.3.1 Commercial Plants

Table 2.5 Industrial Fischer-Tropsch synthetic oil projects existing and planned [Morita, 2001]

Name of company	Scale of production (bpd)	Location
Existing plants		
Sasol	20 000	Sasolburg, South Africa
Sasol	105 000	Secunda, South Africa
Qatar Petroleum + Sasol	30 000	Qatar
PetroSA	30 200	Mossel bay, South Africa
Shell SMDS	12 500 – 15 000	Bintulu, Malaysia
Construction / feasibility studies under way		
Chevron and Sasol	30 000	Nigeria
Shell	140 000	Qatar
Sasol	80 000	China
Sasol	80 000	South Africa

2.3.2 Fischer-Tropsch Reactors in Commercial Use

Commercially there are two FT operating modes, the HTFT (300 - 350℃) process and the LTFT (200 – 240℃) process. Other than temperature a key distinguishing factor between the HTFT and LTFT reactors is that there is no liquid phase present outside the catalyst particles in HTFT reactors [Steynberg *et al*[b]., 2004]. The formation of a liquid phase in a HTFT reactor will cause the catalyst particles to agglomerate (snow ball effect) thereby leading to loss of fluidization and "slumping" of the catalyst bed.

FT reactions are highly exothermic, it is therefore very important to remove the heat of reaction from the catalyst particles in order to avoid overheating of the catalyst. If the catalyst particles were to overheat it would result in an increased rate of deactivation due to sintering and fouling and an increase of undesired products, especially methane [Dry, 2002]. To remove the excess heat, high rates of heat exchange are achieved by forcing synthesis gas at high linear velocities through long narrow tubes packed with catalyst particles to achieve turbulent flow, or by operating a fluidised bed or slurry reactor.

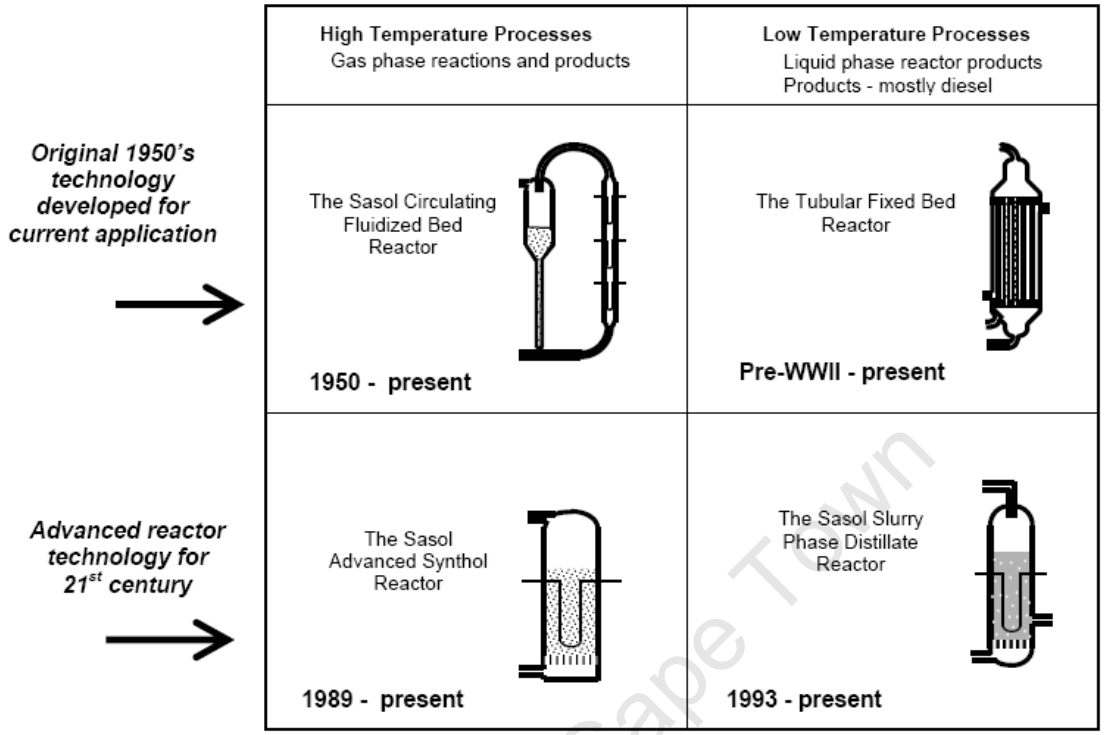

Figure 2.2 Fischer-Tropsch reactors in commercial use [Steynberg *et al*., 2004]

2.4 Mechanism of the Fischer-Tropsch Synthesis

2.4.1 Adsorption of Hydrogen and Carbon Monoxide

Hydrogen reacts either in the molecular state or via dissociative adsorption [van der Laan *et al.*, 1999]. Most transition metals are able to dissociate hydrogen on the catalyst surface with heats of chemisorption for hydrogen on group VIII metals increasing in the order Co, Ni, Fe [Vannice, 1975]. Chemisorbed hydrogen has a high surface mobility and it is therefore assumed that hydrogen in the chemisorbed mono-atomic state reacts with other surface species during the FTS [Claeys and van Steen, 2004]. This also implies that chemisorbed mono-atomic hydrogen can spill over onto the support and in this way the catalyst support acts as a hydrogen atom reservoir [Conner and Falconer, 1995]. The influence of spilt-over hydrogen has never been quantified in kinetic rate equations, but it may have a significant effect.

The adsorption of carbon monoxide on transition metal surfaces can be dissociative or molecular. Studies by Sung and Hoffmann (1985) have shown that on the left side of the first row of transition metals up to and including iron, the adsorption is likely to be dissociative and on the right side from cobalt it is likely to be molecular.

Three different modes of chemisorbed carbon are known from spectroscopic studies i.e. atop, bridged and vicinal.

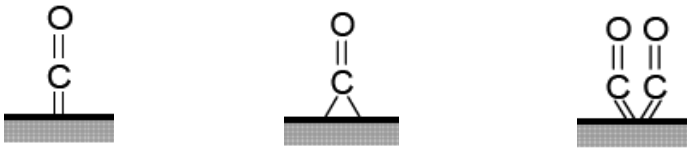

Figure 2.3 Modes of chemisorbed carbon [Claeys and van Steen, 2004]

When chemisorbed carbon monoxide dissociates on the catalyst surface it yields surface carbon and surface oxygen. The surface carbon can diffuse into the bulk of the metal catalyst yielding metal carbides or remain on the surface of the catalyst to form graphitic carbon.

With iron catalysts, iron carbides are formed during FTS. In pure hydrogen atmospheres the carbides of iron and other Fischer-Tropsch metals all readily reduce forming the metal, therefore the stability of these carbides in synthesis gas atmospheres depends on the relative rates of the carbiding and reducing reactions [Dry, 1981]. In general, during FTS various states of carbon monoxide are present on the catalyst surface and displace hydrogen from the metal.

2.4.2 Proposed Mechanisms for Fischer-Tropsch Synthesis

The Fischer-Tropsch synthesis is a polymerization reaction with the in-situ formation of monomers from synthesis gas. All reaction pathways proposed in literature have three different reaction sections:

- Formation of chain starter (initiation)
- Chain growth (propagation)
- Desorption (Chain termination)

For a FT mechanistic model to be acceptable it must be able to account for all of the unique aspects of the FT product [Dry., 1996] e.g.

- FT products are predominantly linear and aromatics are only formed at higher temperatures.
- The olefin content is high and the ratio of paraffin to olefins is much lower than thermodynamic prediction.
- Olefins are predominantly terminal (alpha olefins).
- There is a large amount of mono-methyl branching. Likewise ketones are predominantly methyl ketones.
- The degree of branching decreases as chain length increases.

Given the unique aspects above and the vast product spectrum possible (paraffins, olefins, alcohols, carbonyls, acids and aromatics), a great deal of controversy still exists as to the chemical identity of the monomeric building block and the propagation of the hydrocarbon chain on the catalyst surface [van Dijk., 2001]. Several mechanisms have been published with the four most popular (alkyl, alkenyl, enol and CO-insertion), recently reviewed by Claeys and van Steen (2004). It must be appreciated that given the complexity of the FT reaction it is generally accepted that more than one mechanism may operate on the catalyst surface at any one time.

'Alkyl' mechanism

The alkyl mechanism is currently the most widely accepted mechanism for chain growth in FTS [Claeys and van Steen, 2004]. Chain initiation occurs via dissociative chemisorption of carbon monoxide on the catalyst surface. The surface oxygen can be removed by reaction with hydrogen resulting in water or by reaction with carbon monoxide to form carbon dioxide. The surface carbon species are sequentially hydrogenated yielding surface methylidyne (CH), surface methylene (CH_2) and surface methyl (CH_3) species. The surface methyl species being regarded as the chain initiator and the surface methylene species the monomer responsible for chain growth. Primary product formation is achieved by β-hydrogen abstraction or hydrogen addition yielding α-olefins or n-paraffins respectively. Although no evidence for the formation of primary alcohols via this mechanism exists, it is thought to be possible via the coupling of a hydroxyl group with an alkyl group.

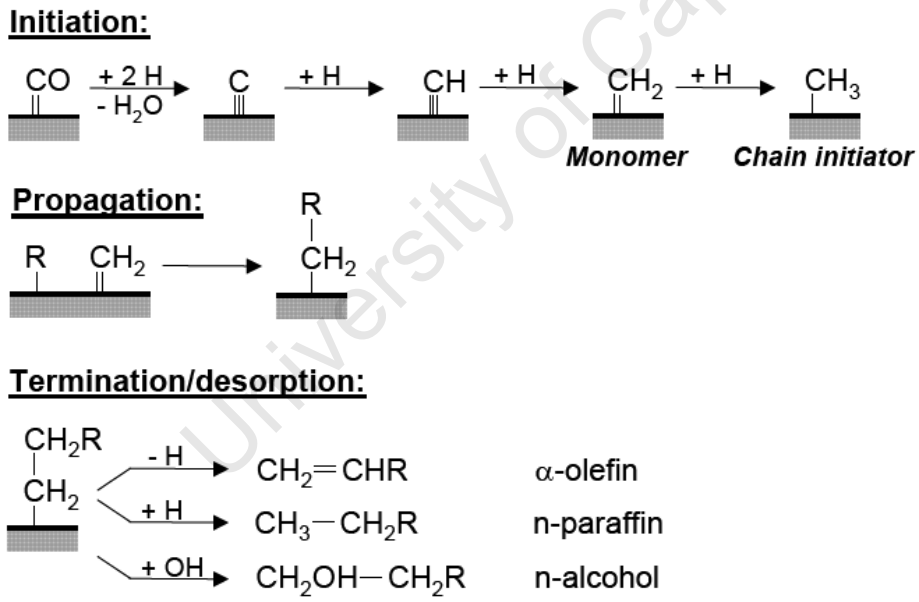

Figure 2.4 The "alkyl" mechanism [Claeys *et al.*, 2004]

'Alkenyl' mechanism

The formation of the monomer is identical to that of the "Alkyl" mechanism where the surface carbon species is hydrogenated to yield a surface methylene species. The

addition of a surface methylene species and a surface methylidyne species yields the chain initiator (vinyl surface species) and chain propagation occurs via a stepwise addition of the methylene surface species to the vinyl species (Figure 2.5). Finally desorption via hydrogen addition yielding α-olefins takes place. This mechanism was originally proposed by Maitlis *et al*. (1996) but fails to explain the primary formation of n-paraffins or n-alcohols.

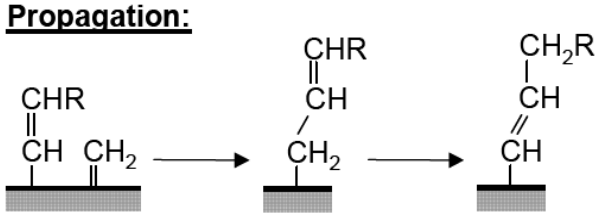

Figure 2.5 Propagation step of the alkenyl mechanism showing the vinyl surface species [Claeys and van Steen, 2004]

'Enol' mechanism

This reaction mechanism was originally proposed by workers at the Bureau of mines (1951) and involves oxygen containing (enol) surface species. The enol (CROH) surface species are formed from the hydrogenation of chemisorbed carbon monoxide and chain growth occurs via a condensation reaction of two enol species and the removal of water. Termination of the carbon chain yields aldehydes, n-alcohols and α-olefins as primary products. The enol mechanism fails to explain the primary formation of n- paraffins.

'CO-insertion' mechanism

This mechanism is regarded as the main reaction pathway for the formation of oxygenates and is based on the known carbon monoxide insertion from coordination chemistry and homogeneous catalysis. Chemisorbed carbon monoxide is the monomer and the chain initiator is thought to be a surface methyl species. The formation of the surface methyl species differs from the "alkyl" mechanism with regard to the elimination of oxygen from the surface species (Figure 2.6).

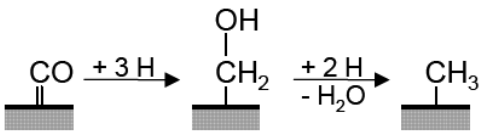

Figure 2.6 Formation of the methyl surface species in the CO-insertion mechanism [Claeys *et al*., 2004]

Chain growth occurs via carbon monoxide insertion into the metal-alkyl bond which in turn leads to an acyl (CRO) surface species. Hydrogenation of the acyl species produces water and an enlarged (by one carbon atom) alkyl species. Termination or desorption of the alkyl species to form n- paraffins or α-olefins follows the same path as proposed for the alkenyl mechanism (Figure 2.5). Chain termination may also involve the oxygen containing surface species leading to the formation of aldehydes and alcohols as primary products.

2.5 Selectivity of the Fischer-Tropsch Synthesis

2.5.1 Influence of Process Conditions on Fischer-Tropsch Selectivity

Process parameters such as temperature, total pressure, partial pressure, hydrogen to carbon monoxide ratio, space velocity and residence time all have an influence on the FT product selectivity. Because of this it becomes exceptionally complicated to determine the effects of just one parameter while taking the effects of the additional parameters into account.

Aside from the effect of process conditions on FT selectivity, the nature of the catalyst and its reduction or activation before synthesis will have a significant effect on the FT selectivity and must therefore be taken into account whilst carrying out experiments.

Temperature

An increase in the reactor operating temperature results in a shift toward products with a lower carbon number on iron, cobalt and ruthenium catalysts [Donnelly and Satterfield, 1989; Dry, 1981]. At low temperatures (<190℃) ruthenium and nickel catalysts are

selective towards high molecular mass compounds (waxes) but at higher temperatures (>300°C) methane is the main product formed. Cobalt catalysts at low temperatures (<175°C) produce large amounts of alcohols but with increasing temperature (>200°C) almost no oxygenated molecules are found. Dry (1981) also observed the decrease in alcohols and acids over an iron catalyst with increasing temperature. Donnelly and Satterfield (1989), as well as Anderson (1984), observed an increase in the olefin to paraffin ratio over potassium-promoted precipitated catalysts with increasing temperature. Dictor and Bell (1986) and Dry (1981) observed a decrease in the olefin selectivity with increasing temperature for un-alkalised iron oxide powders and fused iron catalysts respectively. Furthermore, the degree of branching increases and the amount of secondary product formed (such as ketones and aromatics) increases with increasing temperature. Dry (2002) states that the effect of temperature on product selectivity is consistent for all FT catalysts and these shifts are in line with thermodynamic expectations as given in section 2.5.2.

Table 2.6 Influence of process parameters on the Fischer-Tropsch selectivity [Claeys. 1997, van Dijk. 2001].

Increasing parameter	Chain length	CH_4 selectivity	Olefin selectivity	Oxygenate selectivity	Olefin to Paraffin ratio	Chain branching
Temperature	–	+	*	–	+	+
Pressure (Total)	+	–	*	+	+	–
H_2/CO (feed)	–	+	–	–	–	+*
$P_{Hydrogen}$ (reactor)	–	+	–			*
$P_{Carbon\ monoxide}$ (reactor)	+	–	+			*
Residence time	+*	+*	–	–	–	+*
Space velocity	*	–	+	–		*
K (Fe catalyst)	+	–	+	+		–

Note: Increases with increasing parameter **+**; decreases with increasing parameter **–**; complex relation *; differences in literature **+***.*Pressure and synthesis gas composition*

When the H_2/CO ratio of the feed gas is kept constant and the total reactor pressure is increased there is little or no effect on hard wax selectivity (product fraction boiling above 500℃) over iron based LTFT catalysts, but over iron HTFT and cobalt catalysts the wax selectivity was observed to increase with increasing total reactor pressure [Dry, 1981, 2004]. Over both iron and cobalt catalysts the oxygenate selectivity increased with increasing total pressure, but the olefin content of the products showed no clear trend as the pressure was increased [Dry, 1981; Anderson, 1984].

If the total pressure is kept constant and the H_2/CO entry ratio (P_{H2}/P_{CO} ratio) is decreased the overall product spectrum over both cobalt and LTFT iron catalysts shifts to a higher molecular mass as well as increasing the olefin and alcohol contents [Dry, 1981; Donnelly and Satterfield 1989]. The reason for this observation is that, as the carbon monoxide partial pressure in the reactor is increased, the higher the catalyst surface coverage of carbon and oxygen containing monomers become, hence the higher the probability of chain growth as well as olefin and oxygenate formation. Conversely, as the H_2/CO ratio is increased the higher the partial pressure of hydrogen in the reactor the higher the probability of chain termination by hydrogenation. By comparison of Sasol data Dry (2004) has shown that the partial pressures of carbon dioxide and water also play an important role in the FT selectivity as they will have a negative effect on the chemisorption of both carbon monoxide and to greater extent hydrogen. The selectivity is then not simply dependent on the H_2/CO ratio but on a more complex ratio such as:

$$P_{H2}{}^{a} / \left(P_{CO}{}^{b} + P_{CO2}{}^{c} + P_{H2O}{}^{d} \right) \qquad (2.9)$$

The partial pressures of hydrogen, carbon monoxide, carbon dioxide and water in the reactor will depend on several factors of which the main contributing factors are: composition and linear gas velocity of the synthesis gas, the usage ratio (LTFT) or Ribblett ratio (HTFT) of the reaction, the contraction of gas, the extent of conversion, the extent of WGS and the recycle ratio.

Residence time and space velocity

The longer a primary product such as an olefin or alcohol resides in the FT reactor the greater the probability of secondary reaction (see section 2.5.3). In general the residence time or space time (τ) is the time necessary to process one reactor volume of fluid, based on the reactor entrance conditions [Fogler, 1999].

The space velocity (SV) is defined as:

$$SV = \frac{1}{\tau} \tag{2.10}$$

Mathematically, space velocity appears to be the reciprocal of residence time but there is a difference in the definition of the two quantities. For the residence time the entering volumetric flow rate is measured at the reactor entrance conditions, while for SV other conditions are used [Fogler, 1999]. For FT reactor systems the SV most often used is the gas hourly space velocity (GHSV) where the volumetric flow rate (per hour, $\dot{v}$) is measured at normalized (n) temperature and pressure (273.15 K and 1.013 bar).

$$GHSV = \frac{\dot{v}}{g(catalyst)} \tag{2.11}$$

2.5.2 Thermodynamic Aspects of the Fischer-Tropsch Synthesis

When the Fischer-Tropsch product selectivity as calculated from thermodynamic equilibrium is compared to the selectivity found in practice, significant deviations are observed. Thermodynamic calculations by Tillmetz (1976) predicted the major products to be methane, carbon dioxide and graphite. In practice methane is much lower than thermodynamically predicted, graphite is almost absent and the bulk of the product is high molecular mass hydrocarbons and oxygenates. These deviations from thermodynamic equilibrium indicate that the selectivity of the Fischer-Tropsch reaction is mainly a result of competing reaction rates.

Even though the observed FT selectivity is far from thermodynamic equilibrium, the equilibrium calculations give valuable information on attainable equilibrium yields and product distributions which are independent of mechanism and catalyst. This information can therefore be useful to identify trends in selectivity and differences between catalysts.

The calculation of the Gibbs free energy of reaction for the formation of various compounds from the hydrogenation of carbon monoxide shows that it is energetically possible to produce a wide variety of hydrocarbons and organic molecules at commercial FT conditions (Gibbs free energy of reaction < 0).

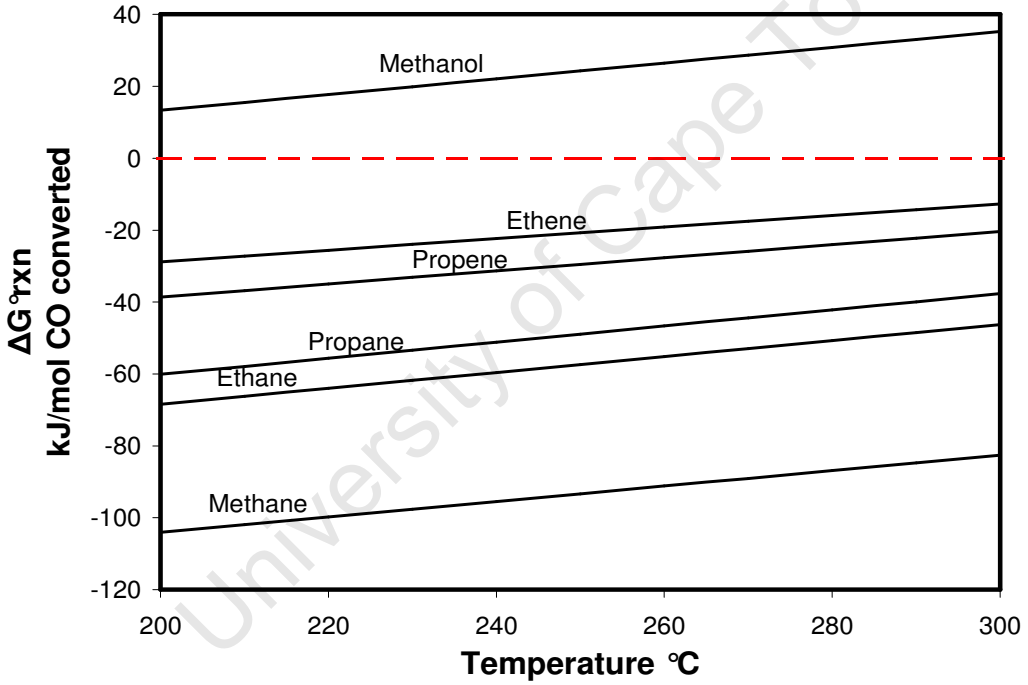

Figure 2.7 Gibbs free energy of reaction as a function of temperature per mol of carbon monoxide converted for the formation of reactions 2.12 – 2.16, data for Gibbs free energy from Aspen Plus 2006

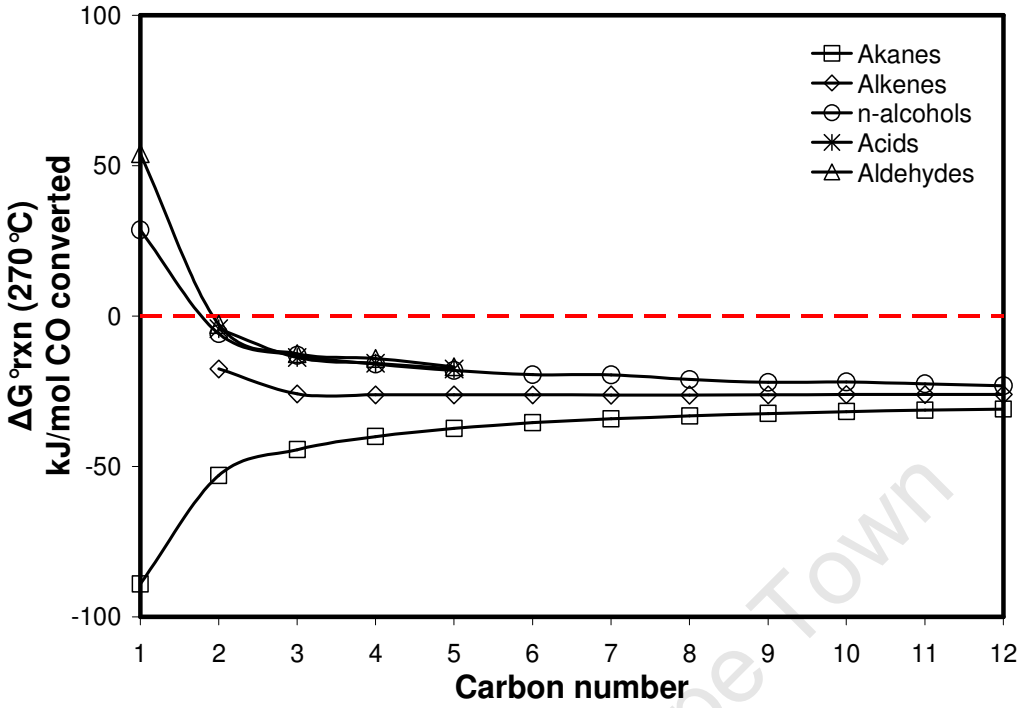

Figure 2.8 Gibbs free energy of reaction (270 °C) as a function of carbon number per mol of carbon monoxide converted for the formation of reactions 2.12 – 2.16 below, data for Gibbs free energy from Aspen Plus 2006

Paraffins: $$CO + \left(\frac{((2 \bullet n) + 1)}{n} \right) H_2 \longrightarrow \frac{1}{n} C_n H_{2n+2} + H_2O \quad (2.12)$$

Olefins: $$CO + 2H_2 \longrightarrow \frac{1}{n} C_n H_{2n} + H_2O \quad (2.13)$$

Alcohols: $$CO + 2H_2 \longrightarrow \frac{1}{n} C_n H_{2n+1} OH + \left(\frac{(n-1)}{n} \right) H_2O \quad (2.14)$$

Aldehydes: $$CO + \left(\frac{((2 \bullet n) - 1)}{n} \right) H_2 \longrightarrow \frac{1}{n} C_{n-1} H_{2n-1} CHO + \left(\frac{(n-1)}{n} \right) H_2O \quad (2.15)$$

Acids (n≠1): $$CO + \left(\frac{((2 \bullet n) - 2)}{n} \right) H_2 \longrightarrow \frac{1}{n} C_{n-1} H_{2n-1} COOH + \left(\frac{(n-2)}{n} \right) H_2O \quad (2.16)$$

Figures 2.7 and 2.8 demonstrate the variation in Gibbs free energy of reaction with temperature and carbon number. Shorter carbon chains are thermodynamically favored

for the n-paraffins. With paraffins being the most stable organic products formed at a given carbon number. In general the thermodynamic stability for a given carbon number of FT products can be summerised as: paraffins > olefins > alcohols ≥ aldehydes ≥ acids.

Thermodynamic equilibrium calculations for the operability of possible secondary reactions allows for the identification of classes of components as reactants and products. Comparison of the thermodynamic equilibrium data with the observed FT product has enabled conclusions concerning primary and secondary products to be made. These are summerised in table 2.7.

Further conclusions that can be made from the comparison of thermodynamic equilibrium and observed experimental results:

- 1- Olefins are the dominant hydrocarbons produced in FTS (reaction 1) and secondary conversions of alcohols did not produce 1- olefins (reaction 3), this indicates that 1-olefins are primary products of the FTS.
- The fact that alcohols are not formed from the hydration of olefins in secondary reactions (reaction 3) and the observation from reaction 4 indicates that alcohols are primary FT products.
- The findings from reactions 5.1 and 5.2 imply that acetic acid is not formed by subsequent oxidation of ethanol by water, nor is acetaldehyde formed by de-hydrogenation of ethanol. The reverse of reactions 5.1 and 5.2 are however possible. This implies that aldehydes and acids are also primary products.

Table 2.7 Summary of findings from thermodynamic data regarding primary and secondary products of Fischer-Tropsch synthesis.

Reactions		Comparison of thermodynamic equilibrium and observed experimental results	Reference
$CO + H_2 \rightarrow alkene + H_2O$	(1)	• Formation of olefins from synthesis gas at commercial FTS conditions is thermodynamically possible.	Figures 2.7 and 2.8
		• Thermodynamically olefins should be virtually completely hydrogenated to paraffins (reaction 2). Olefins are however the most dominant hydrocarbons produced.	[Dry, 2004]
$alkene + H_2 \leftrightarrow alkane$	(2)	• Thermodynamically ethene hydrogenation should be more complete than that of propene. The observed ratio is indeed lower.	[Dry, 2004]
		• Thermodynamically the C5 to C8 olefin to paraffin ratio decreases with increasing carbon number. This is observed from product analysis.	[Dry, 2004]
$alcohol \leftrightarrow alkene + H_2O$	(3)	• The reaction is thermodynamically possible but was not observed to take place for FTS (in the presence of carbon monoxide). The reverse reaction is not thermodynamically feasible.	[Weitkamp *et al.*, 1953]
$alcohol + H_2 \leftrightarrow alkane + H_2O$	(4)	• At the hydrogen pressure in the reactor the observed ratio of ethanol to ethane is higher than expected thermodynamically.	[Dry, 2004]
$alcohol + H_2O \leftrightarrow acid + 2H_2$	(5.1)	• Ethanol, acetic acid and acetaldehyde are in thermodynamic equilibrium. This has been shown experimentally at 600 K.	[Dry, 2004]
$alcohol \leftrightarrow aldehyde + H_2$	(5.2)	• At temperatures < 510 K the ratios for both reactions (acid/alcohol and aldehydes/alcohol) are much higher than the expected ratios.	[Dry, 2004]

2.5.3 Secondary Reactions

Secondary reactions in the FTS are defined by Novac *et al.,* (1982) as reactions following the re-adsorption of primary products on surface sites that do not display chain growth. More recently Madon *et al*., (1991), Iglesia *et al*., (1993) and Schulz and Claeys[b], (1999) have shown that this definition is unsatisfactory as some secondary reactions may well proceed on chain growth sites. There is a great deal of literature which deals with secondary olefin reactions, this has been reviewed by Iglesia *et al*., (1993), van der Laan and Beenackers, (1999) and, Schulz and Claeys[a], (1999). The degree of secondary reactions depends on the reaction conditions (temperature, partial pressures and residence time) and the type of catalyst used.

The secondary reactions of 1-olefins during FTS are:

- Hydrogenation to the corresponding paraffin.
- Incorporation into growing chains and chain initiation.
- Isomerisation of olefins via double bond shift and skeletal isomerisation (branching).

and to a lesser extent:

- Hydroformylation to form alcohols and aldehydes.
- Hydrogenolysis and cracking.

Hydrogenation to the corresponding paraffin

Olefins and paraffins are believed to be primary products in the FTS; on the other hand the secondary hydrogenation of olefins to the corresponding paraffin is well known to take place over FT catalysts [Schulz *et al*., 1994]. As illustrated in Figure 2.9. The re-adsorbed surface species can grow further and/or desorb as an olefin or paraffin, the latter reaction leading to the hydrogenation of the re-adsorbed olefin.

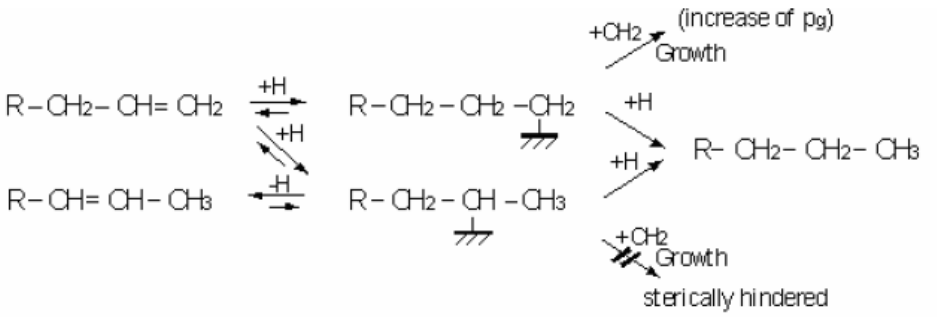

Figure 2.9 Secondary reactions (hydrogenation, double bond isomerisation and chain growth) of olefins [Schulz and Claeys[a], 1999].

Secondary hydrogenation can be inhibited by high carbon monoxide and water partial pressures in the reactor [van der Laan and Beenackers, 1999; Iglesia *et al.*, 1993]. This suggests that there is competitive adsorption of olefins, carbon monoxide and water for the same catalytic sites. The results of Dry (2004) explain the inhibition of hydrogenation to be due to the fact that increasing partial pressures of carbon dioxide and water have a negative effect on the chemisorption of carbon monoxide but to greater extent hydrogen. Secondary hydrogenation of added olefins was observed to increase with increasing carbon number due to increased adsorption strength [Schulz and Gokcebay, 1982].

Incorporation into growing chains and chain initiation

The incorporation of olefins into hydrocarbon chains must not be mistaken with chain initiation by readsorbed olefins. Jordan and Bell (1986) illustrated that oligomerisation of olefins leads to an oscillating product distribution (maxima at even carbon numbers) at very high ethene/carbon monoxide ratios. Given that olefin incorporation into hydrocarbon chains is a similar reaction to oligomerisation and that an oscillating product distribution is not observed for the FT reaction, it seems unlikely that incorporation of olefins occurs to a large extent in the Fischer-Tropsch synthesis. The results also indicated that the incorporation of olefins into growing chains may be inhibited by high partial pressures of carbon monoxide and therefore the incorporation of olefins into growing chains at FT conditions is negligible [van Dijk., 2001].

Figure 2.9, illustrates the initiation of further chain growth by re-adsorbed olefins. This reaction is widely regarded as the most important secondary reaction of 1- olefins [van Dijk, 2001; van der Laan and Beenackers, 1999]. Iglesia *et al*. (1991 and 1993) found that the reactivity of added α- olefins in chain initiation reactions on ruthenium catalysts decreased in the order: ethene >> propene ≥ 1-butene ≈ C_{5+} α- olefins. Chain initiation resulting from re-adsorbed olefins reverses the termination probability to olefins, leading to a higher chain growth probability and higher paraffin selectivity.

Isomerisation of olefins via double bond shift and skeletal isomerisation (branching)

The double bond isomerisation model proposed by Schulz and Claeys[a] (1999, Figure 2.9) shows the re-adsorption of a 1- olefin on the catalyst surface. The alkyl chain can bond to either the terminal or penultimate carbon atom (the carbons opposite the double bond). The terminally bonded alkyl species can be hydrogenated to the corresponding paraffin, continue growth or desorb as a 1- olefin. If the alkyl chain bonds to the catalyst surface on the penultimate carbon atom it can be hydrogenated to the corresponding paraffin or desorb as an internal olefin.

Chain growth is sterically hindered by the hydrocarbon species itself. Isomerisation of added olefins at different reaction conditions via the double bond shift reaction (Figure 2.9) resulted in almost identical distributions [Schulz and Claeys[a], 1999]. This suggests that olefins with internal double bonds are formed mainly by secondary reactions in the FTS. Claeys (1997) noted that the thermodynamic equilibria of these distributions were not reached. An explanation is that the proportions in which the isomers return to the gas phase are determined by the energetics of their conformations in the adsorbed state and not by those in the free molecule [Bond, 2005].

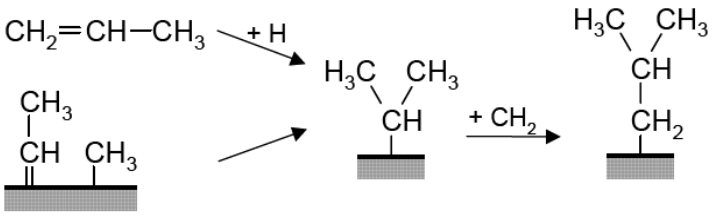

Figure 2.10 Reaction pathways for the formation of branched products as proposed by Claeys and van Steen (2004).

The branched products of FTS consist mainly of mono-methyl branched compounds with small amounts of di- and tri-methyl and ethyl-branched compounds. No quaternary carbon atoms have been observed in FT products [Claeys and van Steen., 2004]. The formation of branched compounds is believed to occur by an alkyl species bonded to the catalyst surface by its penultimate carbon atom (Figure 2.10). Figure 2.10 illustrates that the formation of branched products in FT may proceed via both primary and secondary routes. The formation of branched compounds over iron catalysts increases with increasing partial pressure of carbon monoxide. This might be related to the primary formation of branched compounds. At high reaction temperatures a decrease in the formation of branched compounds relative to the formation of linear compounds with increasing partial pressure of carbon monoxide was observed by Claeys and van Steen, (2004). This may be due to the inhibition of the re-incorporation of reactive product compounds in the chain growth pathway leading to branched compounds.

Anderson (1984) assumed chain branching probabilities were carbon number independent. Schulz *et al*. (1988) extended Andersons model and included an exponentially decreasing chain branching rate constant on the basis that, as the chain length increased, the steric hindrance towards the formation of long chain branched compounds increased. More recently the work of Shi *et al.* (2005) support the findings of Anderson by also concluding that at LTFT conditions the fraction of branched products does not vary significantly with carbon number.

2.5.4 Chain Length Dependency of Secondary Reactions

At set process conditions and steady state operation, secondary reactions are assumed to be function of the chain length. In slurry reactor operation the catalyst is suspended in the hydrocarbon liquid and its pores are filled with liquid wax. Possible fundamental processes responsible for this are [Kuipers *et al*., 1995; Claeys and van Steen, 2004]:

- Carbon number dependent **diffusivity** of liquid products

- Carbon number dependent **solubility** in liquid products
- Carbon number dependent **physisorption strength** of products on catalyst surfaces

Carbon number dependent diffusivity in liquid products

Diffusion limitations of reactants to catalytic sites and vice versa may occur for the case where there is a decrease in diffusion coefficient with increasing chain length. This could then influence the FTS rate and selectivity [van der Laan and Beenackers, 1999]. Iglesia *et al.* (1993) states that an increase in the diffusion limitation with increasing chain length leads to enhanced residence time of the products in the catalyst pores. For this to hold, the opposite would have to apply i.e. the presence of a liquid phase in the absence transport limitations will not increase the rate of secondary reactions (solubility in a liquid phase has no effect on the rate). Iglesia and co-workers (1993) modeled the steady state product distribution by introducing an exponential decay of the diffusion coefficient with carbon number. For which they reported an empirical equation (2.17) describing a strong influence of chain length on diffusivity for olefins and paraffins.

$$D_n = D_{n,0} \times e^{-0.3n} \tag{2.17}$$

This was however not confirmed by experimental data; e.g. Erkey *et al*. (1990) determined the carbon number dependency to be approximately three times lower than that reported for equation 2.17. Furthermore, van Dijk (2001) points out that polymer dynamics predict a proportional dependency of the diffusion coefficient on carbon number and experiments on a polycrystalline cobalt foil in the absence of diffusion limitations by Kuipers et al. (1995) resulted in an exponential decrease of the olefin to paraffin ratio with chain length. Thus it can be concluded that the enhanced residence time of olefins with increasing chain length cannot stem from diffusion effects alone.

Carbon number dependent solubility in liquid products

For FTS in a gradientless slurry reactor the chain length solubility of hydrocarbons in the slurry phase will play a significant role in final product selectivity as the residence time

will increase with increasing carbon number τ_N (the mean reactor residence time of a hydrocarbon with carbon number N).

Various authors, Schulz *et al*. (1988), Tau *et al*. (1990) and Kuipers *et al*. (1995) have noted that an increase of the chain length dependent solubility results in an increase of the residence time and hence higher readsorption rates. van der Laan and Beenackers,(1999) defined an ideal liquid as an inert, non-adsorbing, non polar liquid with all activity coefficients equal to unity (i.e. the chemical potential of any component is the same in the gaseous, liquid and adsorbed states). Therefore as defined by van der Laan and Beenackers, (1999), if the liquid phase of FTS is "ideal" then it will not influence the reaction rate. However in real cases the liquid phase may affect the reaction rate. By taking a typical scheme of an olefin reincorporation model, Botes (2008) derived a set of equations for the chain growth probability and the olefin to paraffin ratio. Assuming that the fugacity of the olefin determines the rate of secondary readsorption and since the Henry coefficient of olefins strongly decreases with increasing carbon number, the equations predict a decrease in the probability for chain growth and an increase in the olefin to paraffin ratio unless the rate constant for the secondary conversion of primarily formed paraffins/olefins and/or the rate constant for the secondary conversion of primarily formed olefins are a function of the carbon number. The increasing solubility of olefins with carbon number cannot explain the chain length deviations in the Fischer-Tropsch synthesis.

Carbon number dependent physisorption strength of products on catalyst surfaces

The physisorbed state is a transition state between the chemisorbed and vapor phase and is governed by Van der Waals forces. The physisorption of hydrocarbons therefore has an influence on the extent of secondary reactions. The experimental results of many authors have been summarised by van der Laan and Beenackers, (1999) (i.e. Komaya and Bell (1994) and Pichler *et al.* (1967)). van der Laan and Beenackers, concluded that the adsorption equilibrium constants increase exponentially with increasing chain length, resulting in an enrichment of long chain hydrocarbons on the catalyst surface.

2.6 Models for Predicting the Fischer-Tropsch Selectivity

Although the FTS results in a highly complex organic mixture there is a high degree of ordered multiplicity (repeating selectivity patterns) in different carbon number fractions [Schulz *et al*., 1988]. This implies that the FT reaction proceeds via a stringent kinetic system whereby organic molecules are formed from the stepwise addition of a C_1 monomer species. The high degree of order in the FT product is well suited for selectivity modeling [Claeys and van Steen, 2004].

2.6.1 Ideal Anderson-Schulz-Flory Distribution with One Sort of Product

If the values of the reaction rate constants for the repetitive stepwise addition of a C_1 monomer are regarded as being carbon number independent; no chain branching and the formation of only one type of product is assumed. The products of FTS can be described with only one parameter i.e. the probability of chain growth (P_G) or alpha (α) [Schulz *et al*., 1988].

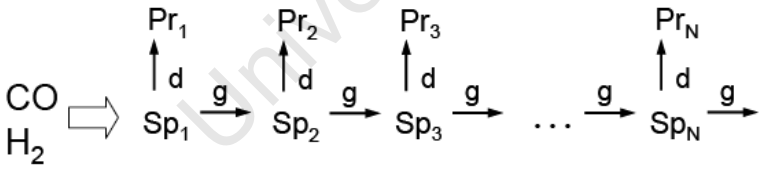

Figure 2.11 Ideal chain growth with one sort of products [Claeys and van Steen, 2004]. (Sp: surface species, Pr: product, N: carbon number, d: desorption, g: growth)

For ideal chain growth as shown in Figure 2.11 the molar product distribution can be represented as:

$$x_N = (1-p_g)\bullet p_g^{N-1} \qquad (2.18)$$

When the molar content of a product compound x_N with N carbon atoms is plotted logarithmically straight lines are observed and the chain growth probability can be determined from the slope:

$$\lg x_N = \lg \frac{(1-p_g)}{p_g} + n \bullet \lg p_g \qquad (2.19)$$

Assuming ideal Anderson-Schulz-Flory (ASF) kinetics places constraints on the theoretically achievable product selectivity's.

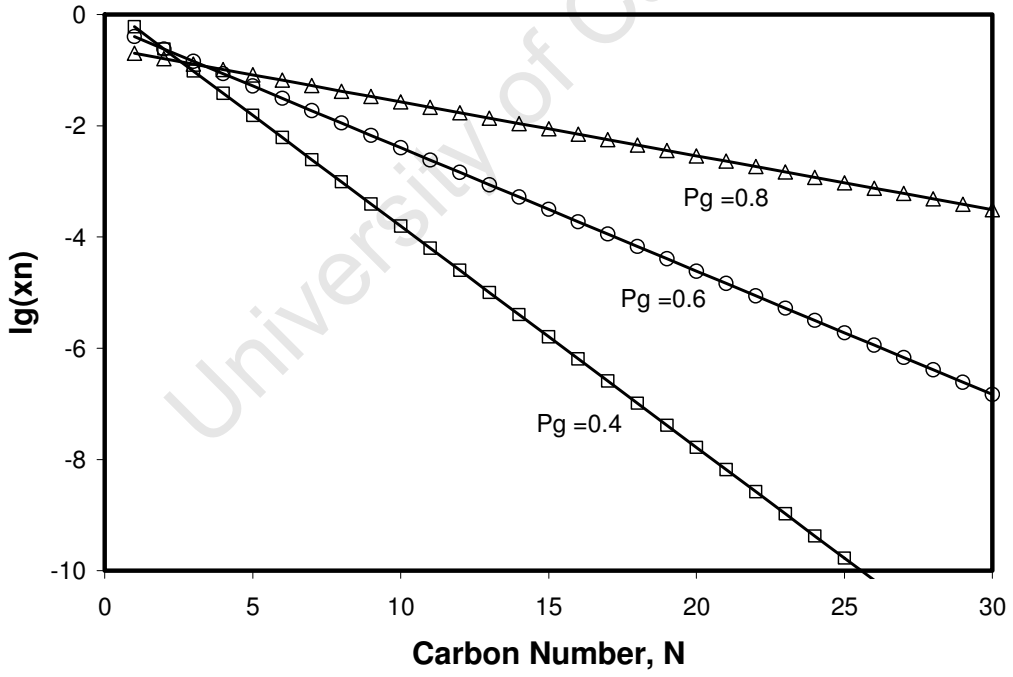

Figure 2.12 Logarithmic molar product content versus carbon number (Ideal ASF product distributions were assumed).

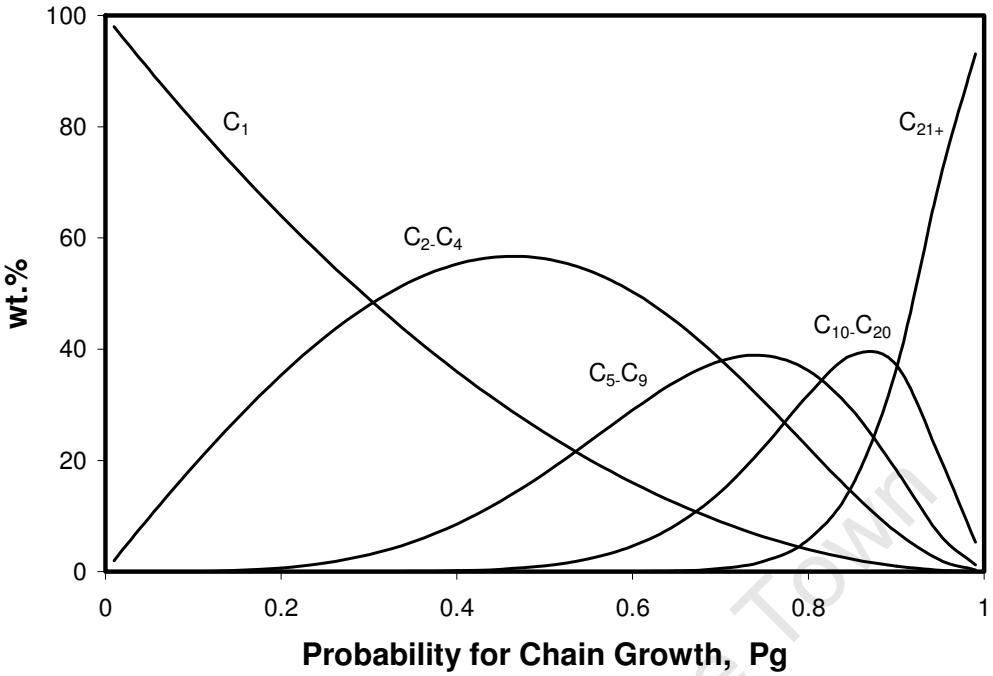

Figure 2.13 Calculated product compositions (wt.%) as a function of chain growth probability (Pg): the highest carbon number was taken to be 100 and ideal ASF product distributions were assumed.

Figure 2.12 shows the logarithmic molar product content versus carbon number at different values for chain growth as calculated from equation 2.19. The chain growth probability is observed to increases with decreasing temperature, increasing partial pressure of carbon monoxide and increasing amount of alkali promoter [Dry., 2004, Donnelly *et al*., 1986]

Figure 2.13 shows that by assuming ideal ASF kinetics, constraints are placed on the theoretically achievable product weight fractions. Only methane can be produced with a selectivity of 100 wt.% and if the desired product is gasoline (C5 – C9) the maximum yield according to ideal ASF kinetics is approximately 40 wt.% at a chain growth probability of 0.75.

2.6.2 Deviations from Ideal Anderson-Schulz-Flory Distribution

Real product distributions obtained from the FTS often show deviations from ideal ASF. The four most commonly observed deviations are:

- Higher than expected molar methane content.
- Lower than expected molar C_2 content.
- An increase in the chain growth probability with increasing carbon number.
- Chain length dependent olefin content, decreasing with increasing carbon number.

Other than the higher than expected methane content, the deviations from ideal ASF kinetics are most easily explained by the occurrence of secondary reactions as discussed in section 2.5.3.

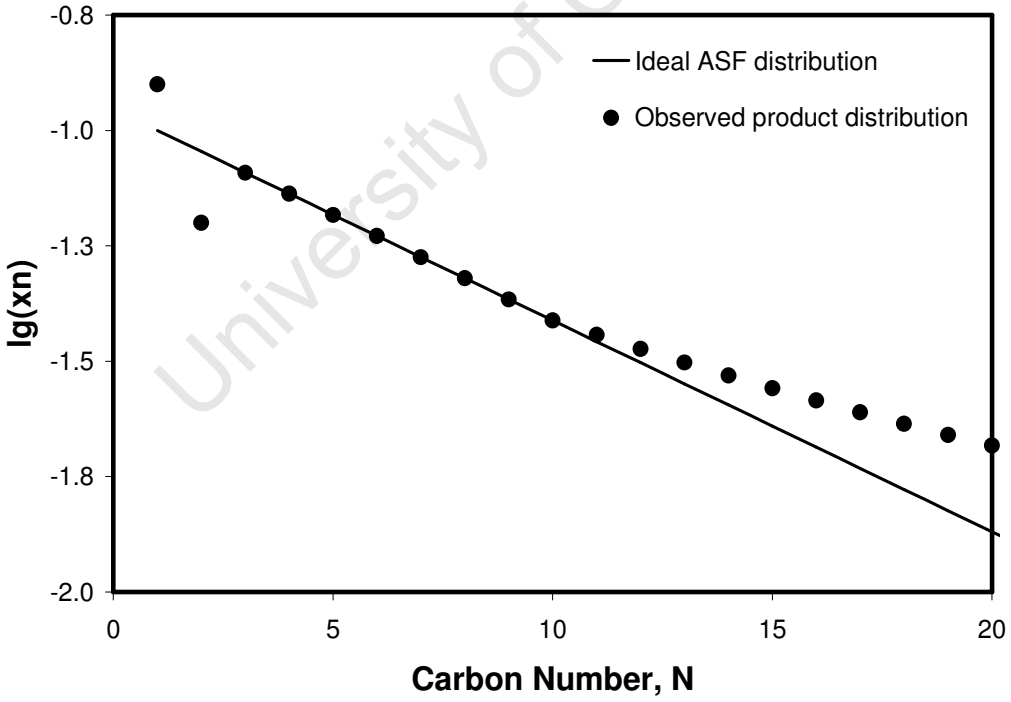

Figure 2.14 Deviations from ideal ASF distribution

Higher than expected molar methane content

On “common” FT catalysts it is not clear which process is responsible for the increased methane production. In the absence of mass and heat transfer limitations with common H_2/CO ratios and reaction temperatures, the increased methane yield is probably due to an increased surface mobility of the methane precursor [Wojciechowski, 1988; Sarup and Wojciechowski, 1988]. Furthermore, of the several active FT sites, one may result in a site that favours the formation of methane [Riedel *et al*., 2003].

2.6.3 Further Selectivity Models

Although the ideal ASF distribution with the formation of one sort of product is a good approximation, in practice ideal ASF kinetics is not observed and more than one product is formed. Many authors [Geerlings *et al.* (1999), van der Laan *et al.* 1999; Iglesia *et al*. 1993; Zimmerman 1992] have developed selectivity models in order to predict the FT selectivity at various reaction and process conditions, as well as with different catalysts.

2.7 Macro Kinetics of the Fischer-Tropsch Synthesis

As discussed in section 2.4, the FTS is a complex system comprising a large number of surface species and elementary reaction steps. The result is that FT reaction kinetics are often described by empirical power law expressions [van der Laan, 1999]. Langmuir-Hinshelwood-Hougen-Watson (LHHW) and Eley-Rideal type of rate equations have also been applied based on a reaction mechanism for the formation of the hydrocarbon forming reactions[van der Laan, 1999], but the success of this approach up to now has been questionable [Schulz and Zein El Deen, 1977]. The derivation of reliable kinetic equations is however essential for scaling up calculations with respect to reactor design and the selection of optimal operating conditions.

2.7.1 Iron based Fischer-Tropsch kinetics

There are many reviews [Botes, 2008] dealing with various kinetic studies over iron FT catalysts. A handful of the equations are discussed below.

The Anderson – Dry equation (2.20) includes a term for water inhibition and the hydrogenation of chemisorbed CO is assumed to be the rate determining step. Furthermore, it assumes that CO and H_2O adsorb more strongly than either H_2 or CO_2. Anderson (1956) first derived equation (2.20), later Dry (1976) derived the same equation from the enol/carbide mechanism.

$$r_{FT} = A\frac{P_{CO}P_{H_2}}{P_{CO} + k_{H_2O}P_{H_2O}} \tag{2.20}$$

Huff and Satterfield (1984) derived equation (2.21) based on the Anderson Dry equation. However, they account for a linear decrease in the adsorption parameter, k, with the partial pressure of hydrogen. Equation 2.21 can be derived from either the carbide or enol/carbide mechanisms. The hydrogenation of the surface carbon and the surface enol are regarded as the rate determining steps for the respective mechanisms.

$$r_{FT} = A\frac{P_{CO}P_{H_2}}{P_{CO} + \frac{kP_{H_2O}}{P_{H_2}}} \tag{2.21}$$

The study by Ledakowicz *et al.* (1985) was carried out on a potassium-promoted precipitated iron catalyst in a continuously stirred tank slurry reactor. The catalyst had a high WGS activity; as a consequence the partial pressure of H_2O in the reactor was negligible. Therefore, the rate determining step was assumed to be the competitive adsorption between CO and CO_2 and equation (2.22) was proposed.

$$r_{FT} = A\frac{P_{H_2}P_{CO}}{P_{CO} + kP_{CO_2}} \tag{2.22}$$

Van Steen and Schulz (1999) disputed the need of a rate-determining step in the derivation of a kinetic expression for the Fischer-Tropsch synthesis. They discarded the LHHW method of a single rate-determining step in favour of another approach based on the irreversibility of the FT reaction, describing the kinetics of consumption of CO for the formation of organic compounds in the Fischer-Tropsch synthesis (equation 2.23).

$$r_{c,org} = A\frac{\dfrac{P_{H_2}^{3/2}P_{CO}}{P_{H_2O}}}{\left(1 + k\dfrac{P_{H_2}P_{CO}}{P_{H_2O}}\right)^2} \tag{2.23}$$

Botes *et al*. (2006), argued that the derivation of a LHHW-type kinetic expression for the FT reaction is valid as long as that the monomer is quickly removed by subsequent reaction steps after its formation (i.e. fast enough to not influence the overall reaction rate). More recently Botes (2008) published equation 2.24 where he excludes the water inhibition term:

$$r_{FT} = A\frac{P_{H_2}^{0.5}P_{CO}}{(1 + k_{CO}P_{CO})^2} \tag{2.24}$$

There is little agreement in the literature as to what the form of the rate equation over iron based FT catalysts should be. The main debate has recently focused on whether or not; H_2O and possibly CO_2 inhibit the FT reaction rate [Botes *et al*., 2006; Botes 2008]. For the FT rate equations which account for water inhibition it is believed that H_2O may compete with CO for active sites, or even oxidize the active iron “carbide” phase of the catalyst.

At low conversions or if the rate inhibition of H_2O and CO_2 are considered to be negligible, equations 2.20, 2.21 and 2.22 reduce to:

$$r_{FT} = kP_{H_2} \tag{2.25}$$

Table 2.8 Kinetic studies for FTS on iron catalysts [van der Laan., 1999].

Catalyst	Reactor	Operating conditions			E_A (K)	Ref.
		T, °C	P, bar	H_2/CO feed	kJ/mol	
Fused Fe/K	Fixed bed	225 - 265	10 – 18	1.2 – 7.2	71	[Dry *et al.*, 1972]
Prec. Fe/K/Cu	Slurry	235 - 265	15 - 30	0.6 – 1.0	86	[Zimmerman *et al.*, 1990(1)]
Fused Fe/K	Fixed bed	250 - 315	20	2.0	85	[Atwood *et al.*, 1979]
Fused Fe	Slurry	232 - 263	4 - 15	0.5 – 1.8	83	[Huff *et al.*, 1984]
Prec. Fe	Slurry	220 - 260	10	0.5 – 0.6	103	[Ledakowicz et al., 1985(2)]
Prec. Fe	Slurry	220 - 280	5 - 12	0.5 – 3.5	89	[Nettlehoff *et al.*, 1985(2)]
Fused Fe	Slurry	210 - 270	5 - 55	0.5 – 3.5	81	[Nettlehoff *et al.*, 1985(2)]
Prec. Fe	Slurry	220 -260	/	0.5 – 0.8	105	[Deckwer *et al.*, 1986(2)]
Prec. Fe	Slurry	220 - 260	/	0.8 – 2.0	80	[Deckwer *et al.*, 1986(2)]

1No temperature dependence of optimal rate equations (c) (Fe/Cu/K) and (g) (100Fe/0.3Cu/0.2K) is given

2Rate equations expressed in liquid concentrations

2.7.2 Water gas shift kinetics

In the iron-based low temperature Fischer-Tropsch synthesis, both water and carbon dioxide are formed. If carbon dioxide is formed by a separate reaction such as the water-gas-shift (WGS) reaction, the relative rates of these two oxygen removal routes will influence the H_2/CO ratio in the reactor.

Botes (2007), has reviewed much of the literature concerning WGS in the Fe-LTFT synthesis and concludes that the bulk of the carbon dioxide is formed by a subsequent reaction (WGS), occurring on a different catalytic site than FT. If this is the case, then the kinetic equations used to describe FT and WGS reactions will be totally unrelated to each other.

For WGS in the Fe-LTFT synthesis it was originally shown that the formation of CO_2 via WGS could be described by first order kinetics in CO, provided that the WGS reaction was far from thermodynamic equilibrium i.e. equation 2.26 does not account for the reverse WGS and cases close to thermodynamic equilibrium.

$$r_{WGS} = AP_{CO} \qquad (2.26)$$

Botes (2007), selected three reaction schemes and derived comprehensive rate equations (Langmuir-Hinshelwood-Hougen-Watson type expressions) accounting for the inhibiting effects of various intermediates. The models were evaluated against new kinetic measurements, the most appropriate being:

$$r_{WGS} = A \bullet \frac{P_{CO}P_{H_2O} - \frac{1}{K_{WGS}} P_{H_2}P_{CO_2}}{\left(1 + k_{H_2O}P_{H_2O} + k_{OH}\frac{P_{H_2O}}{P_{H_2}^{0.5}}\right)^2} \quad (2.27)$$

The terms in the denominator account for the effects of vacant sites, site occupation by adsorbed molecular water and site occupation by hydroxyl groups respectively.

2.8 Chapter Summary and Relation to Present Study

Several mechanisms have been published with the four most popular being the “alkyl”, “alkenyl”, “enol” and “CO-insertion” mechanisms. The alkyl mechanism is currently the most widely accepted mechanism for chain growth in FTS [Claeys and van Steen, 2004]. It must however be appreciated that given the complexity of the FT reaction it is generally accepted that more than one mechanism may operate on the catalyst surface at any one time.

Even though the observed FT selectivity is far from thermodynamic equilibrium, the comparison of the thermodynamic equilibrium data with the observed FT product has enabled authors to make conclusions concerning the primary and secondary products of FTS. Furthermore it is shown that the changes in selectivity as a function of temperature are in line with thermodynamic expectations. For example methane selectivity, olefin to paraffin ratio and degree of branching increase with increasing temperature while the selectivity for organic oxygen containing products decrease.

It is well known that α-olefins undergo secondary reactions during FTS and a large variety of secondary reactions (hydrogenation, re-incorporation, and isomerisation) have been proposed to occur. The extent and nature of the secondary reactions depends on the reaction and process conditions (i.e. temperature) as well as catalyst properties. Chain length dependent effects such as diffusion, solubility and physisorption cause an increase in the reactor residence time, which may result in a preferred secondary

conversion of long chain olefins and a decrease of olefin contents at higher carbon number fractions [Claeys and van Steen, 2004].

Selectivity models must account for positive deviations in ideal ASF kinetics as well as predict FT selectivity on porous FT catalysts at industrial conditions. Much work has already been done to understand the effect of the partial pressure of kinetically relevant compounds, such as CO and H_2, on the product selectivity [Schulz *et al.*, 1994]. In this dissertation, the effect of temperature while keeping the partial pressure of the kinetically relevant components constant is investigated using a precipitated iron catalyst in a gradientless slurry reactor.

The effect of temperature and chain length on the solubility of the product compounds in the slurry phase plays a significant role in the final product selectivity. The likelihood for secondary reactions increases with increasing chain length, but decreases for a given carbon number fraction with temperature. Thus, the observed product distribution as a function of temperature is a result of the complex interplay between primary and secondary reactions, with the latter affected by one or a combination of diffusivity, physisorption and the product solubility.

Chapter 3

Experimental Setup and Procedures

3.1 Philosophy behind the Experimental Program

The main aim of the thesis is to determine the catalyst activity and product selectivity in the absence of mass transport limitations as a function of reactor temperature while keeping the reactor partial pressures, catalyst and catalyst activation procedure constant. The partial pressures of the kinetically relevant components are to be kept constant, by changing the space velocity to obtain similar levels of conversion.

3.2 Reactor Used and Transport Limitations

For ideal reactors i.e. plug flow reactors (PFR) and continuous-flow stirred-tank reactors (CSTR), design equations can be derived using mass balance equations for each species involved.

For a PFR, concentration gradients of reactants and products as well as temperature gradients are established between the inlet and outlet of the reactor as shown in Figure 3.1. The existence of a temperature gradient does not allow for the mass balance of reacting components and the energy balance to be considered separately. To overcome the problems associated with temperature gradients in PFR reactors the reaction can be carried out at very low conversions (i.e. isothermal reaction conditions).

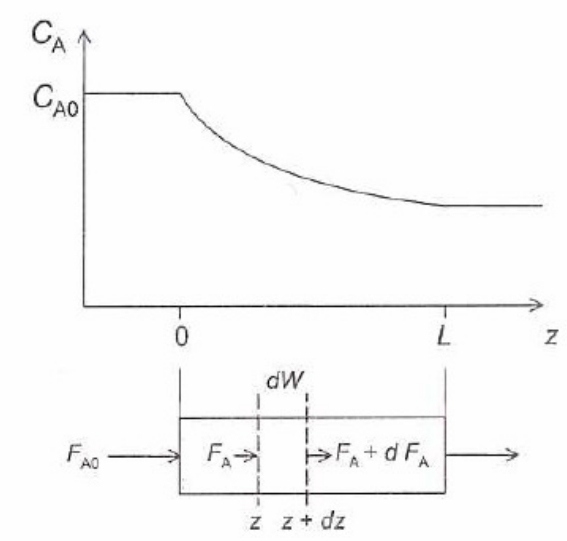

Figure 3.1 Reactant concentration versus position in a PFR [van Santen *et al.*, 1999]

To determine the reaction rate over an integral PFR reactor, the conversion vs. W/F_{Ao} data pertaining to the same temperature must be integrated for the reactant A.

$$\frac{W}{F_{AO}} = \int_{x1}^{x2} \frac{dx}{r_A} \tag{3.1}$$

where:

W = mass of catalyst

F_{Ao} = Molar flow rate of reactant A at inlet

x = Conversion

r_A = Reaction rate (per unit mass of catalyst)

For CSTR reactors the concentration of reactants remains “constant” in the reactor and equation 3.1 becomes,

$$F_{AO}\Delta x = r_A W \tag{3.2}$$

And the rate of reaction per unit mass of catalyst, r_A follows directly from the measured conversion.

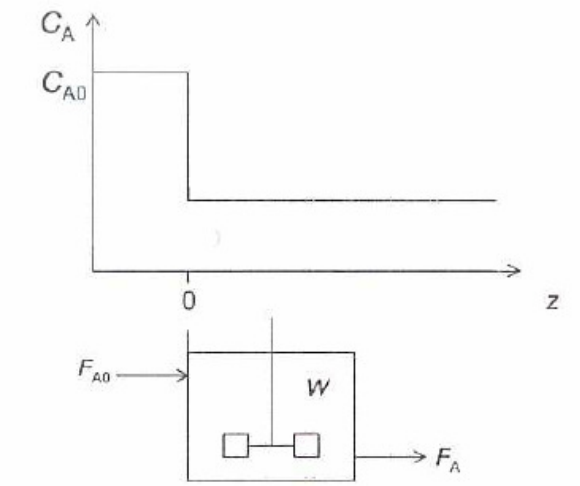

Figure 3.2 Reactant concentration versus position in a CSTR [van Santen *et al.*, 1999]

The operation of differential or continuously stirred tank reactors (CSTR) such as Berty and slurry reactors is simplified by the fact that the reactants and products are completely mixed (i.e. there are no concentration gradients in the reactor). Therefore, the concentration/partial pressure of components at the exit of the reactor will be the same as at all points inside the reactor. The high rate of mixing also allows for good heat removal from the reaction zone (isothermal operation) and eliminates gas bypass or channelling.

For this study all experiments were carried out in a CSTR, but instead of a single phase there are three phases present (gas, liquid and solid). The existence of three phases complicates the experimental operation of the reactor as transport between phases is required for the reaction to take place (i.e. temperature and concentration gradients). Therefore, when measuring the rate of reaction, the rate of the slowest or rate limited step is measured.

To eliminate internal and external transport limitations from the reacting system, small catalyst particles were used (particle diameter < 190 micron) and the reacting phases were completely mixed (see chapter 4 and 5).

3.3 Experimental Setup

The experimental system (Figure 3.3) consists of mass flow controllers, a Parr slurry reactor, a hot pot, a cold pot and a back pressure regulator. On-line GC's (TCD and FID) analyse the tail gas and the synthesis gas, while off-line GC's are used to analyse the liquid products. Synthesis gas is either fed from gas cylinders (H_2, 99.999%; CO: 99.97%) or from the commercial auto thermal reformers (ATR). The synthesis gas used for all experiments has a H_2/CO ratio of 2 and argon is co-fed as an internal standard for the TCD gas analysis.

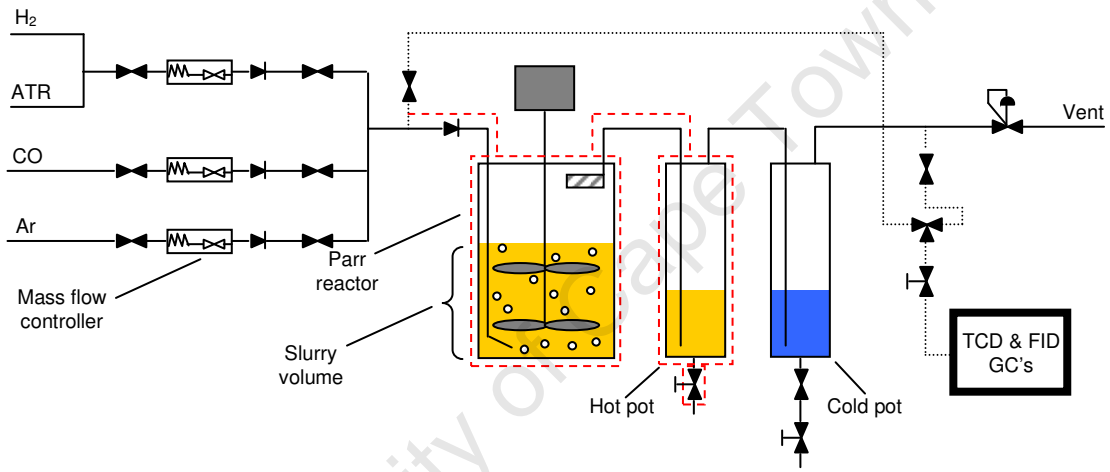

Figure 3.3 Flow Diagram of Experimental Setup; red dashed lines indicate heated sections.

A CSTR reactor is used in this study with a total volume of 1000 ml and an operational slurry volume of approximately 500 ml at 250℃. Reactor internals such as the stirrer, thermowell and gas feed line take up the remaining volume thereby increasing the slurry level to just below the filter.

The reactor has a double-blade stirrer to ensure good mixing of the slurry (liquid and solid) and the gas phase under reaction conditions. The feed line enters at the top of the reactor and ends below the bottom stirrer in order to ensure good gas mixing. Both the gaseous and liquid products leave the reactor through a filter to ensure that all the catalyst remains in the reactor. The temperature in the reactor is measured by two thermocouples placed in a thermowell. The mixed (liquid and vapour) product from the

reactor passes into the hot pot which is kept at 200℃. In the hot pot all the liquid is collected along with some condensed vapour ("wax"). The remaining vapour stream then passes through a cold pot which is chilled to 25℃. The temperature is measured at the outlet of the cold pot by a thermocouple in contact with the gas phase. In the cold pot, water and organic product compounds are condensed out.

The water phase and the oil phase are analysed on off-line gas chromatographs (TCD and FID). The remaining tail gas is sampled from a point before the back-pressure regulator with the remainder of the gas passing through the back pressure regulator and out to the vent. The composition of the tail gas is determined by on-line gas chromatographs.

3.3.1 Catalyst precursor loading

The catalyst used in this study is a precipitated iron catalyst where all samples originated from the same batch. Detailed information regarding the manufacture and catalyst characterisation are given by Biel (2004), Malherbe (2007) and Dry (2004).

Before loading of the catalyst precursor, 490 grams of wax is melted in the reactor at 150ºC. After the wax has melted the catalyst precursor is added to the wax medium. The reactor is then closed and pressurized to 14.5 barg, using argon and the temperature is increased to 250℃. For all experiments the same amount of catalyst precursor (i.e. 10 grams) was used.

3.3.2 Catalyst Activation and Switch Over to Synthesis

Catalyst activation is carried out *in-situ* with synthesis gas and continued until a specified FT activity is reached (rather than activating the catalyst for a specified amount of time). This serves to ensure that all catalysts have the same initial FT activity when synthesis is started.

Catalyst activation was done at 250℃, 14.5 bar(g) and at a synthesis gas space velocity of 10000 ml(n)/g_{cat}.hr; the synthesis gas having a H_2/CO ratio of 2:1. Once the specified

FT activity is reached the knock-out pots are drained and the reactor is switched over to synthesis. The temperature is set to the required value for the experiment and the space velocity is adjusted to obtain ≈ 20% carbon monoxide conversion to FT products, $X_{CO\ to\ FT\ products}$ (see section 3.5.4). During synthesis, knock-out pots are drained and gas samples are taken daily for off-line and online FID and TCD/FID analysis respectively (see section 3.4).

3.4 Product Analysis

3.4.1 One Dimensional Gas Chromatography

Two online gas chromatographs (GC's) were used to analyse the gaseous streams viz. feed and tail-gas. A gas chromatograph equipped with a thermal conductivity detector (TCD) was used to analyse for the permanent gases H_2, CO, CO_2, Ar and CH_4 whilst a gas chromatograph equipped with a flame ionisation detector (FID) was used to analyse organic compounds in the gas phase (including CH_4).

Impurities/inerts in the feed synthesis gas such as CH_4, CO_2 etc. are quantified by the TCD/FID and subtracted from the products formed in order to achieve accurate conversion and selectivity data as well as reliable mass balances.

The liquid samples were analysed using off-line GC's. The aqueous phase, collected at a temperature of 25℃ was separated into a water and oil fraction and analysed on the off-line FID's. The details of the gas chromatographic separations are summarised in Table 3.1.

Table 3.1 One dimensional GC product analysis

Species	GC	Column	Temperature (℃)	Detector
H2	HP 6890	Chemlab Molecular Sieve 5Å, Packed 1m x 1/8in	110	TCD
CO, CO_2, CH_4, Ar, N_2	HP 6890	Restek Shin Carbon 80/100 µ, Packed 2m x 1/8in	110	TCD
Organics in feed & tail gas	HP 6890	Varian CP Sil 5 CP, Capillary 25m x 150µm x 2µm	35 - 180	FID
Organics in oil	HP 6890	J & W PONA, Capillary 50m x 200µm x 0.5µm	35 - 250	FID
Organics in water	HP 6890	J & W PONA, Capillary 50m x 200µm x 0.5µm	35 - 120	FID

For detailed selectivity studies in FTS, one dimensional gas chromatography is not sufficient for the quantification of the minor compounds (Figures 3.4 and 3.5) such as branched compounds, dienes, oxygenates, aromatics etc. This is caused by the large number of components with similar physical properties that co-elute from the GC column, making detailed analysis impossible.

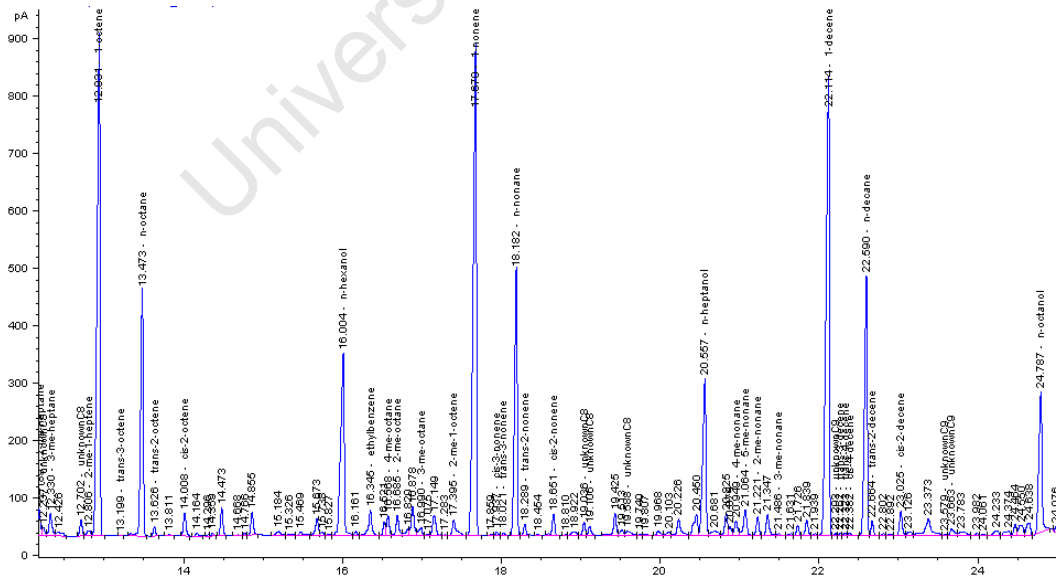

Figure 3.4 GC analysis of C_8 to C_{10} oil fraction.

Figure 3.4 shows the major products (α-olefins, n-paraffins, 1-alcohols, as well as the cis- and trans-olefins) in the C_8 to C_{10} oil fraction and the ordered multiplicity in which they appear. They are easily identified and quantified.

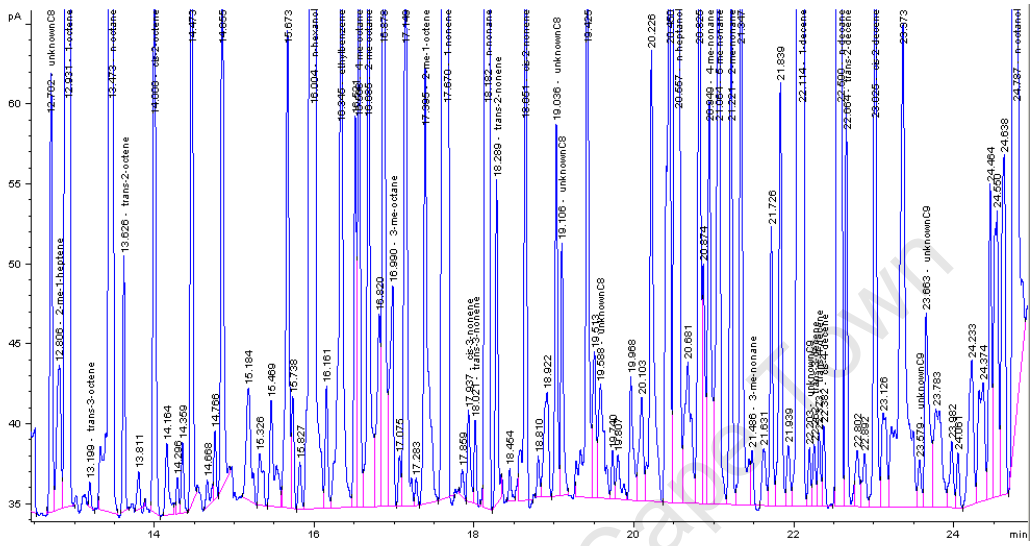

Figure 3.5 Magnified GC analysis of C_8 to C_{10} oil fraction.

Figure 3.5 shows the same GC trace as in Figure 3.4 but at a higher magnification. This Figure clearly shows the peak overlap and co-elution of minor products like branched compounds, oxygenates and aromatics having similar residence times.

3.4.2 Comprehensive Gas Chromatography

Comprehensive GC is a relatively new analytical method which allows for the routine analysis of complex organic mixtures (i.e. high separation power), making it possible to separate and quantitatively determine the major, as well as, the minor products (branched products as well as carbonyls, dienes, acids, cyclics, aromatics and secondary alcohols) of the FTS.

A comprehensive GC system can be described as a “continuous heart cutter” where effluent from the first column is “focused” into a series of nearly ideal injections onto a

second, high speed analytical column. The interface between the first and second column is known as the modulator.

The operation of the loop modulator is schematically shown in Figure 3.6. The sample leaving the first column is trapped at the entrance to the delay loop (1st stage) by a cold jet. Firing of the hot jet remobilizes the sample and it enters the delay loop. While the now focused sample moves around the delay loop (a few hundred milliseconds), the hot jet is turned off again and a cold spot reforms (2nd stage). The sample in the delay loop reaches the second cold spot and once again becomes trapped. The next firing of the hot jet releases the focused sample into the second column and simultaneously admits another sample from the first column into the delay loop. The delay loop is generally made up of the first part of the second column.

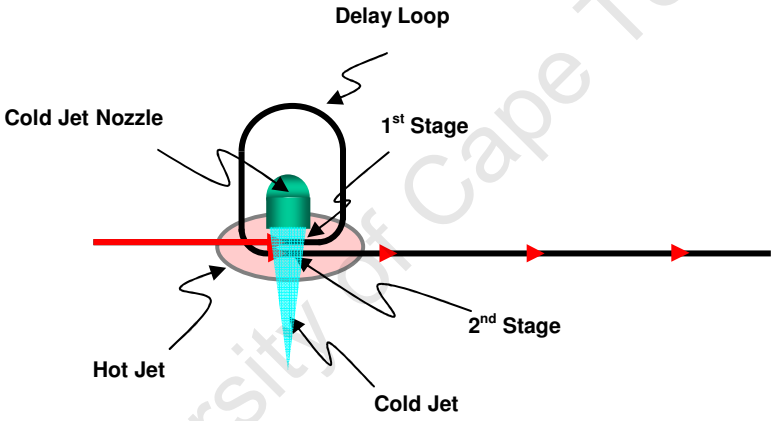

Figure 3.6 Schematic of a loop modulator [Ledford *et al.*, 2005]

To obtain maximum separation, the mechanisms on the two columns can be by two different molecular properties, molecular size (volatility) and polarity. These two properties are independent of each other as there is no direct correlation between molecule size and polarity. Therefore, the first column retention times can be plotted against the second column retention times. The result is a separation that arranges organic compounds according to their chemical group on one axis and by their carbon numbers on the other axis.

The best separation of the FT oil fraction was found to be with a non-polar column followed by a polar column (i.e. separation by boiling point and then by polarity). Table 3.2 describes the columns and program settings used, while Figures 3.7 and 3.8 show a full multidimensional GC analysis.

Table 3.2 HP6890 GC x GC set-up for FT oil analysis

Column order	**1**	**2**
Column	Varian CP Sil 5 CP, Capillary 25m x 150µm x 2µm	J & W HP-INNOWAX, Capillary 50 x 200 µm x 0.4µm
Temperature (℃)	30 - 240	30 – 240
Modulation time (s)	4	/
Detector	/	FID

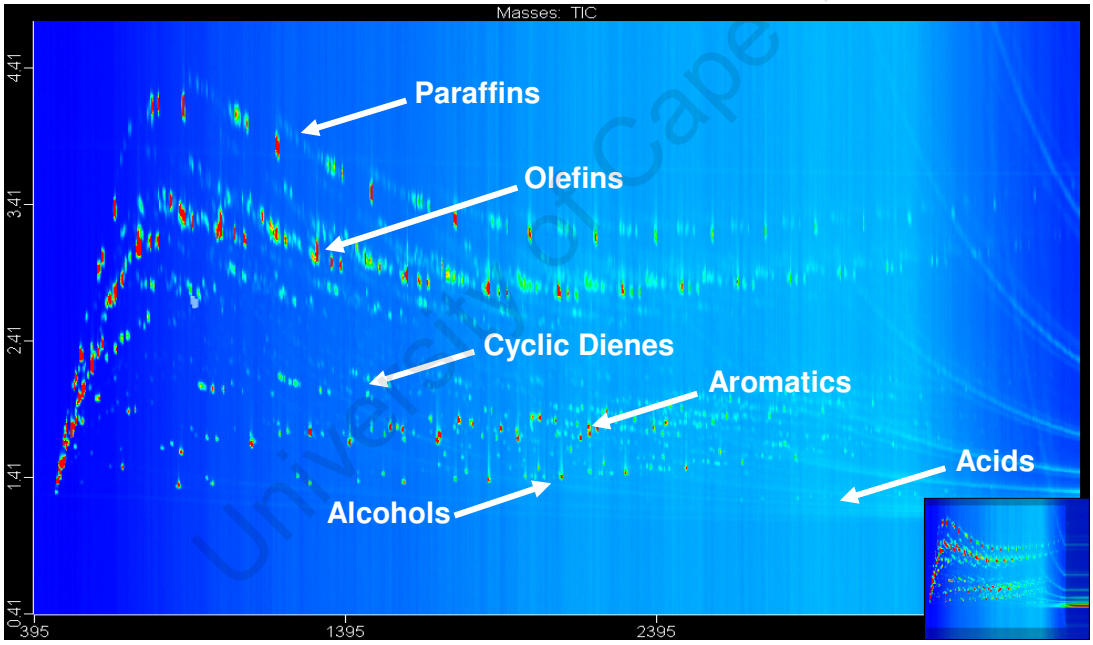

Figure 3.7 Comprehensive multidimensional GC analysis of total oil fraction

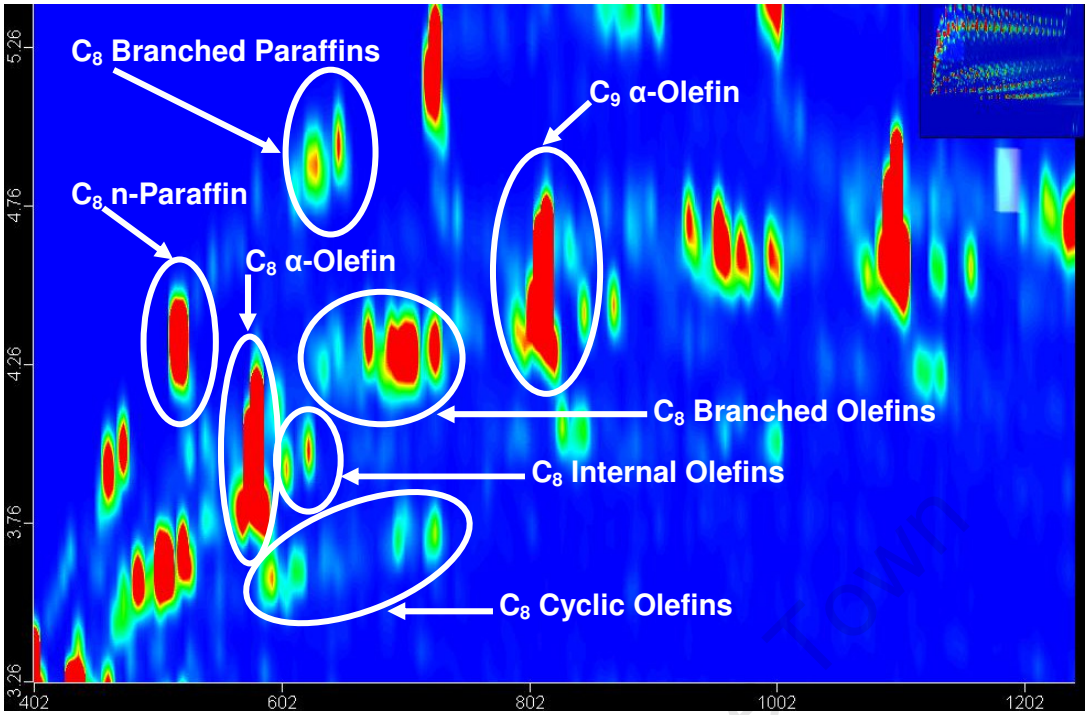

Figure 3.8 Comprehensive multidimensional GC analysis of C_8 paraffins and olefins in the oil fractions

3.4.3 Acid number determination

The acid number is determined by adding a few drops of indicator (phenolphatlein) to a known mass of reaction water product. The sample is then titrated with a KOH solution until the indicator changes colour.

$$Acid\ number = \frac{W_{KOH}}{W_{rw}} = V \bullet C_{KOH} \bullet \frac{56.1}{W_{rw}} \qquad (3.3)$$

where:

W_{KOH} = mass of KOH used to titrate (mg)

W_{rw} = mass of reaction water (g)

V = volume of KOH solution used to titrate (cm^3)

C_{KOH} = concentration of KOH in solution ($mol.dm^{-3}$)

3.5 Data Workup

3.5.1 Argon as internal standard for TCD analysis

Argon is added to the feed as an internal standard as it is chemically inert and therefore is not consumed or generated during the reaction. Using the fact that argon is inert and given that the amount (ml(n)/h) of argon in the feed is known, all the other components in the feed and product gas streams can be quantified. From this, the conversion, kinetics and methane selectivity data can be calculated.

$$F_i = f_i \bullet \frac{AC_i}{AC_{Ar}} \bullet F_{Ar} \tag{3.4}$$

where:
F_i = molar flow rate of compound *i*
F_{Ar} = molar flow rate of argon (internal standard)
f_i = compound specific calibration factor, relative to the response of argon
AC_i = area counts for compound *i* from GC
AC_{Ar} = area counts for argon from GC

The flow rate of water is calculated from an oxygen balance, i.e. the flow rates from the inlet and outlet of the reactor for CO and CO_2.

$$F_{H_2O} = F_{CO,in} - F_{CO,out} + F_{CO_2,in} - F_{CO_2,out} \tag{3.5}$$

The flow rate of the C_2+ organic product compounds can be found by relating to the flow rate of methane, which is linked to the flow rate of argon.

3.5.2 Methane as external standard for on-line FID analysis

The tail and fresh feed gas contain a mixture of organic compounds and permanent gases (H_2, CO, CO_2, Ar and N_2). A FID detector only detects organic compounds, therefore the analysis of the tail and fresh feed gas do not add up to 100% of the sample analysed. For this reason an external standard of methane is used to quantify the hydrocarbons in the tail gas and fresh feed.

The external standard can only be used when a fixed amount of sample is injected into the GC (accomplished using a sample loop) as for online gas analysis. The external standard method can therefore not be used with the ampoule sampling technique as the volume of the ampoule is not constant.

The quantification of hydrocarbons for the online FID analysis is as follows:
A gas of known concentration (known methane volume %) is injected in the same manner as the tail and fresh feed samples in order to replicate the amount of sample injected. From this known methane volume of sample (%), an area count is obtained from the GC detector and the volume fraction (%) of all the other hydrocarbons in the tail gas and fresh feed can be calculated.

$$\frac{C_{CH4Y}}{C_{CH4X}} \bullet n = \frac{AC_Y}{AC_X} \tag{3.6}$$

$$\therefore C_{CH4Y} = \frac{AC_Y}{AC_X} \bullet \frac{1}{n} \bullet C_{CH4X} \tag{3.7}$$

The calculation for any hydrocarbon is then:

$$C_{HC,N} = \frac{AC_N}{AC_X} \bullet \frac{1}{n} \bullet C_{CH4X} \tag{3.8}$$

where:
C = concentration (vol %)
AC = area counts from GC

x = methane sample of known concentration
Y = methane sample of unknown concentration
N = hydrocarbon of unknown concentration
n = carbon number of the sample with unknown concentration

The same methodology is followed in the water FID analysis for determining the organic content, as water is not detected by the FID. Instead of methane a oxygenate mixture of known concentration is used as an external standard.

3.5.3 Quantification of products in the oil FID

Oil samples can be normalized to 100% (i.e. all compounds in the oil sample can be identified and summed to the total oil mass) therefore it is not necessary to use an external standard for quantification.

3.5.4 Calculation of Conversion

Carbon Monoxide Conversion
According to the definition of conversion [Fogler, 1999], the total amount of carbon monoxide converted (X_{CO}) is:

$$X_{CO} = \frac{F_{COin} - F_{COout}}{F_{COin}} \tag{3.9}$$

Carbon Monoxide Converted to Fischer-Tropsch Products
As discussed in chapter 2, iron Fischer-Tropsch catalysts are also active for the water-gas shift reaction (only the net production of carbon dioxide was observed over the temperature range investigated). This complicates the calculation for the conversion of carbon monoxide to FT products, as the amount of carbon monoxide converted to carbon dioxide via the forward WGS reaction must be accounted for (i.e. the amount of carbon monoxide converted to carbon dioxide must be subtracted from equation 3.8). The amount of carbon monoxide consumed in the WGS reaction cannot be measured directly and must therefore be calculated from the net production of carbon dioxide from

the WGS reaction. Finally, the conversion of carbon monoxide converted to FT products over an iron catalyst with forward WGS is calculated by:

$$X_{CO\ to\ FT\ products} = \frac{\left(F_{COin} - F_{COout}\right) - \left(F_{CO_2 out} - F_{CO_2 in}\right)}{F_{COin}} \bullet 100 \quad (3.10)$$

Synthesis Gas Conversion

The FT reaction consumes synthesis gas (H_2 and CO) and produces organic products. The WGS reaction consumes one molecule of CO for every molecule of H_2 produced, and therefore does not affect the total molar amount of synthesis gas in the system. The synthesis gas conversion is therefore the fraction of the reactive feed that has been converted to desired products and is numerically independent of the WGS reaction.

$$X_{CO+H_2} = \frac{\left(F_{COin} + F_{H_2 in}\right) - \left(F_{COout} + F_{H_2 out}\right)}{\left(F_{COin} + F_{H_2 in}\right)} \bullet 100 \quad (3.11)$$

3.5.5 Calculation of Reaction Rates

For ideal gradientless reactors, those in which temperature and concentration gradients are negligible or altogether absent, the reaction rate can be calculated by means of simple mass-balance equations.

The rate of formation of organic Fischer-Tropsch products can therefore be calculated from the amount of carbon monoxide consumed, minus the amount of carbon dioxide formed via the WGS reaction.

$$r_{FTS} = \frac{\left(F_{COin} - F_{COout}\right) - \left(F_{CO_2 out} - F_{CO_2 in}\right)}{m_{mass\ of\ cat\ loaded}} \quad (3.12)$$

where:

r_{FTS} = rate of the Fischer-Tropsch Synthesis

m = mass of catalyst loaded into the reactor

The rate of the water gas shift reaction is determined from the total CO_2 formed:

$$r_{WGS} = \frac{\left(F_{CO_2 out} - F_{CO_2 in}\right)}{m_{mass\ of\ cat\ loaded}} \tag{3.13}$$

3.5.6 Calculation of Product Selectivity

For the FTS the selectivity to organic compounds is of particular interest. Therefore, the selectivity towards an organic compound *i,* is calculated relative to the amount of carbon monoxide converted to FT products (excluding carbon dioxide formed via the WGS reaction). By representing the selectivity data as carbon atom selectivity, the distribution of carbon atoms towards specific product compounds is given; thereby showing the carbon efficiency towards useful or targeted products.

$$S_{i\ C-atom} = \frac{F_i}{\left(F_{CO\,in} - F_{CO\,out}\right) - \left(F_{CO_2\,out} - F_{CO_2\,in}\right)} \bullet C\#_i \bullet 100 \tag{3.14}$$

where:

S = selectivity (C-atom %)

$C\#_i$ = carbon number of compound *i*

3.5.7 Miscellaneous Calculations

Partial pressure in the reactor

Because the reactor is completely mixed (CSTR), the composition at the exit of the reactor is the same as all points inside the reactor (i.e. no concentration gradients). Therefore, the partial pressures inside the reactor can be calculated from the analysed composition of the exit stream:

$$P_i = \frac{F_{i\ out}}{\Sigma F_{out}} \bullet P_{total} \tag{3.15}$$

where:

P_i = partial pressure of component *I* (bar)

P_{total} = total reactor pressure (barg)

Usage ratio

The usage ratio is defined as the amount of hydrogen consumed relative to the amount of carbon monoxide consumed.

$$Usage\ ratio = \frac{F_{H_2\ in} - F_{H_2\ out}}{F_{CO\ in} - F_{CO\ out}} \tag{3.16}$$

Gas hourly space velocity

The gas hourly space velocity (GHSV) is calculated by:

$$GHSV = \frac{\dot{V}_{syngas\ in}}{m_{mass\ of\ cat\ loaded}} \tag{3.17}$$

where: $\dot{V}$ = Volumetric flow rate (ml(n)/s)

3.6 Experiments

During activation, on-line samples were taken periodically and analysed by TCD to determine the catalyst activity. Once the desired activity was reached, the reactor was switched over to synthesis conditions.

After setting the temperature to the desired value for the experiment, the GHSV was changed to obtain 20 % conversion of carbon monoxide to FT products; (increasing the GHSV resulted in decreased conversion and vice versa). For the experiments at higher temperatures, the catalytic activity was very high and it was difficult to achieve a high enough space velocity to achieve a CO to Fischer-Tropsch product conversion of 20 %.

Once 20 % conversion of carbon monoxide to FT products was reached, samples were taken on a daily basis and full mass and carbon balances were done (FID and TCD). A minimum of two days of synthesis without changing the process conditions was required to reach steady state. After which samples were analyzed by the methods above to obtain selectivity data used in chapter 4.

The source of the synthesis gas was changed from the auto-thermal reformer (ATR) to cylinders after run PR 20. This was due to the inconsistent delivery of gas from the ATR. The composition of the cylinder derived feed was mixed in such a way to be the same as for the ATR gas and no differences with regard to catalyst activity were observed after the switch was made.

Table 3.3 Summary of experiments where reaction temperature was varied.

Experiment no.	Run name	Temperature (℃)	Catalyst mass (g)	ATR or cylinder feed
1	PR31*	260	10	Cylinder
2	PR 17	220	10	ATR
3	PR 34	230	10	Cylinder
4	PR 20	245	10	ATR
5	PR 29	250	10	Cylinder
6	PR 24	260	10	Cylinder
7	PR 18	270	10	ATR

* This experiment was carried out to determine the effect of stirrer speed on the FT and WGS reaction rates, no selectivity data was collected for this experiment.

Chapter 4

Results

4.1 Mass Transport Limitations

4.1.1 External mass transport limitations

The reaction rates for the Fischer-Tropsch synthesis and the water gas shift reaction were measured as a function of stirrer speed. The catalyst was activated as per the normal activation procedure described in section 3.3.2. Synthesis was carried out at 260℃ in order to have high catalyst activity (270℃ was not tested as catalyst deactivation was a concern).

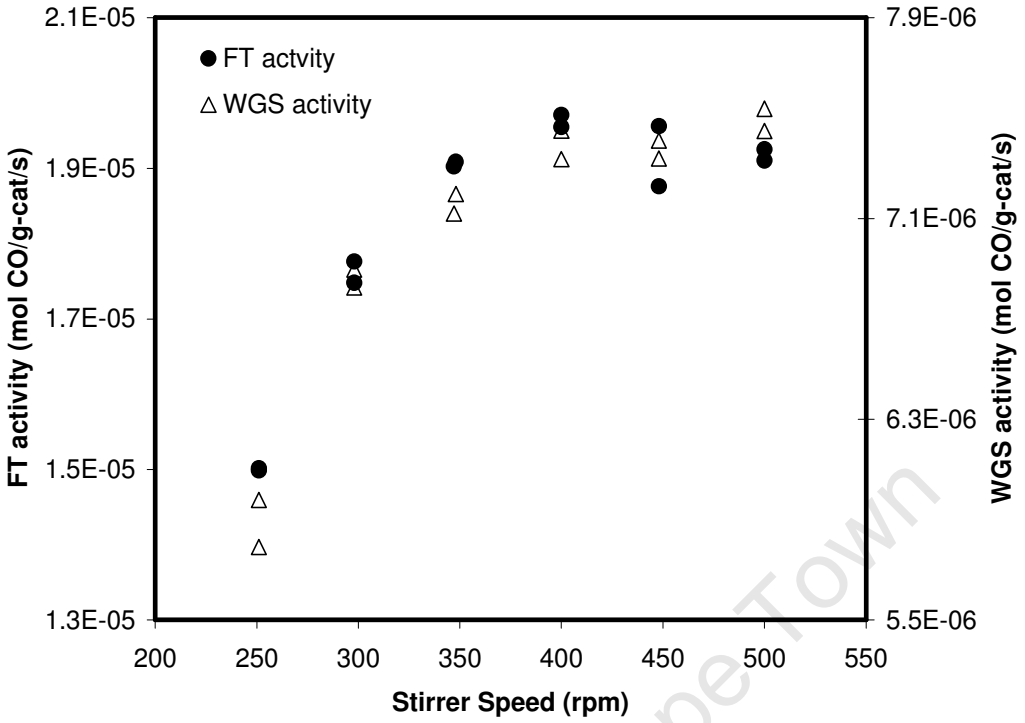

Figure 4.1 Fischer-Tropsch activity (mol CO/g-cat/s) at 260℃ as a function of stirrer speed (rpm)

Two samples were taken at each stirrer speed and analysed by on-line GC equipped with a TCD. The measured rate of reaction increased with increasing stirrer speed up to approximately 400 rpm after which the reaction rates for both the Fischer-Tropsch and water-gas shift reactions remained constant. The increase in reaction rates can be attributed to enhanced gas-liquid mass transfer with increasing stirrer speed. The section of Figure 4.1 where the reaction rates become independent of the stirrer speed indicates the region in which the reaction is not controlled by external (gas-liquid) mass transfer limitations. Consequently, it can be concluded that for the current reactor setup with high catalyst activity (at reaction temperatures of 260℃), stirrer speeds in excess of 400 rpm are sufficient to eliminate external mass transfer limitations.

The experiment above (effect of stirrer speed on external mass transfer limitations) was completed independently to the experiment at 260℃ for which selectivity data was collected. Unless otherwise specified, the data for the 260℃ selectivity point is presented in the remaining sections of this chapter.

4.1.2 Internal mass transport limitations

The Weisz-Prater criterion (C_{WP}) was used to check for the presence of internal mass transfer limitations: If C_{WP} «1, there are no internal diffusion limitations and consequently the concentration gradients within the catalyst particle are negligible. If however C_{WP} »1, internal diffusion limits the reaction severely [Fogler, 1999].

$$C_{WP} = \frac{-r_A(obs) \bullet \rho_c \bullet R^2}{D_e \bullet C_{As}} \tag{4.1}$$

where:

$-r_A(obs)$ = experimentally observed reaction rate (mol/g-cat•s)

ρ_c = catalyst density, (g/cm^3)

R = radius of spherical catalyst particle, (cm)

C_{As} = concentration of carbon monoxide in the liquid phase, (mol/cm^3)[1]

D_e = effective diffusivity of carbon monoxide in $C_{22}H_{46}$ (slurry medium), (cm^2/s)

The liquid in the reactor was assumed to be paraffinic with an average carbon number of 22 and is thus modeled as *n*-$C_{22}H_{46}$. The effective diffusivity, D_e of carbon monoxide in liquid FT product (FT product not including FT product in the gas phase) was calculated using the Wilke-Chang correlation. The Wilke-Chang correlation is used for estimating the diffusion coefficients at infinite dilution. For this case the solute A, is carbon monoxide and the solvent B, is the slurry medium ($C_{22}H_{46}$ n-paraffin). In engineering work the diffusion coefficient is assumed to be representative of concentrations of A, up to 10 mol% [Millet *et al.*, 1996]. A detailed description of the methods used for the calculation of the diffusion coefficients, effective diffusivity and Weisz-Prater criterion, as well as the parameter values used, is given in appendix A

[1] Henry coefficients used in the calculation of liquid phase carbon monoxide concentrations were calculated as a function of temperature [Marano and Holder, 1997]

Figure 4.2 shows the values for the Weisz-Prater criterion (C_{WP}) as a function of temperature. The increase in C_{wp} with increasing reaction temperature is expected, since the rate of the Fischer-Tropsch reaction increases exponentially with temperature. Therefore, the likelihood of internal mass transfer limitations will also increase with increasing temperature.

The value for C_{WP} remains less than 1 up to approximately 250 °C, at 260 °C it is 1.1 and at 270 °C it is just below 1.2. This indicates that internal mass transport limitations are feasible at high temperatures and may influence both the reaction rates and product selectivities. It is however not clear what a value of 1.2 for the Weisz-Prater criterion actually means in terms of the extent of internal mass transport limitations. For this reason the extent of mass transport limitations at high temperatures are quantified further in chapter 5 where the Thiele modulus and effectiveness factor will be estimated.

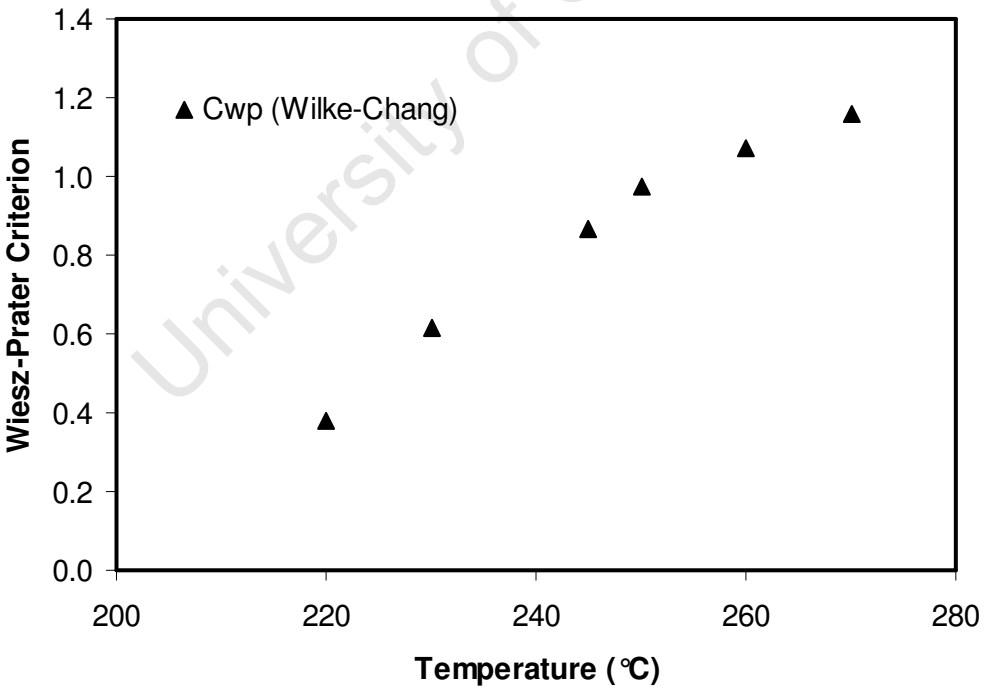

Figure 4.2 Weisz-Prater criterion as a function of temperature

4.2 Conversion and Reactor Partial Pressures

As discussed in the experimental section, the space velocity was varied to maintain the carbon monoxide to Fischer-Tropsch product conversion at approximately 20%. Table 4.1 gives the resulting CO conversion to Fischer-Tropsch products as well as the conversion of CO to CO_2 for each respective temperature tested. It should be noted that an increase in the space velocity will lead to a decrease in the residence time of components in the reactor, and thus may decrease the probability for secondary reactions to occur [van der Laan and Beenackers, 1999].

The space velocity used to obtain a conversion of CO to Fischer-Tropsch products of approximately 20% at 270°C is lower than that at 260°C and only slightly higher than the space velocity for the experiment at 250°C. This might indicate that the catalyst has deactivated before the data obtained at 270°C were collected.

Table 4.1 Average conversions and space velocities as a function of temperature for selectivity periods

Temperature (°C)	**Average $X_{CO\ to\ FT\ prod}$ (%)**	**Average $X_{CO\ to\ CO2}$ (%)**	**Average space velocity measured, (ml(n) / g-cat / h)**
220	20	16	5100
230	21	16	8000
245	18	17	16600
250	22	22	17000
260	20	14	22400
270	26	27	17600

The reactor partial pressures were calculated from the TCD analysis of the tail gas and the total pressure in the reactor. The water content in the tail gas was calculated using an oxygen balance as described in the experimental section.

Figure 4.3 and Table 4.2 show the reactor partial pressures of the kinetically relevant compounds (hydrogen, carbon monoxide, water and carbon dioxide) for the runs performed. The partial pressures of the kinetically relevant components were kept fairly constant over the entire temperature range therefore; the major effects on activity and selectivity observed in this study can thus be attributed to changes in temperature.

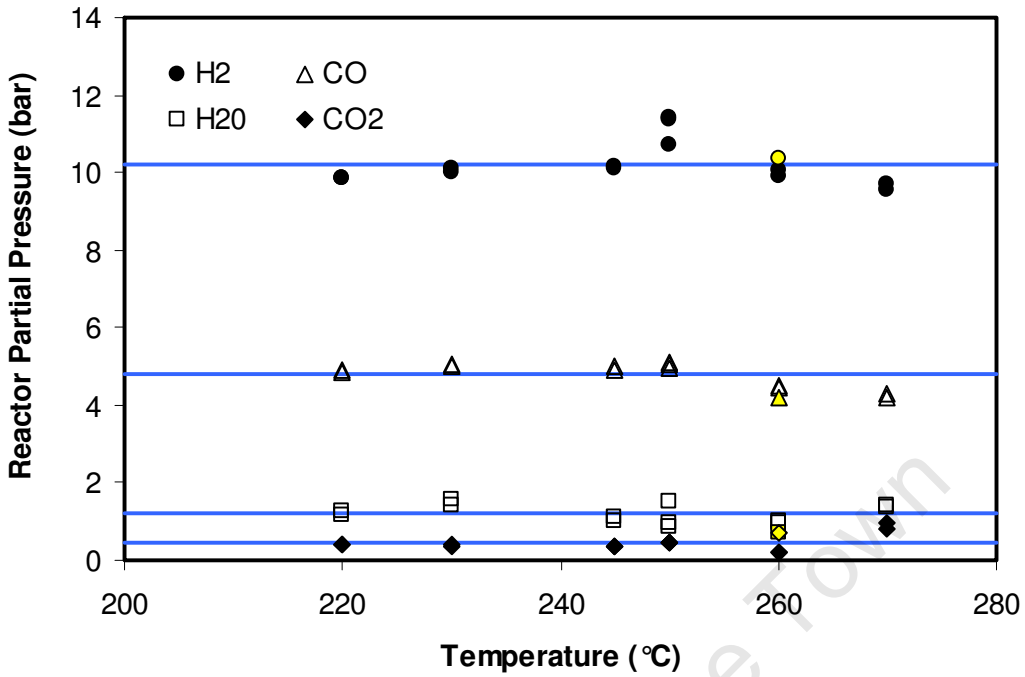

Figure 4.3 Reactor partial pressures as a function of temperature, yellow symbols represent data from the stirrer speed experiment at 260°C

Table 4.2 Average partial pressure (pp) of kinetically relevant components

Component	Average pp (bar)	Maximum pp (bar)	Minimum pp (bar)
Hydrogen	10.2	11.4	9.6
Carbon monoxide	4.8	5.1	4.2
Water	1.2	1.6	0.9
Carbon dioxide	0.5	1.0	0.2

Figure 4.4 shows the deviation of the partial pressure of hydrogen and carbon monoxide for the runs performed at the various temperatures. The partial pressures of H_2 and CO have a maximum deviation of approximately 12 %. This deviation is due to the

increasing difficulty in controlling the Fischer-Tropsch conversion ($X_{CO\,to\,FT\ products}$ ≈ 20%) as the reaction temperature and thus the reaction rate increases.

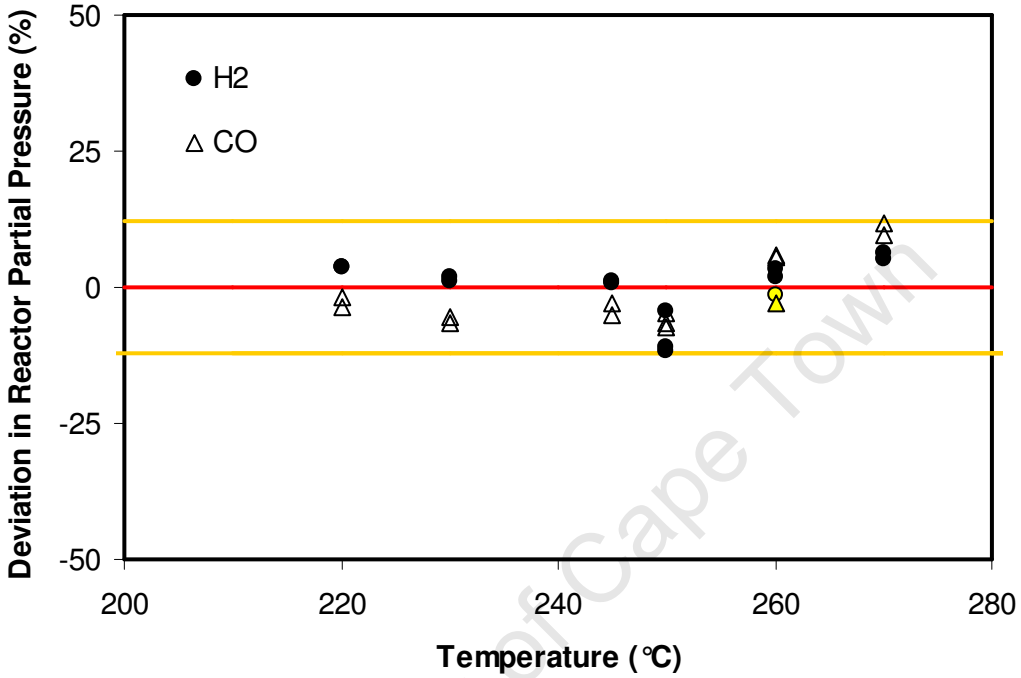

Figure 4.4 Deviation in H_2 and CO partial pressures from their respective averages as a function of increasing temperature, yellow symbols represent data from the stirrer speed experiment at 260°C

4.3 Observed Activity as a Function of Temperature

Figure 4.5 shows the rate of CO consumption for the formation of organic product compounds (FT-activity) and for the formation of CO_2 (WGS activity) as a function of temperature. At 260°C, the rate of CO consumption for the formation of organic product compounds (FT activity) is less than expected based on an exponential extrapolation of the rate of reaction in the range 220-250°C. The rate of CO consumption for the formation of CO_2 (water gas shift activity) is even more severely affected and a lower rate of formation of CO_2 is observed.

The lower than expected, increase in the rate of CO consumption for the formation of organic product compounds (Fischer-Tropsch activity) in the temperature range 250℃ to 270°C may indicate the presence of mass transport limitations or catalyst deactivation. As discussed above, it is not clear to what extent internal mass transport limitations or catalyst deactivation play a role in the rate of CO consumption. This will be discussed further in chapter 5.

The low rate of CO consumption for the formation of CO_2 at 260℃ may be related to the high space velocity used to obtain the desired conversion level for this point ($X_{CO\ to\ FT\ products}$ ≈ 20%). Krishnamoorthy *et al.* (2002) studied the pathways for CO_2 formation during Fischer-Tropsch synthesis and observed the forward rate of CO_2 formation to increase with increasing residence time / conversion. Hence, the formation of CO_2 in the Fischer-Tropsch synthesis is generally accepted to occur via a subsequent (secondary and independent) reaction of CO with H_2O (water-gas shift reaction) [Krishnamoorthy *et al.*, 2002; Zimmerman and Bukur, 1990; van der Laan and Beenackers, 1999; Botes 2008]. At conditions of high space velocity the forward rate of CO_2 formation will decrease since H_2O is removed before it can react.

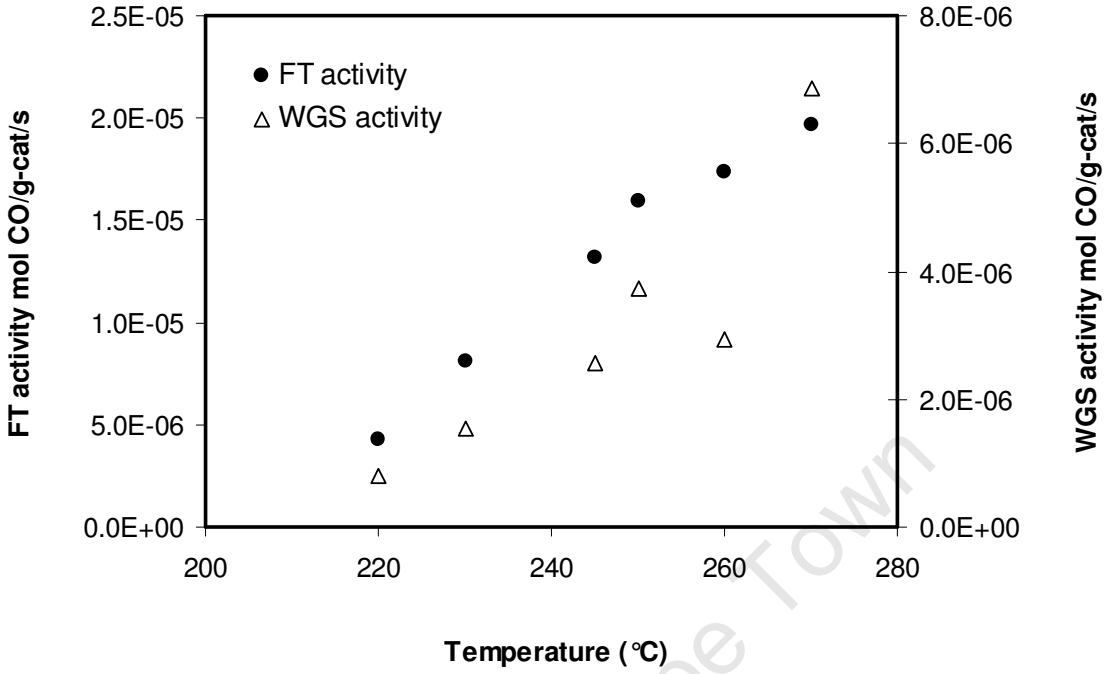

Figure 4.5 Rate of CO consumption for the formation of organic product compounds (Fischer-Tropsch activity) and for the formation of CO_2 (water gas shift activity) as a function of reaction temperature

4.4 Product analysis: One Dimensional vs. Comprehensive Gas Chromatography

The oil fraction obtained in the various experiments were analysed using both the well-established one-dimensional GC-technique and the recently introduced comprehensive GC-technique [Adahchour *et al*., 2006]. Figures 4.6 and 4.7 show a comparison of the results obtained using 1-dimentional (1-D) and comprehensive GC analysis for a typical oil sample (see appendix B).

For both the α-olefin and n-paraffin analysis the comprehensive GC analysis gives a slightly higher selectivity at low carbon numbers while the 1-D-GC analysis gives a slightly higher selectivity at higher carbon numbers. It is postulated that the higher selectivity observed with the comprehensive GC-analysis compared to 1-D analysis at low carbon numbers (C_5 to C_9) can be attributed to better resolution of the individual

peaks by comprehensive GC and hence more accurate integration leading to larger peak areas.

The higher selectivity of the 1-D-GC analysis compared to the comprehensive GC-analysis for high carbon numbers (C_{10}+) is due to the limited separation ability of the 1-D GC. With comprehensive GC, separation is based on orthogonal separation (two column set-up) that separates compounds on the basis of physical properties (boiling point) and chemical properties (functional group). For example internal olefins and 1-olefins with similar boiling points can still be separated based on their different functionalities. As the carbon number increases the number of components that have similar physical properties, e.g. isomers, also increases. This increase of compounds with similar physical properties results in co-elution in a 1-D GC (see chapter 3, Figure 3.5) leading to an increased FID response and hence an "observed" greater selectivity for the major compounds. In comprehensive-GC analysis the problem of co-elution is solved by modulation. Therefore, the selectivity for the major compounds as obtained using comprehensive GC-analysis is a better reflection of the true Fischer-Tropsch selectivity at the conditions tested.

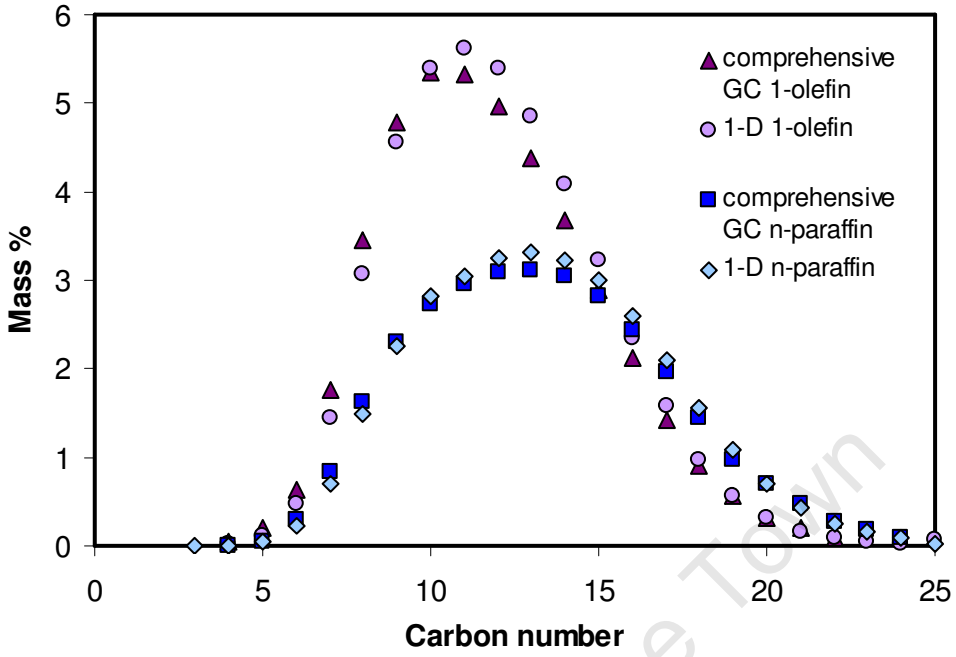

Figure 4.6 Comparison of product selectivity for α-olefins and n-paraffins in the oil fraction of the product obtained in the experiment performed at 230°C as determined by 1-dimensional (1-D) and comprehensive gas chromatography

Figure 4.7 shows the selectivity for n-alcohols-(1) and for internal olefins in the oil fraction as a function of carbon number obtained by the conventional 1D-GC analysis and the newly introduced comprehensive GC technique. The selectivity for 1-alcohols (C_8 to C_{12}) and the internal olefins (C_{10} to C_{18}) show a similar trend as already described for the major product compounds (see Figure 4.6).

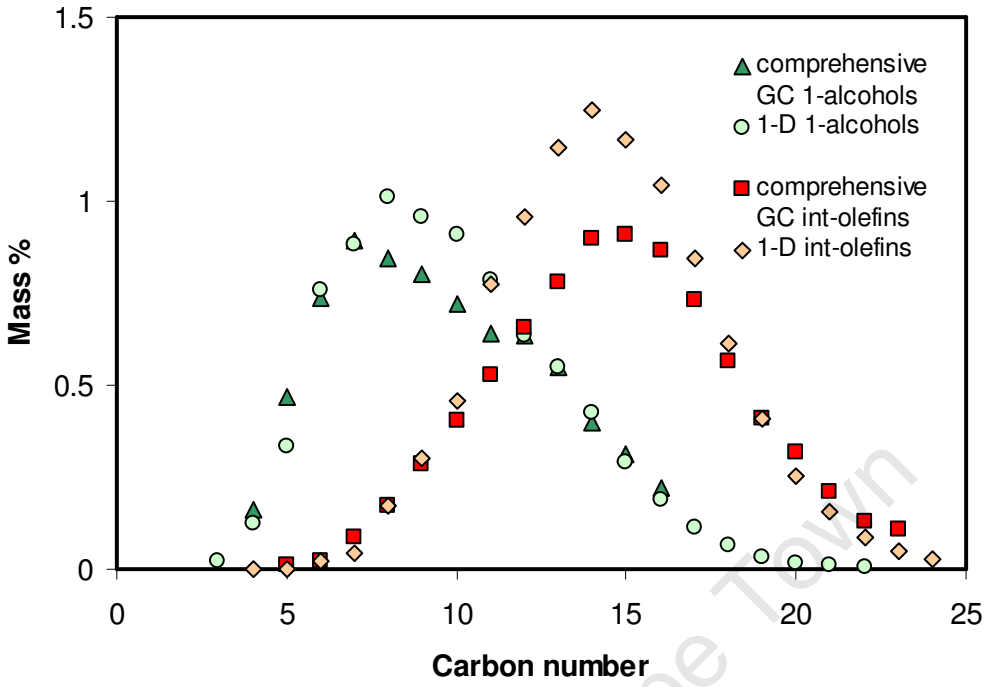

Figure 4.7 1-Dimensional (1-D) vs. comprehensive GC analysis of 1-alcohols and internal olefins

Figure 4.8 demonstrates how comprehensive GC analysis can be used to efficiently separate out the minor components which are normally obscured by the more prominent compounds in the Fischer-Tropsch product. The advantage of comprehensive GC is therefore particular evident in the analysis of the selectivity of minor product compounds.

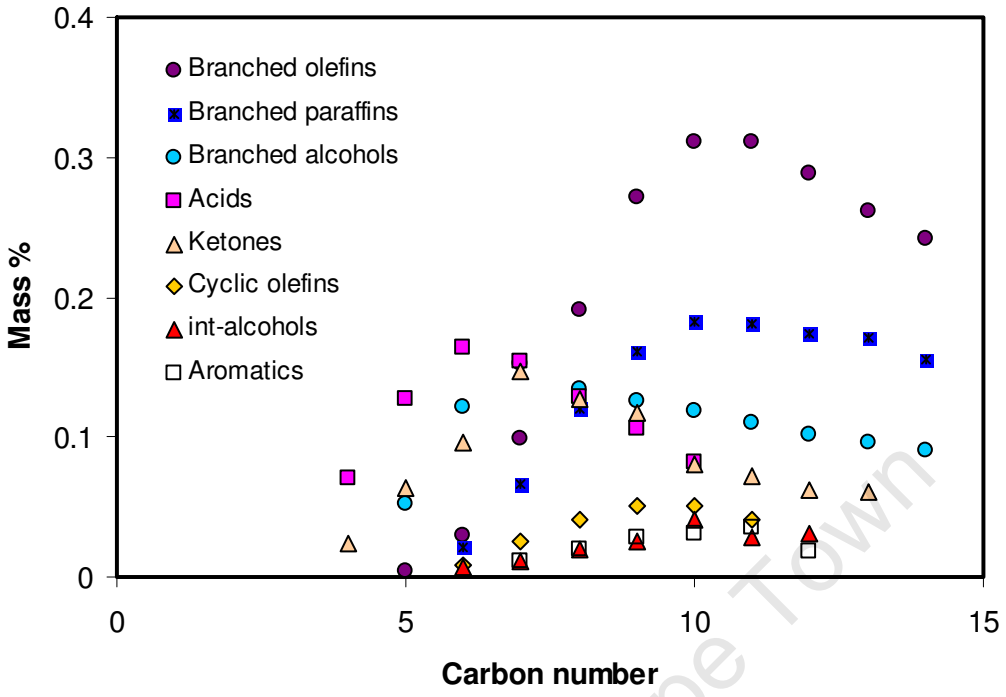

Figure 4.8 Minor organic components identified in the oil fraction by comprehensive GC analysis

4.5 Selectivity

4.5.1 Carbon dioxide selectivity

Figure 4.9 shows the CO_2 selectivity as a function of the reaction temperature. The overall trend for CO_2 selectivity increases "slightly" with increasing temperature; the only exception being the two points at 260°C which are lower than expected. Since the 260°C points are at conditions of relatively high space velocity (Table 4.1) and given the discussion in section 4.3 above, i.e. that the formation of CO_2 occurs via a consecutive reaction of CO with H_2O (the H_2O formed in the Fischer-Tropsch reaction). It is expected that at conditions of high space velocity or low reactor H_2O partial pressure the water-gas shift reaction rate will be low. Furthermore, assuming that no other major side reactions involving CO and H_2O to form CO_2 (water-gas shift) take place over the iron catalyst at the reaction conditions tested, the overall CO_2 selectivity for the Fischer-Tropsch synthesis (including the water-gas shift reaction) will be a function of the water-gas shift reaction rate (i.e. if the WGS reaction rate decreases, so will the CO_2 selectivity).

The results of Figure 4.9 therefore support the view that CO_2 formation via the secondary reaction of CO with primarily formed H_2O (water-gas shift reaction) at reaction conditions far from WGS equilibrium are indeed a major route for the formation of CO_2 in the Fischer-Tropsch synthesis.

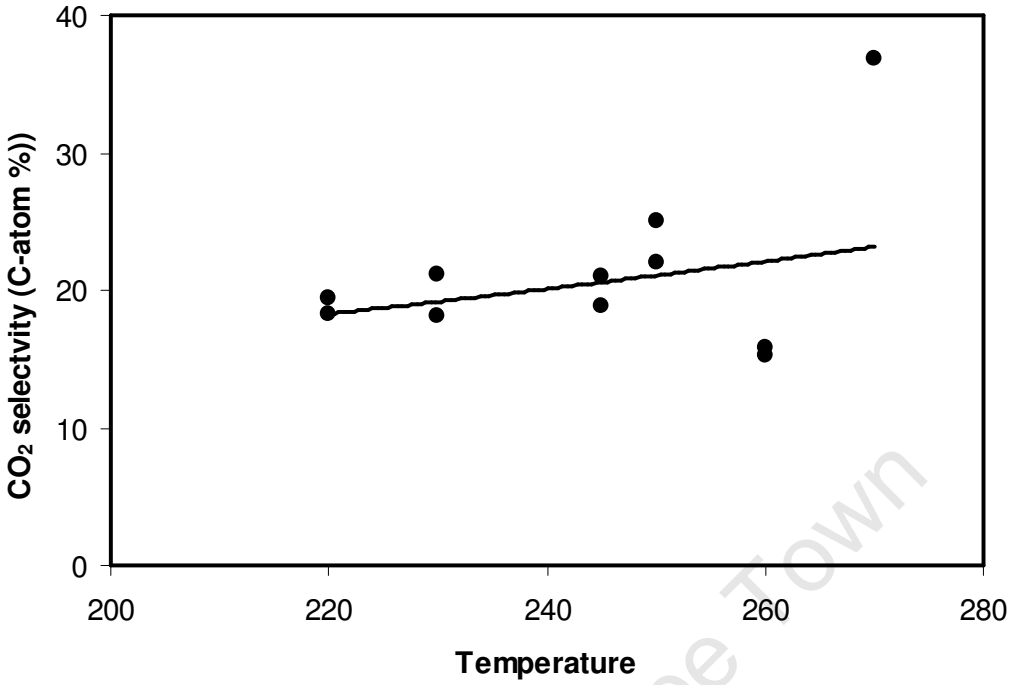

Figure 4.9 CO_2 selectivity (C-atom %) as a function of temperature

The formation of CO_2 in the experiments for this thesis i.e. reaction conditions are far from water-gas shift equilibrium (see Table 4.3) and can thus be regarded as an irreversible, consecutive reaction following the formation of the major product compound water.

Table 4.3 Equilibrium constants and experimentally determined water-gas-shift ratio as a function of temperature

Temperature (℃)	**Equilibrium constant** $K_e(T,P) = \exp\left(\frac{-\Delta Grxn}{RT}\right)$	**Water-gas shift ratio** $K_a = \frac{P_{CO_2} \cdot P_{H_2}}{P_{CO} \cdot P_{H_2}}$
220	149	0.66
230	123	0.49
245	94	0.71
250	86	1.14
260	72	0.41
270	61	1.47

4.5.2 Methane selectivity

In the Fischer-Tropsch synthesis, more methane is typically formed than expected based on the constant (ideal) chain growth probability. This "excess" methane formation is actually larger than that conventionally reported by researchers in the FT field since surface species with more than one carbon atom can desorb by multiple pathways, e.g. hydrogen addition, β-hydrogen abstraction etc. [Claeys and van Steen, 2004]. Desorption by β-hydrogen abstraction, yielding olefins is however not possible for C_1 species. Hence, the desorption probability of the C_1-surface species should theoretically be lower.

The excess formation of methane has up to now not been adequately explained. A popular proposal for the formation of methane is via a different surface species than that responsible for the formation of long chain hydrocarbons in the FT synthesis i.e. hydrogenation of a CH_3 surface species which does not take part in chain growth. Govender *et al.* (2008) has shown by steady-state isotopic transient kinetic analysis (SSITKA) on a co-precipitated potassium promoted iron HTFT catalyst (330°C, 1.2bar and H_2:CO = 15), that methane may be formed from two different surface intermediates (C_α and C_β). The results showed that although C_β accounted for 92% of the $C_{1,tot}$ coverage it was 25 to 50 times less active for methanation than C_α. Furthermore, the chain-initiation reaction (C-C coupling) involves a combination of C_α and C_β to form the C_2 surface intermediate.

The formation of methane can be controlled kinetically and in general the rate of desorption relative to the rate of chain growth is inhibited by carbon monoxide and favoured by hydrogen. It is also well known that the rate of desorption is strongly favoured by an increase in the reaction temperature [Claeys and van Steen, 2004].

Figure 4.10 shows the methane selectivity determined from FID GC-analysis as a function of reaction temperature. In general the methane selectivity is very low, but increases with increasing reaction temperature. Given that the partial pressures of carbon monoxide and hydrogen were kept relatively constant for all selectivity points the

data in Figure 4.10 is in-line with literature [Claeys and van Steen, 2004] i.e. it seems that the increasing reaction temperature leads to an increase in the rate of desorption. There is however some scatter in the data (especially at 230℃). This scatter in Figure 4.10 can be ascribed to inaccuracy of the analysis method for such low concentrations of methane.

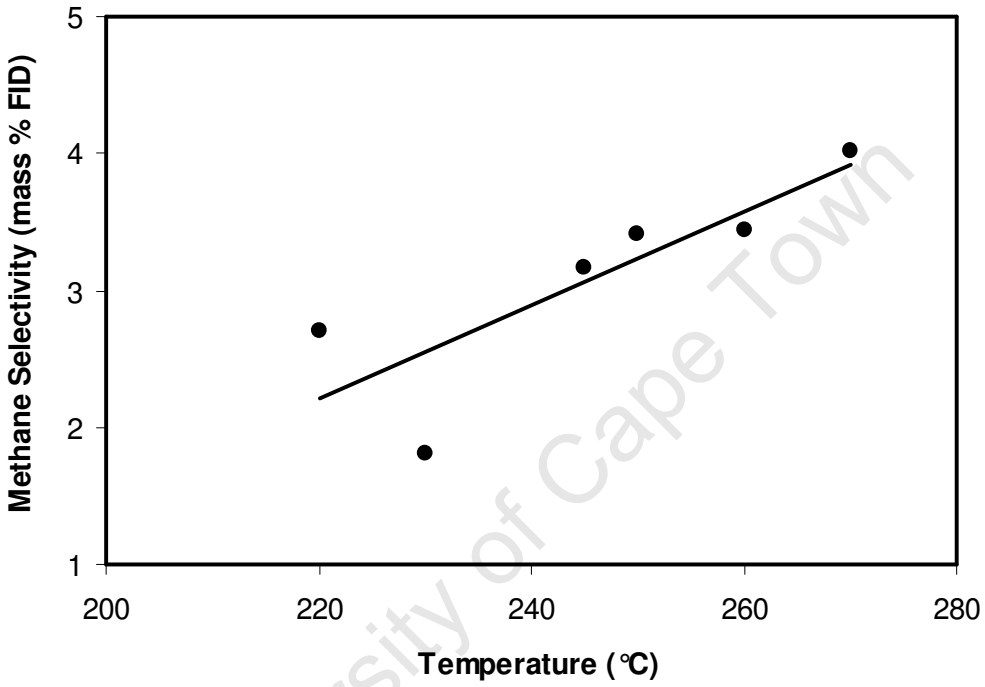

Figure 4.10 Methane selectivity (mass %) as a function of temperature, determined by online FID analysis

4.5.3 Chain growth probability

When performing Fischer-Tropsch selectivity experiments in a slurry reactor, it is imperative that the products of Fischer-Tropsch synthesis can be distinguished from the initial slurry medium. Since the initial slurry medium is usually a heavy paraffinic wax, this task becomes increasingly complicated with Fischer-Tropsch products that have high chain growth probabilities. To prevent any uncertainty in the selectivity results, especially with regard to the experiments at low temperatures (high chain growth

probabilities), the composition of the initial slurry medium was analysed by FID. The results show that a carbon number range of C_1 to C_{14} will be representative of the true Fischer-Tropsch synthesis product, since analysis of the initial slurry medium showed less than 0.05 mass% per carbon number in the C_{15} fraction and lower. Furthermore the initial slurry medium contains predominantly n-paraffins with insignificant amounts of other compounds.

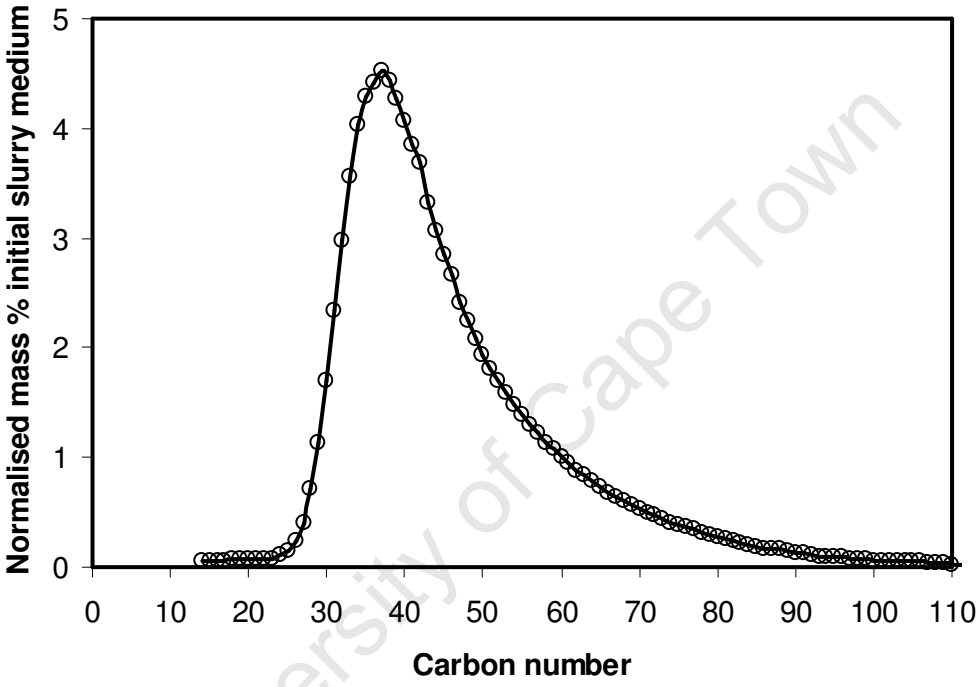

Figure 4.11 Composition of the initial slurry medium

The chain growth probability is expected to decrease with increasing temperature (see Chapter 2.6). This would result in a shift towards a shorter carbon number product and an increase in the methane content (see Table 2.6 and Figure 4.10).

The deviations from the ideal chain growth mechanism as discussed in section 2.6 are clearly illustrated in Figure 4.12, where the Anderson-Schulz-Flory plot for the total product is given: i) the C_1 content in the organic product spectrum is higher than expected based on extrapolation of the C_3-C_5 fraction, ii) the content of the C_2 products is lower than expected based on extrapolation of the C_3-C_5 fraction with the exception for

the experiment performed at 220℃ and iii) there is an increase in the chain growth probability with increasing carbon number, this is especially evident for carbon numbers larger than 7/8.

The deviations from ideal ASF behavior are most easily explained by the occurrence of secondary reactions of olefins as discussed in section 2.5.3. There is however some debate over the extent of secondary reactions in the iron based Fischer-Tropsch synthesis. Botes (2008) argued that secondary hydrogenation and incorporation does not take place over iron-based FT catalysts, (the only exception being ethylene).

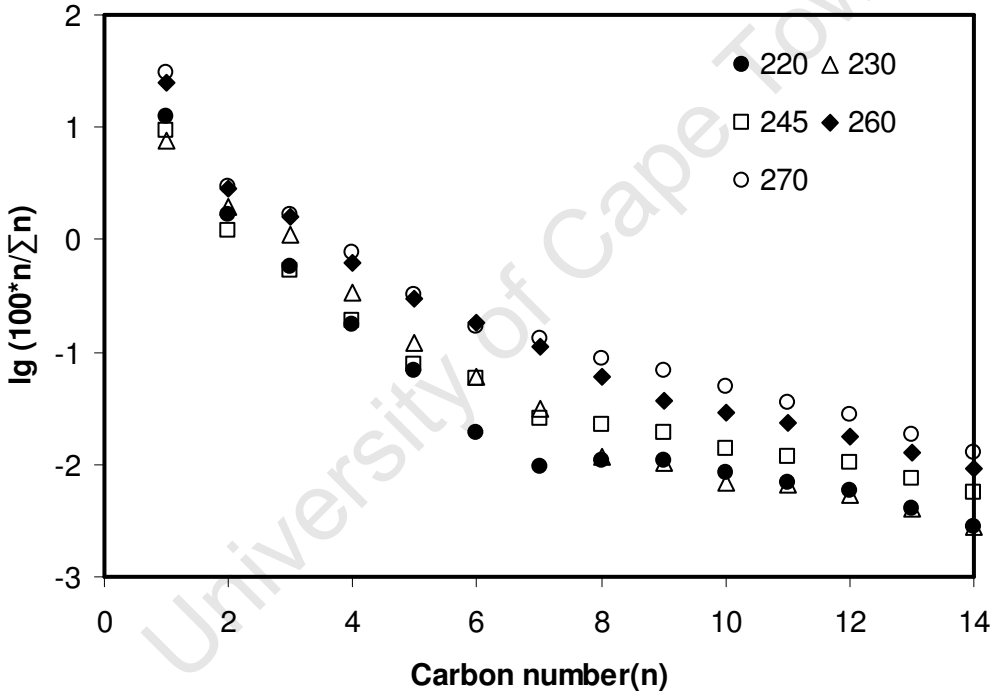

Figure 4.12 Anderson-Schulz-Flory plots (each carbon number represents the total Fischer-Tropsch product for that carbon number)

The carbon number ranges, C_3 to C_7 and C_8 to C_{14} were used to evaluate the chain growth probability as a function of the reaction temperature (see Figure 4.13). Overall the chain growth probability in the range C_8 to C_{14} decreases with increasing temperature from 0.91 at 220℃ to 0.87 at 270℃. This is in line with literature [Donnelly and Satterfield, 1989], but realistically the decrease in chain growth probability is quite small

considering the 50℃ variation in temperature. Interestingly, the chain growth probability in the range C_3 to C_7 is observed to increases from 0.63 at 220℃ to 0.75 at 270℃.

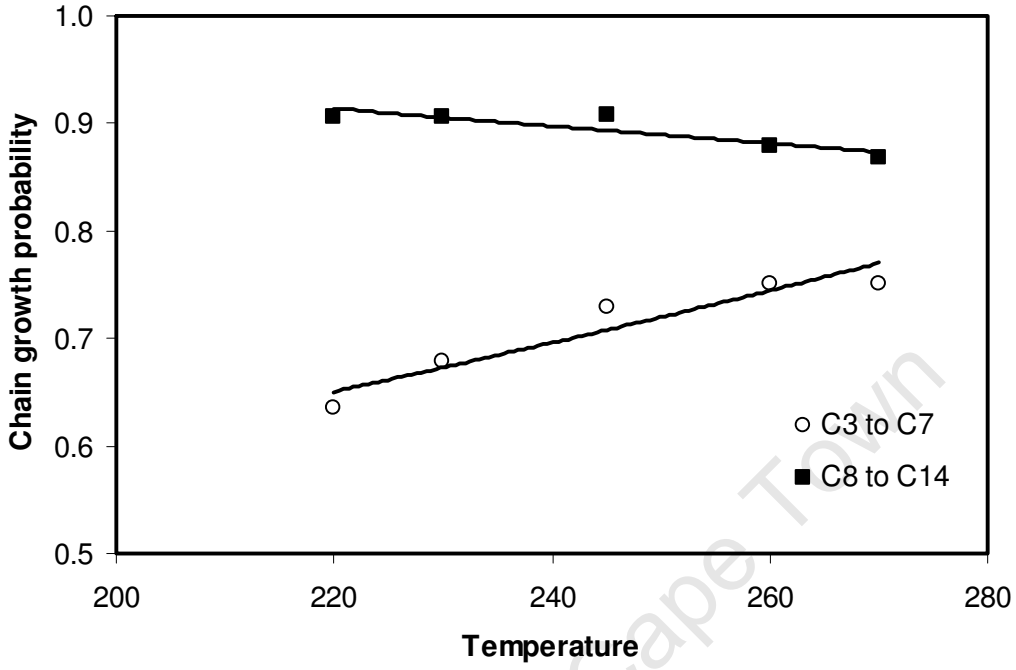

Figure 4.13 Chain growth probabilities in the range C_3 to C_7 and in the range C_8 to C_{14} as a function of reaction temperature as determined from the Anderson-Schulz-Flory distribution shown in Figure 4.12

4.5.4 Hydrocarbon selectivity

4.5.4.1 Olefin content in the fraction of linear hydrocarbons

As the initial slurry medium is composed predominantly of C_{14+} n-paraffins (Figure 4.11). The data for the Fischer-Tropsch product olefin content in the fraction of linear hydrocarbons above a chain length of C_{14} will be erroneous, giving lower olefin contents in the fraction of linear hydrocarbons. The data for C_{14+} are therefore not reported in Figure 4.14.

1-Olefins and n-paraffins are believed to be formed as primary products in the Fischer-Tropsch synthesis [Schulz and Gokcebay, 1982]. Furthermore, secondary hydrogenation of olefins to the corresponding paraffin is well known to take place over Fischer-Tropsch catalysts [Schulz *et al*. 1994]. The fraction of olefins relative to the fraction of linear hydrocarbons therefore yields valuable information regarding the extent of secondary hydrogenation of primarily formed α-olefins.

Figure 4.14 shows the linear olefin content in the fraction of linear hydrocarbons as a function of carbon number for the experiments performed at the various reaction temperatures. The linear olefin content in the fraction of linear hydrocarbons for the C_3 hydrocarbons is slightly higher, especially for the low reaction temperatures of 220 and 230°C. From C_3 onwards a carbon number dependent decrease in the linear olefin content relative to the fraction of linear hydrocarbons is observed. Schulz and Gokcebay (1982) observed the same trend and attributed it to an increase in the paraffin content via hydrogenation of the corresponding olefin.

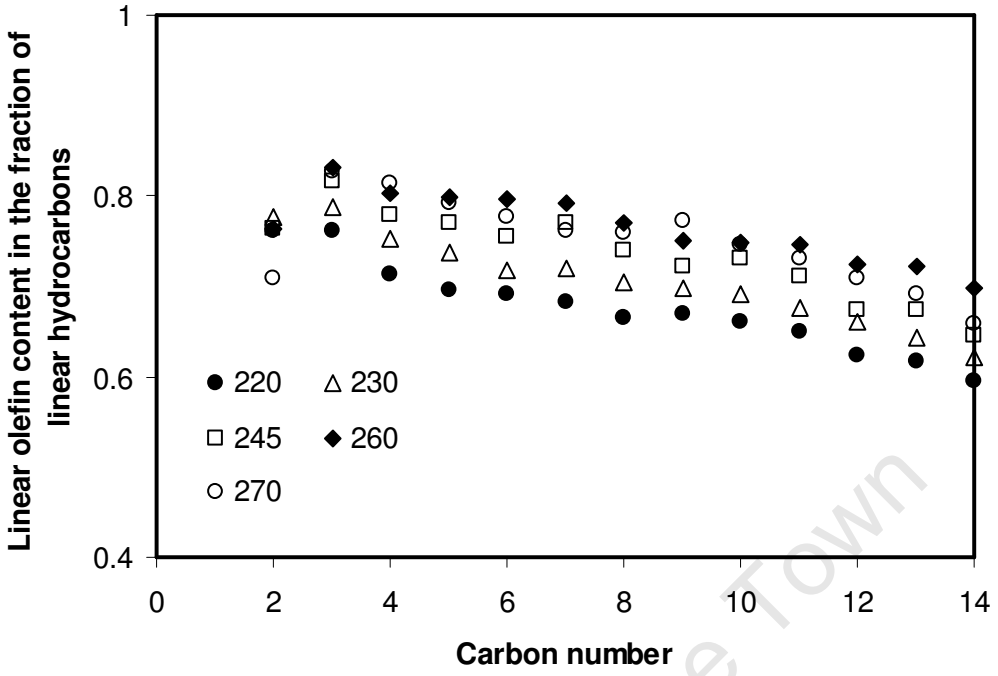

Figure 4.14 Linear olefin content (α-olefins plus linear internal olefins) in the fraction of linear hydrocarbons (linear paraffins plus linear olefins) as a function of the carbon number

Figure 4.15 shows the linear olefin content in the fraction of linear hydrocarbons for a specific carbon number as a function of the reaction temperature. The olefin content in the fraction of C_2 hydrocarbons is relatively constant over the temperature range tested, although it seems to pass a maximum with increasing temperature, whereas the olefin content in the fraction of linear C_3, C_6 and C_{10} hydrocarbons increases with increasing temperature. The slight decrease of the olefin content in the C_2 fraction for reaction temperatures higher than ca. 240°C might be attributed to the high reactivity of ethene for secondary reactions, particularly secondary hydrogenation as described by Botes (2008) and Schulz and Claeys[a,b] (1999). The observed increase in the olefin content for C_3 and higher carbon numbers might be attributed to the increase in the rate of desorption as an olefin relative to the rate of desorption as a paraffin.

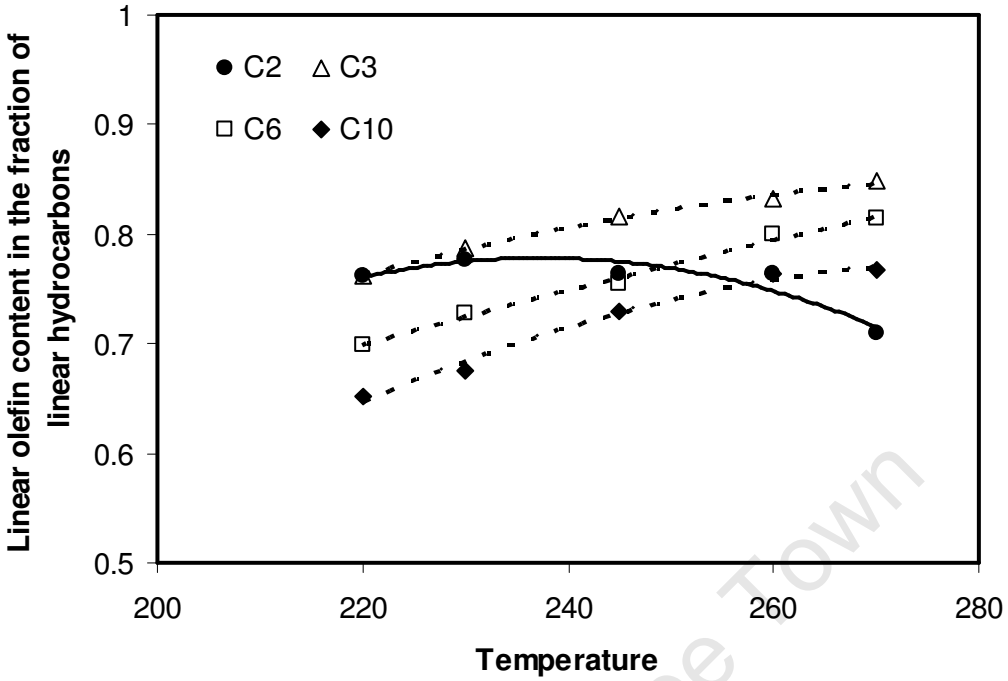

Figure 4.15 Linear olefin content (α-olefins plus linear internal olefins) in the fraction of linear hydrocarbons (linear paraffins plus linear olefins) as a function of temperature for selected carbon numbers

4.5.4.2 Olefin double bond isomerisation

Since the initial slurry medium is comprised of n-paraffins as discussed in section 4.5.3, it will not have any effect on the alpha-olefin content in the fraction of linear olefins (including the C_{14+} fraction).

Figure 4.17 shows the alpha-olefin content in the fraction of linear olefins for product compounds in the oil fraction as a function of carbon number obtained at the reaction temperatures tested. Schulz and Gokcebay (1982) considered the double bond isomers of olefins to be predominantly secondary products of the Fischer-Tropsch synthesis (see Figure 4.16). If this is the case, then the alpha-olefin content in the fraction of linear olefins is a good measure for secondary double bond isomerisation. Figure 4.17 shows that the alpha-olefin content in the fraction of linear olefins decreases with increasing

carbon number, or in other words, the degree of secondary reaction for the formation of internal olefins increases with increasing carbon number.

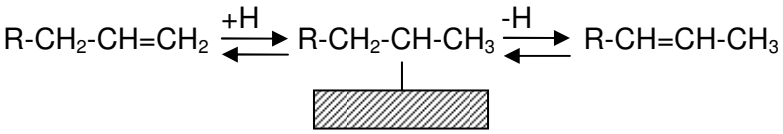

Figure 4.16 Proposed mechanism for secondary isomerisation of double bond

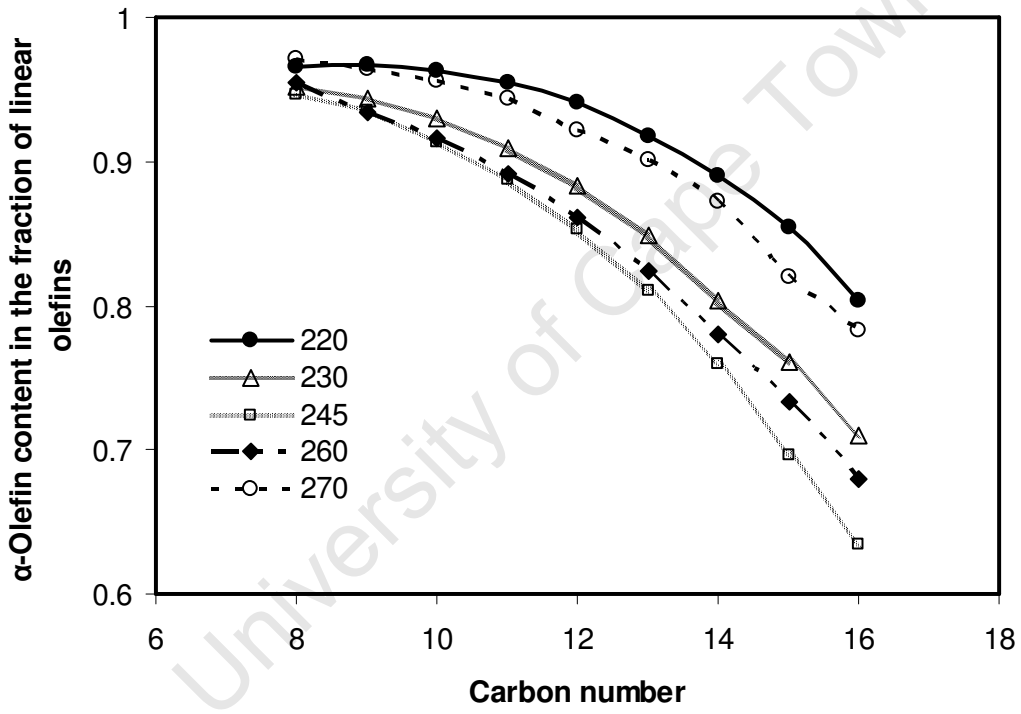

Figure 4.17 α-Olefin content in the fraction of linear olefins (comprehensive GC) as a function of carbon number

Figure 4.18 shows the α-olefin content in the fraction of linear olefins for selected carbon numbers as a function of temperature. The carbon number dependency of the α-olefin content in the fraction of linear olefins is again apparent. Furthermore, the α-olefin content goes through a minimum when plotted as a function of temperature. The α-olefin content in the fraction of linear olefins is therefore a function of temperature and carbon

number. Although the space velocity / residence time of the primarily formed olefins is varied in conjunction with the respective temperatures there is no clear evidence that the space velocity had a significant effect on the α-olefin content in the fraction of linear olefins. In experiments conducted by Schulz and Gokcebay, (1982), the α-olefin content in the fraction of linear olefins only showed a decrease at one of the four space velocities tested (the low space velocity point showing the decrease in α-olefin content). Furthermore, the experiments of Schulz and Gokcebay, (1982), showed the influence of reaction temperature on the α-olefin content to be much greater than that of space velocity over the conditions tested. Therefore, given the fact that the experiments in this thesis were conducted at low carbon monoxide to Fischer-Tropsch product conversions i.e. high space velocities, it is realistic to assume that the effect of space velocity on the α-olefin content in the fraction of linear olefins for these experiments is negligible or at least insignificant relative to the effect of temperature.

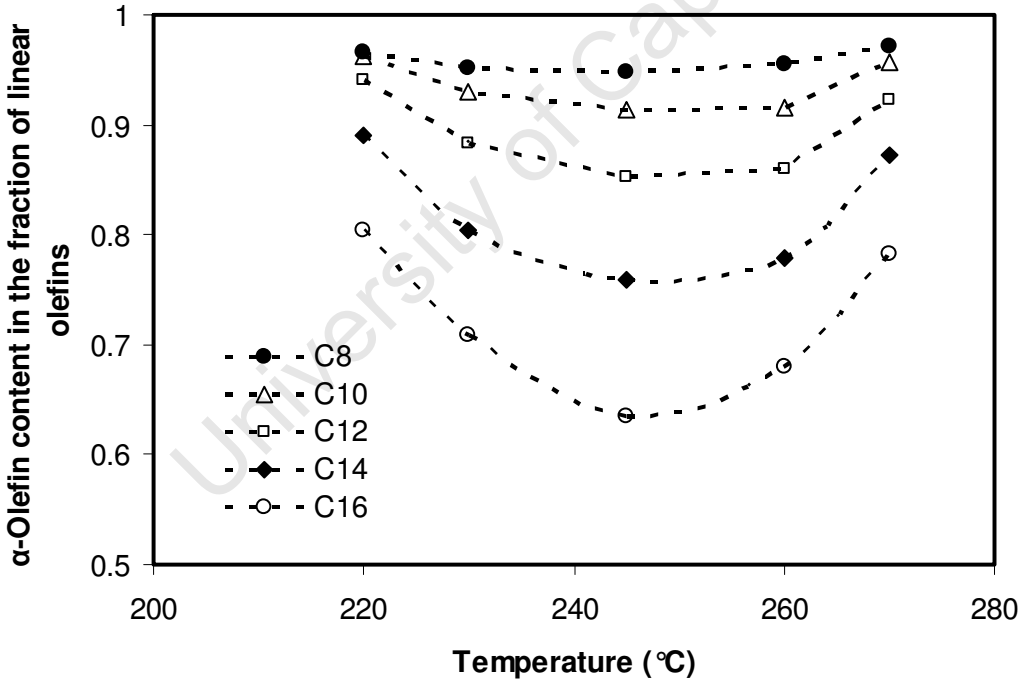

Figure 4.18 α-Olefin content in the fraction of linear olefins (comprehensive GC) as a function of temperature for selected carbon numbers

The parabolic nature of the α-olefin content in the fraction of linear olefins as a function of temperature can therefore be explained by two competing effects.

4.5.4.3 Branching

In previous studies [Shi and Davis, 2005; Schulz *et al.,* 2005], indirect methods such as hydrogenation or bromination of the FT products were used to measure the isomers of each carbon number. This is because, on normal 1-D GC some of the branched alkanes co-elute with branched alkenes and vice versa. In this study however, the branched products were directly quantified in the product oil fraction using comprehensive GC analysis as described in section 3.4 and 4.4.

Figure 4.19 shows the ratio of branched hydrocarbons relative to the total hydrocarbon product for a given carbon number. The ratio remains relatively constant in the C_7 to C_{12} range, which in is line with the findings of Anderson (1984) and Shi *et al.* (2005). Furthermore, the fraction of branched hydrocarbons relative to the total hydrocarbon product increases with increasing temperature, this effect has also been observed by Schulz and Gokcebay, (1982).

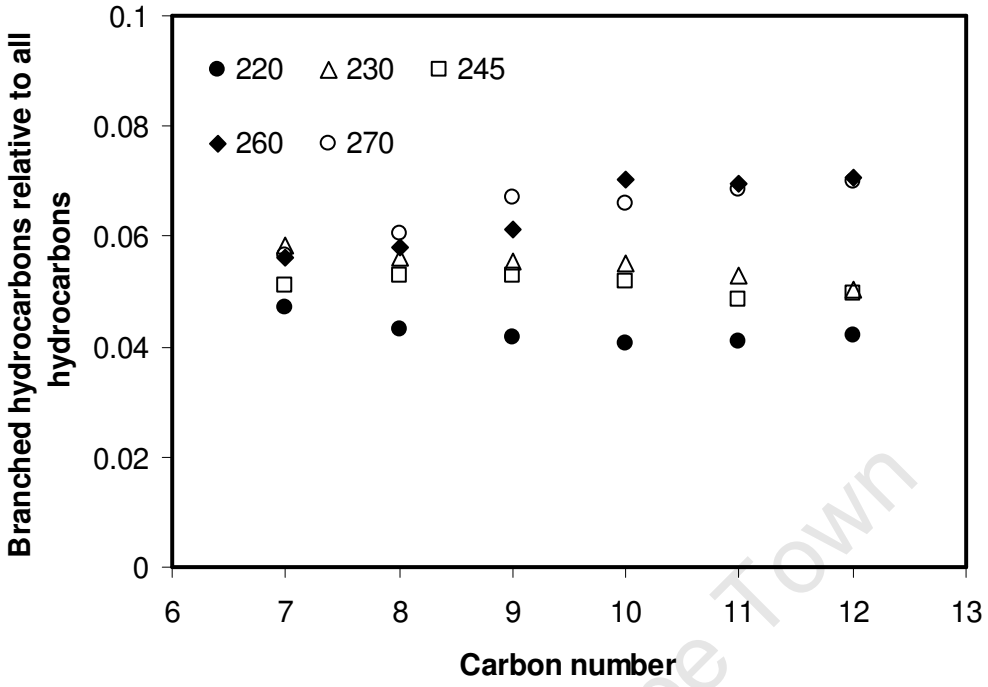

Figure 4.19 Fraction of branched hydrocarbons in the total hydrocarbon (linear plus branched) fraction, from analysis of the oil product by comprehensive GC

Figure 4.20 shows the formation of branched olefins relative to the formation of branched hydrocarbons. The fraction of branched olefins appears to increase with carbon number up to about C_9 and then decreases again. The data at 260℃ do not decrease but remain constant from C_9 to C_{12}. The effect at 260℃ may be related to the high space velocities used for this experiment. The figure therefore, indicates at least two competing effects. Furthermore, the formation of branched olefins relative to the formation of branched hydrocarbons is observed to increase with increasing temperature.

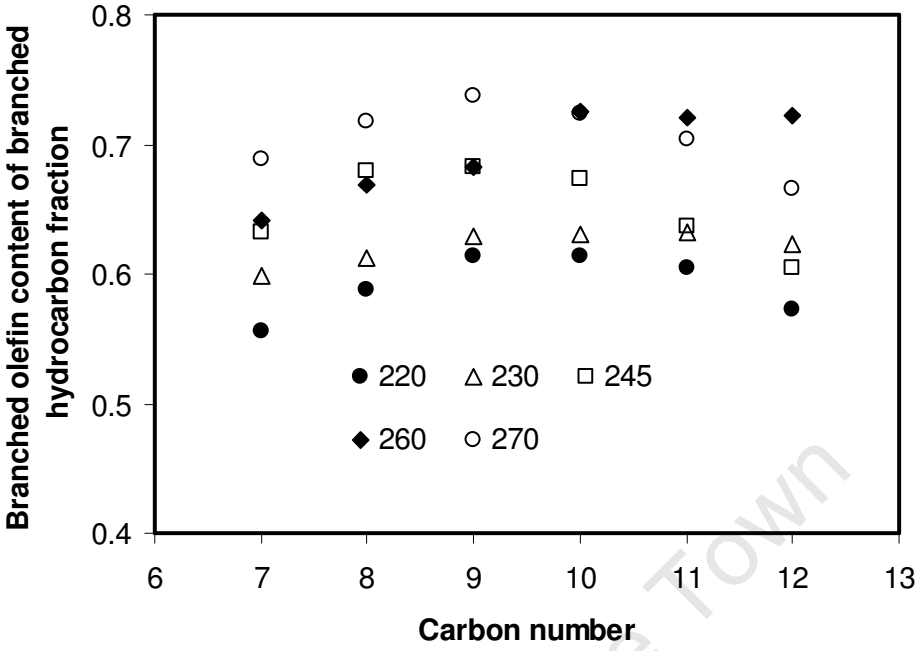

Figure 4.20 Fraction of branched olefins in the total branched hydrocarbon (branched olefin plus branched paraffin) product, from analysis of the oil product by comprehensive GC

4.5.5 Oxygenate selectivity

Oxygenates formed in the Fischer-Tropsch synthesis comprise mainly n-alcohols, carbonyls (aldehydes and ketones) and carboxylic acids (plainly referred to as acids). Other oxygenates such as secondary alcohols and esters are also formed, but in much smaller quantities. Under commercial low temperature Fischer-Tropsch conditions and with commercial iron catalyst formulations the oxygenates make up approximately 6 to 12 wt% of the total FT product with more than 80 wt% of this being n-alcohols [Dry., 2004; Claeys and van Steen, 2004].

The oxygenates seem to behave in a similar fashion as olefins and may take part in secondary reactions such as re-adsorption, hydrogenation and isomerisation [Claeys and van Steen, 2004]. Dry (2004) summarises the effects of process variables on the

formation of n-alcohols and states that their formation is favoured at low temperatures, short residence times (high GHSV) and high total pressures.

4.5.5.1 Alcohol selectivity

Figure 4.21 shows the linear alcohols in the linear hydrocarbon fraction to be low for C_1, increase for C_2 and then decrease again for C_3 to C_{12}. The values for the alcohols in the linear hydrocarbon fraction of C_3 to C_{12} are relatively constant but do show a slight decrease with increasing carbon number. These observations are in line with the observations of Schulz (1999) where the low methanol selectivity is ascribed to thermodynamically unfavorable conditions (see chapter 2, section 2.5.2, Figure 2.7), the high value for C_2 is due to the preferred reaction of OH with:

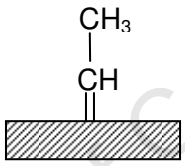

And, the values for oxygenates in the C_2+ fraction are approximated, to be independent of carbon number.

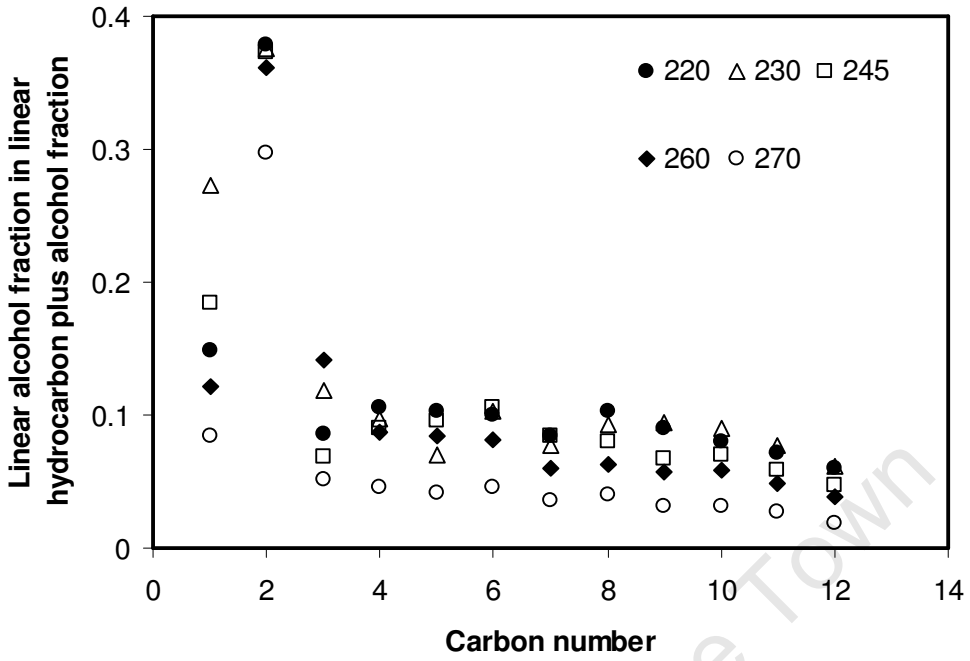

Figure 4.21 Linear alcohols in the linear hydrocarbon plus linear alcohol product as a function of carbon number

The effect of process conditions on the n-alcohol selectivity as described by Dry (2004), predict that the linear alcohols will decrease due to increasing temperature and will increase due to the decreasing residence time. The increase in reaction temperature was accompanied by a proportional increase in the space velocity in these experiments to maintain constant carbon monoxide to Fischer-Tropsch product conversions. The results of the linear alcohol selectivity as a function of reaction temperature shown in Figure 4.22 are therefore not entirely representative of the effect of temperature alone. Having said this, the effect of temperature on the linear alcohol selectivity for these experiments seem to be slightly greater that the effect of space velocity as a small decrease in the linear alcohols is still observed with increasing temperature.

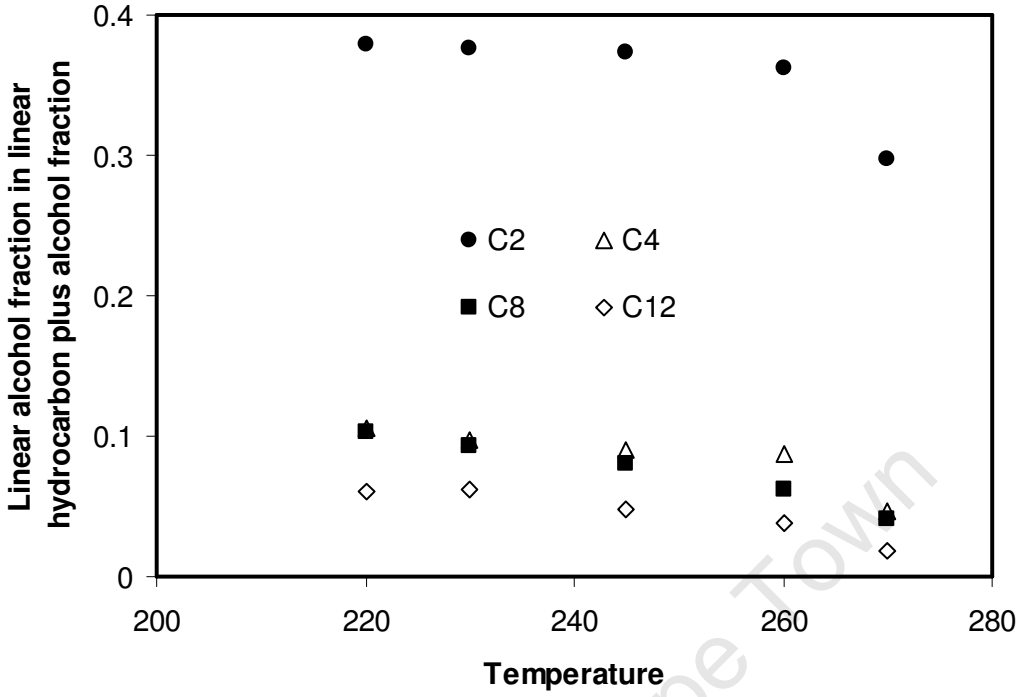

Figure 4.22 Linear alcohols in the linear hydrocarbon plus linear alcohol product as a function of temperature

4.5.5.2 Acid selectivity (water fraction)

Figure 4.23 shows the acid number of the product water fraction as a function of the reaction temperature. The acid number is a measure for the amount of acids formed in the Fischer-Tropsch synthesis, which are predominantly found in the water phase. The acid number of the water fraction decreases with increasing temperature. This implies that with increasing reaction temperature the formation of acids in the Fischer-Tropsch synthesis is reduced.

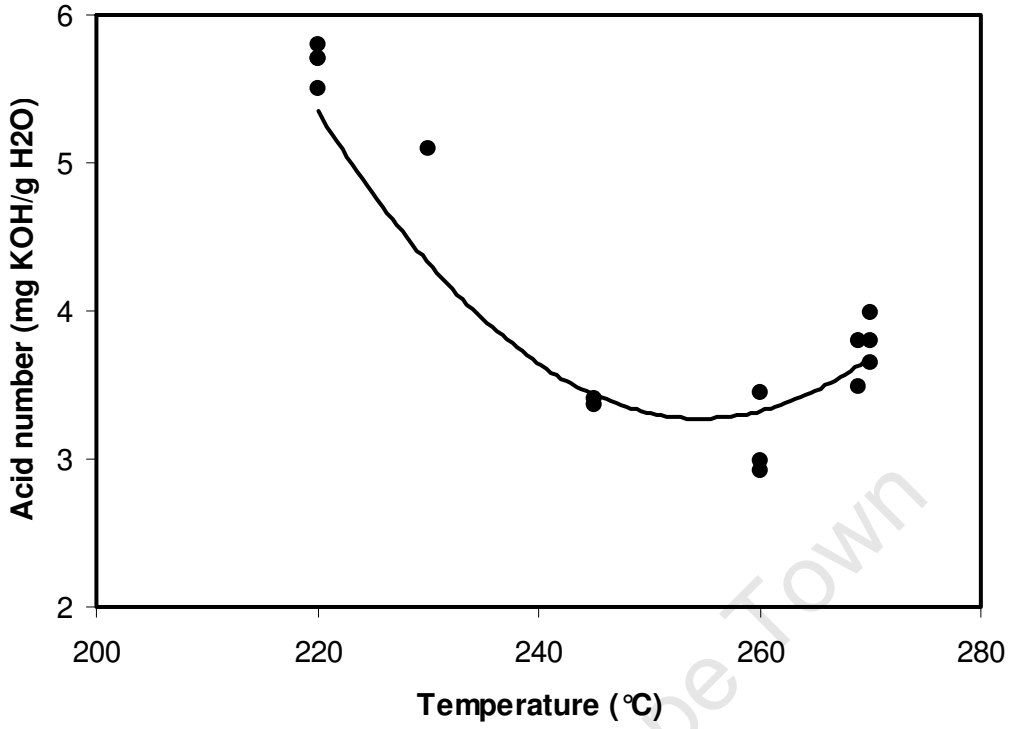

Figure 4.23 Acid number of the product water fraction as a function of temperature (mg KOH/g H_2O)

4.5.6 Cyclic olefin and aromatic selectivity in the oil fraction

It is generally assumed that cyclic compounds and aromatics are not formed in the low temperature Fischer-Tropsch (LTFT) synthesis. This is a valid approximation since in most cases the cyclic olefins together with the aromatics account for less than 1% of the total Fischer-Tropsch product. The formation of minor components such as the cyclic and aromatic compounds are however of mechanistic interest as they can give insight into the active sites and intermediates for the formation of the major components. Furthermore, as fuel specifications around the world become increasingly stringent it is crucial that Fischer-Tropsch processes are designed with a sound knowledge of selectivity including the selectivity of minor products such as aromatics.

4.5.6.1 Cyclic olefins

Figure 4.24 shows the cyclic olefin content in the linear hydrocarbon fraction as a function of carbon number. With increasing carbon number the amount of cyclic olefins decreases (except for the data at 260℃ which is most likely due to the high space velocities at this point). It is also known that the thermodynamic stability of cyclic olefins decreases with increasing carbon number.

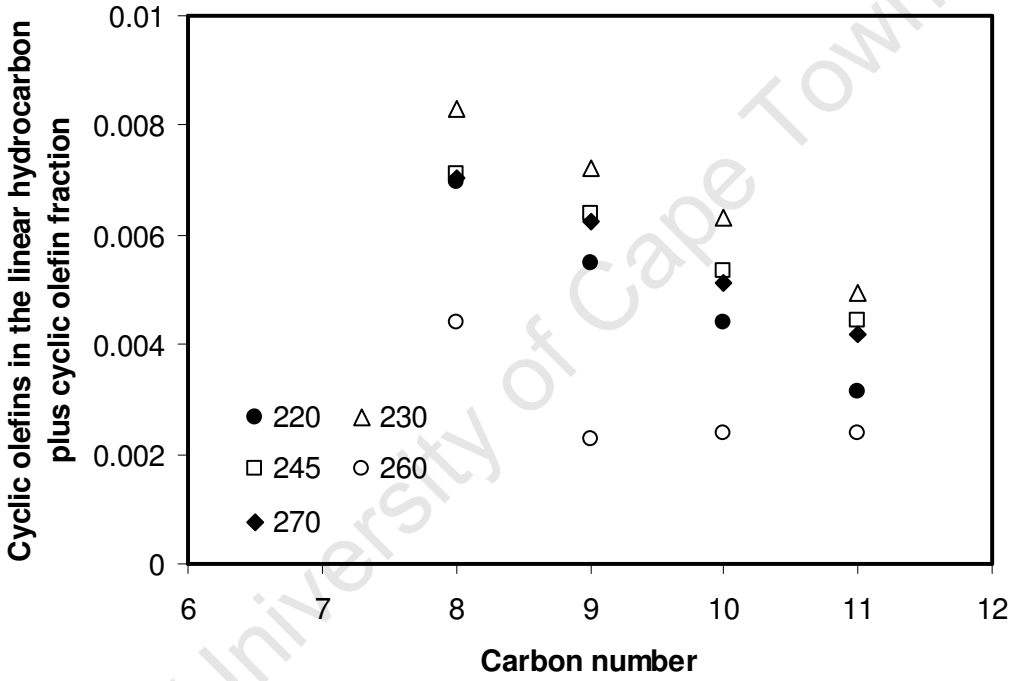

Figure 4.24 Cyclic olefins in the linear hydrocarbon plus cyclic olefin fraction as a function of carbon number

Figure 4.25 shows almost no effect of temperature on the cyclic olefin selectivity in the linear hydrocarbon fraction, the data at 260℃ being the exception. As in figure 4.24 above, the lower cyclic olefin selectivity in the linear hydrocarbon fraction might be due to the high space velocity for the point at 260℃. If so, this suggests that the cyclic olefins in the linear hydrocarbon fraction increase with increasing temperature but

decrease with increasing space velocity. Furthermore, the decrease in selectivity at high space velocity indicates that cyclic olefins may be formed via a secondary reaction.

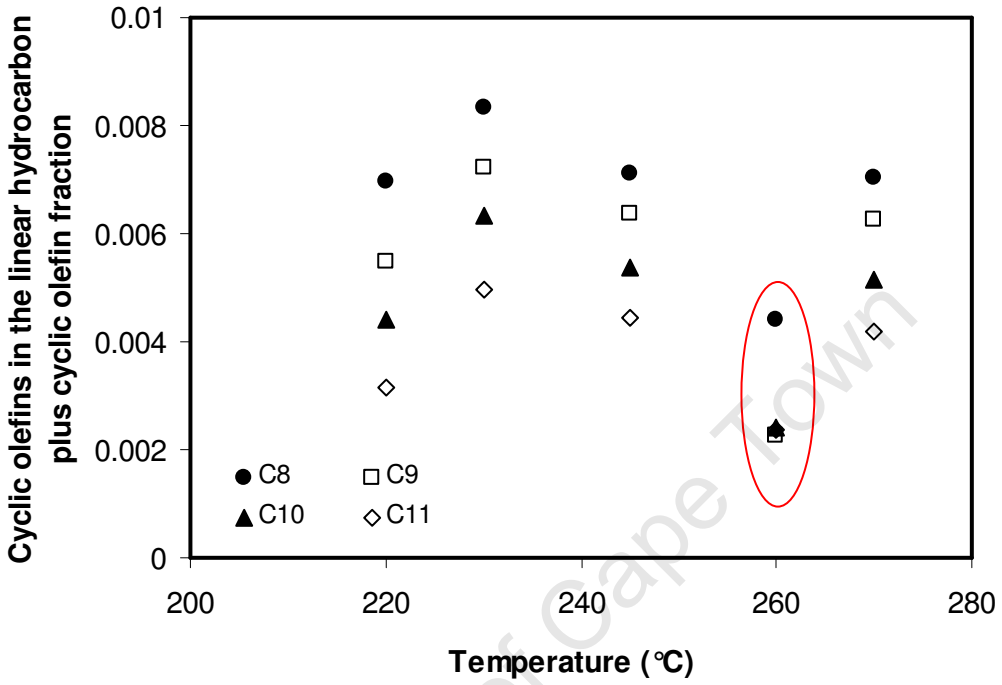

Figure 4.25 Cyclic olefins in the linear hydrocarbon plus cyclic olefin fraction as a function of temperature

4.5.6.2 Aromatics

Figure 4.26 shows the aromatics content as a function of carbon number and Figure 4.27 as a function of temperature. The aromatic content increases with increasing carbon number. The selectivity data at 245°C is far higher than for the other carbon numbers. This is especially apparent in Figure 4.27 but no explanation can be given at this point since there seems to be scatter in the data. If however the data for 245°C was lower, then a similar tend as in Figure 4.18 is observed i.e. a parabola shape indicating two competing effects each of which are conversely affected by temperature.

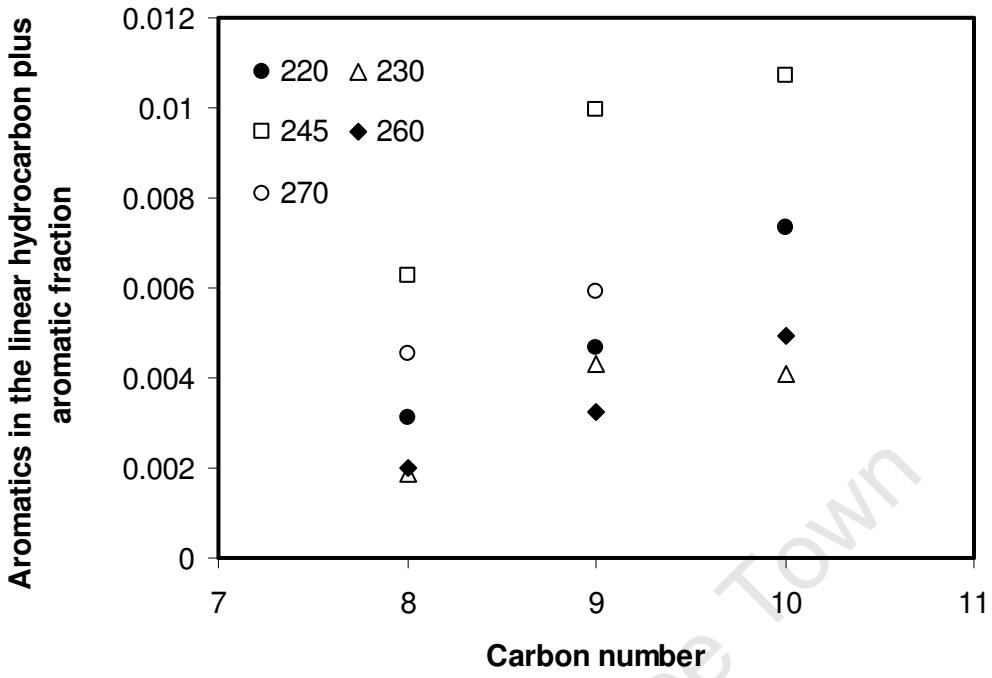

Figure 4.26 Aromatics in the linear hydrocarbon plus aromatic fraction as a function of carbon number

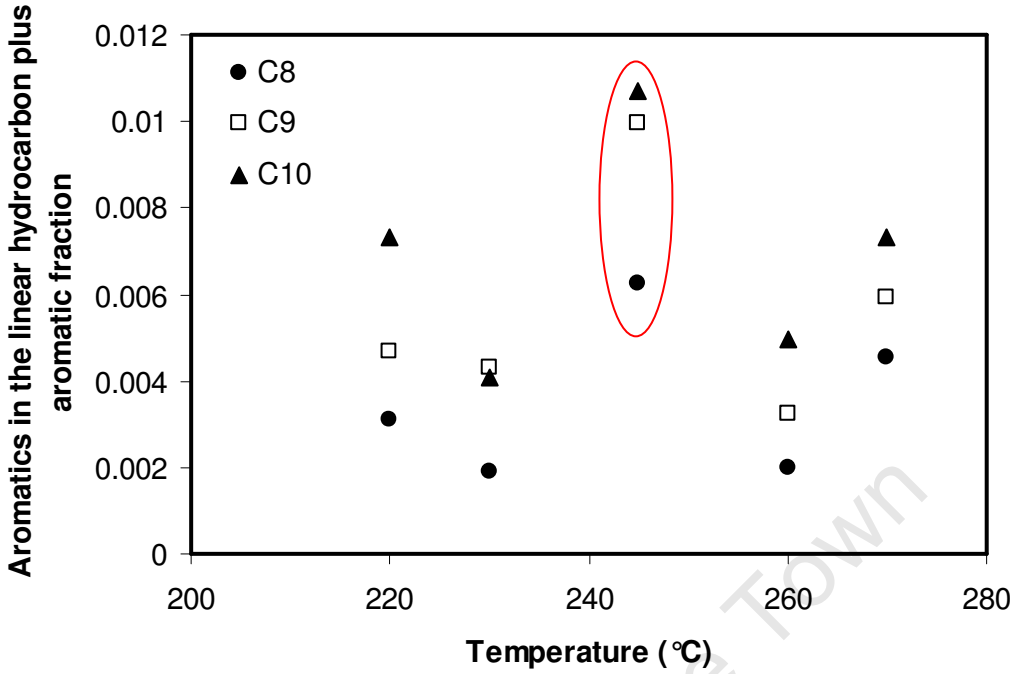

Figure 4.27 Aromatics in the linear hydrocarbon plus aromatic fraction as a function of temperature

Chapter 5

Discussion

5.1 Mass transfer limitations

Since the main aim of this thesis is to determine the catalyst activity and product selectivity as a function of reactor temperature while keeping the reactor partial pressures constant, it is especially important to determine the extent of diffusion limitations, if any, as this may impact on the discussions to follow.

The effect of stirrer speed on the activity at 260°C was investigated (see Figure 4.1 and section 4.1.1). It was concluded that the stirrer speed of 500 rpm was sufficiently high to eliminate external mass transfer limitations in the experiments.

Since only one catalyst particle diameter was utilised, the likelihood for internal mass transport limitations was investigated using the Weisz-Prater correlation. The Weisz-Prater correlation yielded a value of C_{wp} up to 1.2 at 270°C. Fogler (1999), states that severe mass transport limitations only occur at values of C_{wp} much larger than 1. Consequently it is not clear at this stage to what extent mass transport limitations may have occurred within the catalyst particles, especially in the experiments performed at the higher reaction temperatures.

For this reason the effectiveness factor (η_{FT}) and Thiele modulus (M_T) are estimated for all temperatures / experiments below. In this approach, the kinetics of the Fischer-Tropsch synthesis was approximated using equation 2.24 where the equation is simplified to pseudo-first order in CO (appendix A).

5.1.1 Calculation of the Thiele modulus and effectiveness factor

It is well known that the occurrence of internal mass transport limitations results in reduced reaction rates and shifts with regard to product selectivity [Steynberg *et al*[b]., 2004]. This is because severe internal mass transport limitations will lead to large temperature and concentration gradients within the catalyst particle.

The estimated effectiveness factor (Figure 5.1) varies from approximately 0.983 at 220°C to 0.955 at 270°C assuming the catalyst only contains particles with a radius of 95μm [Malherbe, 2006]. This means that for the case of highest internal mass transport limitations i.e. at a temperature of 270°C, the rate differs by less than 5% from that obtained with the partial pressure of CO on the outside of the catalyst particle. The effect of internal mass transport limitations on activity and selectivity are therefore considered to be negligible over the temperature range of the experiments. Consequently, the kinetic and selectivity measurements are not notably influenced by mass transfer limitations.

Using values for the parameters given in appendix A, the Thiele modulus was calculated to vary from 0.23 to 0.38 over the temperature range of this study (Figure 5.2). As a side note, the low values of the Thiele modulus indicate that a large amount of promoter can be added to this catalyst without adversely affecting its performance.

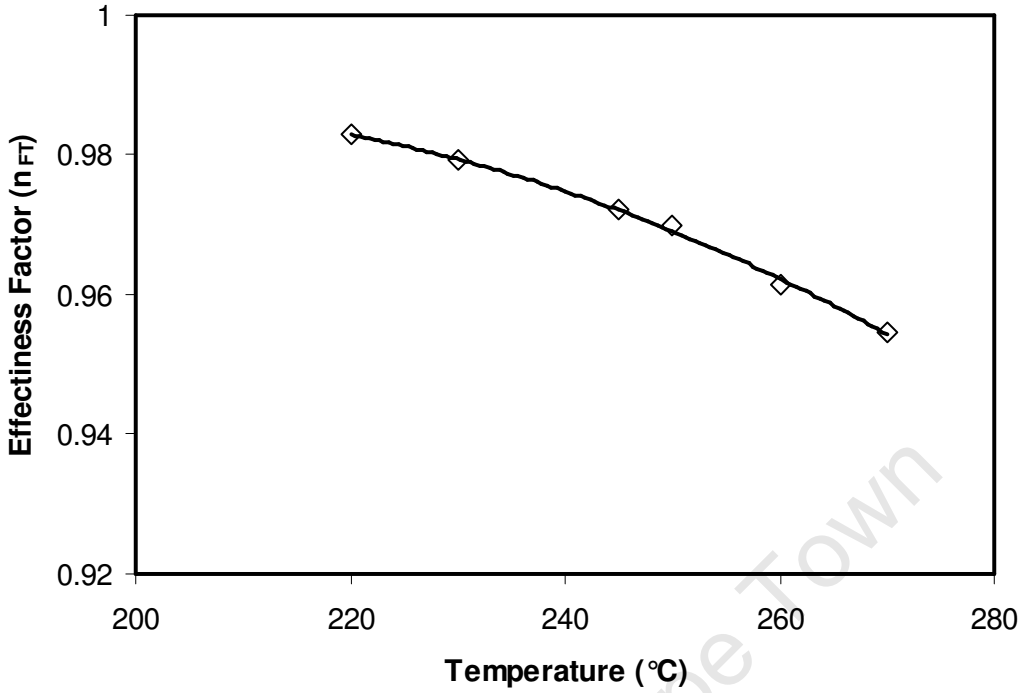

Figure 5.1 Effectiveness factor (η_{FT}) as a function of temperature

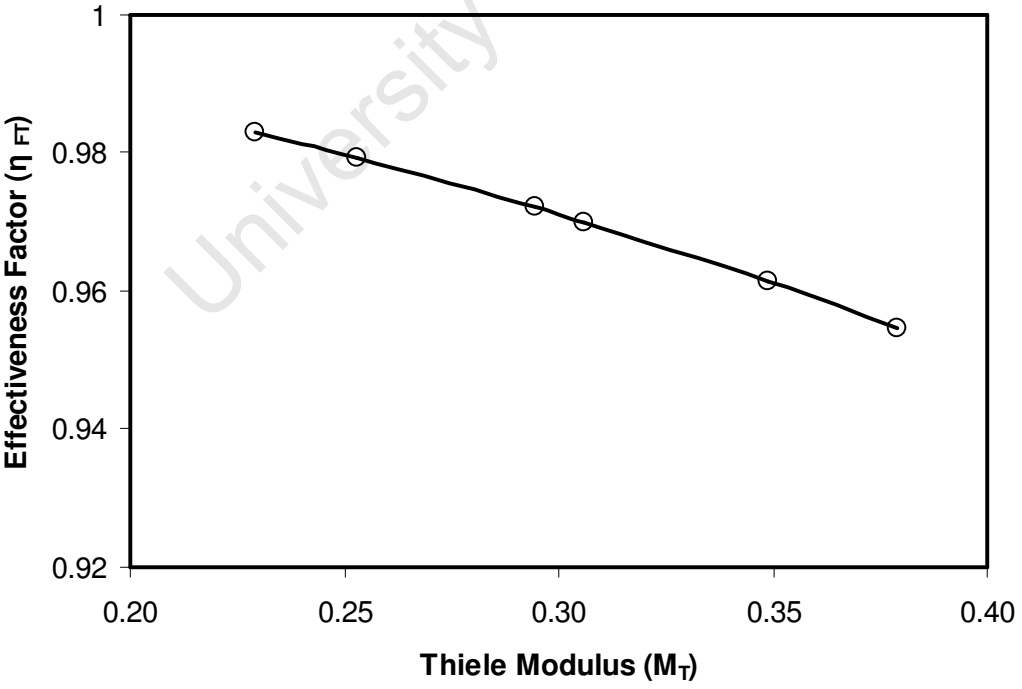

Figure 5.2 Effectiveness factor (η_{FT}) as a function of Thiele modulus (M_T)

5.2 Calculation of activation energy and pre-exponential factor

Given that the effect of mass transfer limitations have been shown to be insignificant over the range of temperatures tested, the activation energy for the Fischer-Tropsch and water-gas shift reactions can be estimated with confidence.

In this thesis the temperature dependence of the rate constant will be evaluated using the Arrhenius equation.

$$A(T) = A^{\circ} e^{\frac{-E_a}{RT(K)}} \tag{5.1}$$

where:

A^o = Pre-exponential factor

R = Universal gas constant

T= Temperature (K)

Since the partial pressures of the kinetically relevant components at each temperature were kept relatively constant, the activation energy for the Fischer-Tropsch and water-gas shift reactions could be obtained directly by applying the linearised form of the Arrhenius equation utilising the rate of reaction:

$$\ln A(T) = \ln A^{\circ} - \frac{E_a}{R} \bullet \frac{1}{T(K)} \tag{5.2}$$

Assuming that:

$$\ln r_{FT,measured} \approx \ln A(T) \tag{5.3}$$

For the general case where the reaction rate can be given by:

$$r_{FT} = A \bullet f(P_i) \tag{5.4}$$

Where

P_i = partial pressure of component i, (bar)

Substituting equation (1) for A

$$r_{FT} = A^{\circ} e^{\frac{-E_a}{RT(K)}} \bullet f(P_i) \tag{5.5}$$

A° and E_a can now be solved by minimisation of:

$$Sqdiff = \frac{\left(r_{FT,measured} - r_{FT,predicted}\right)^2}{r_{FT,measured}} \tag{5.6}$$

When fitting the activation energy and pre-exponential factor by non-linear regression the following re-parameterisation [Anil and Brisk, 1985] is used to reduce the computational difficulties arising from the covariance between the pre-exponential factor and the activation energy:

$$A^{\circ} e^{\frac{-E_a}{RT(K)}} = A^{\circ} e^{\frac{-E_a}{R}\left(\frac{1}{T(K)} - \frac{1}{T^{Ave}(K)}\right)} \tag{5.7}$$

5.2.1 Fischer-Tropsch reaction

To obtain the activation energy and the pre-exponential factor for the Fischer-Tropsch reaction, the rate equation developed by Botes (2008) will be solved by non-linear regression.

$$r_{FT} = A^{\circ} e^{\frac{-E_a}{R}\left(\frac{1}{T(K)} - \frac{1}{T^{Ave}(K)}\right)} \bullet \frac{P_{H_2}^{0.5} P_{CO}}{\left(1 + k_{CO} P_{CO}\right)^2} \tag{5.8}$$

Where

T^{AVE} = Average temperature of experiments (K)

The accuracy of the fitted model relative to the experimental data was obtained from the MARR (mean absolute relative residual) function [van der Laan and Beenackers, 1999]:

$$MARR = \sum_{i}^{n} \left| \frac{m_i^{\exp} - m_i^{\mathrm{mod}}}{m_i^{\exp}} \right| \bullet \frac{1}{n} \bullet 100 \tag{5.9}$$

Even though the fitted value for the activation energy indicated in Table 5.1 is low compared to the majority of published values [Dry *et al.*, 1972, Huff and Satterfield, 1984], it is highly unlikely that this is due to mass transport limitations as discussed above.

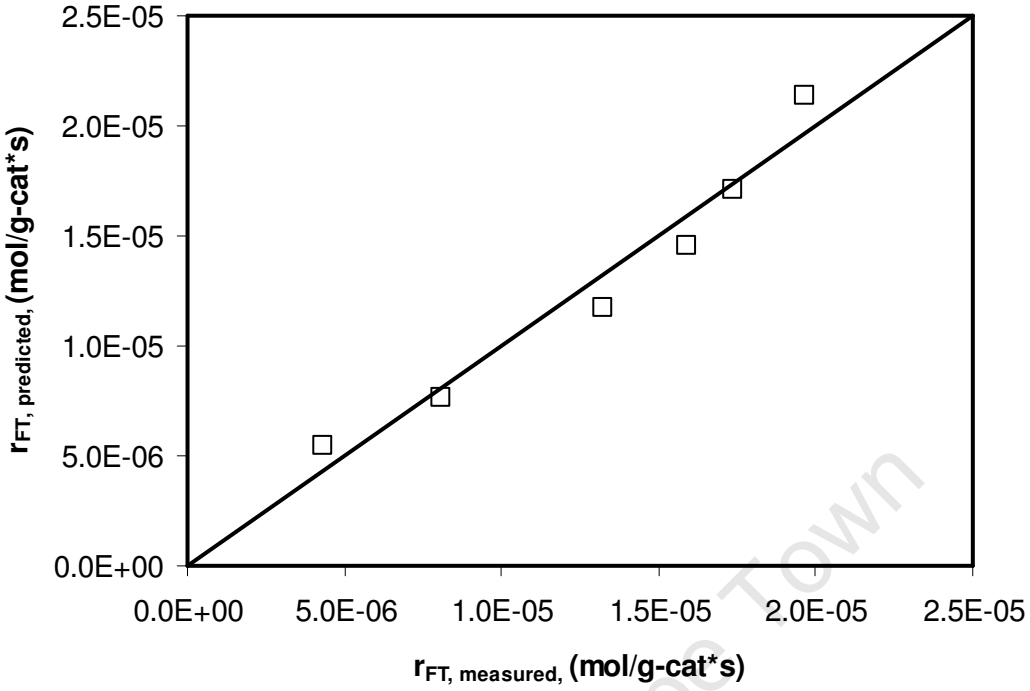

Figure 5.3 Parity plot for the predicted Fischer-Tropsch reaction rate [Botes, 2008] vs. the measured Fischer-Tropsch reaction rate

Applying the same methods as above, the activation energy and pre-exponential factors can be calculated using various other rate equations. Below are the van Steen and Anderson-Dry rate equations, respectively.

$$r_{c,org} = A\frac{\dfrac{P_{H_2}^{3/2}P_{CO}}{P_{H_2O}}}{\left(1+k\dfrac{P_{H_2}P_{CO}}{P_{H_2O}}\right)^2} \tag{5.10}$$

$$r_{FT} = A\frac{P_{CO}P_{H_2}}{P_{CO}+k_{H_2O}P_{H_2O}} \tag{5.11}$$

The adsorption coefficients (k_{CO}, k and k_{H2O}) in the rate equations are also temperature dependent and as such, should be fitted together with the pre-exponential factor and

activation energy. There is however a strong degree of covariance between the pre-exponential factors and the adsorption constants. It is therefore not possible to decouple these kinetic parameters given the experimental data of this thesis. For the purposes of this thesis, the adsorption coefficients are assumed to remain constant over the temperature range 220 to 270°C. In order to obtain the influence of temperature on the adsorption constants an additional study will be required.

Table 5.1 Results for fitting activation energy and pre-exponential factor of the Fischer-Tropsch reaction (adsorption coefficients are assumed to remain constant over the temperature range 220 to 270°C)

FT rate equation fitted:	Adsorption coefficient	Activation energy (Ea - kJ/mol)	Pre-exponential factor (A°)	MARR (%)
Botes-FT (2008)	k_{CO} = 0.1	63.5	4.22	10.5
van Steen *et al.* (1999)	k=0.02	62.5	0.60	11.1
Anderson-Dry (1976)	k_{H2O} = 3.5	66.0	9.45	9.8

5.2.2 Water-gas shift reaction

Following the same approach as for the Fischer-Tropsch reaction, the activation energy and the pre-exponential factor for the water-gas shift reaction are fitted. The rate equation for the water-gas shift reaction developed by Botes (2008) is utilised, where the adsorption coefficients (k_{OH} and k_{H2O}) are assumed to be constant over the temperature range 220 to 270°C. The temperature dependence of the equilibrium constant, (K_{WGS}) is however accounted for.

$$r_{WGS} = A^{\circ} e^{\frac{-E_a}{R}\left(\frac{1}{T(K)}-\frac{1}{T^{Ave}(K)}\right)} \bullet \frac{P_{CO}P_{H_2O} - \frac{1}{K_{WGS}} P_{H_2}P_{CO_2}}{\left(1 + k_{H_2O}P_{H_2O} + k_{OH}\frac{P_{H_2O}}{P_{H_2}^{0.5}}\right)^2} \qquad (5.12)$$

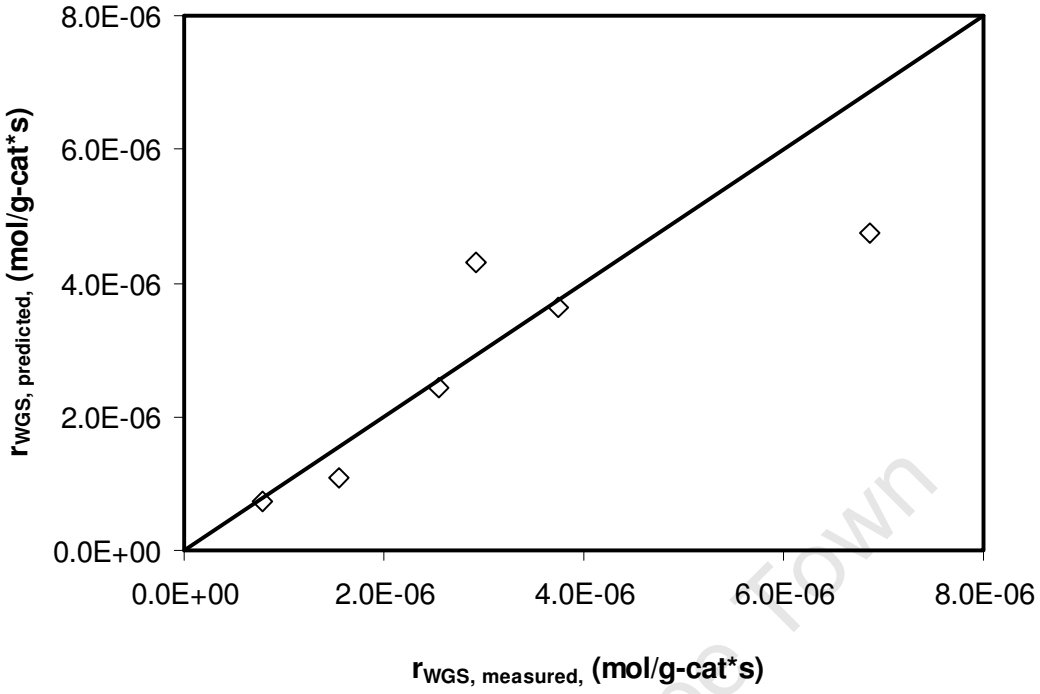

Figure 5.4 Parity plot for the predicted water-gas shift reaction rate (Botes 2008) vs. the measured water-gas shift reaction rate.

Since the water-gas shift reaction is far from equilibrium (see section 4.5.1, table 4.3) and the influence of the water partial pressure on the water-gas shift reaction rate is relatively constant for the data of this thesis (Table 5.2), a simple rate equation (first order in carbon monoxide) can also be applied to describe the water-gas shift reaction rate for this data.

$$r_{WGS} = A^{\circ} e^{\frac{-E_a}{R}\left(\frac{1}{T(K)} - \frac{1}{T^{Ave}(K)}\right)} \bullet P_{CO} \qquad (5.13)$$

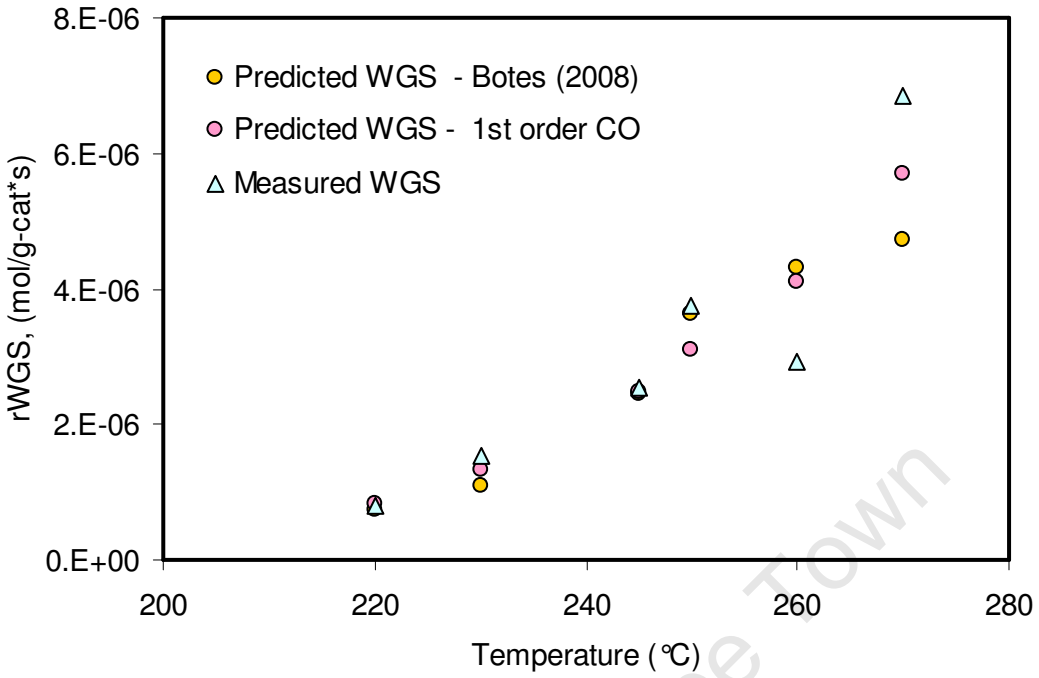

Figure 5.5 Predicted and measured reaction rates for the water-gas shift reaction as a function of temperature

Table 5.2 Results for fitting activation energy and pre-exponential factor of the water-gas shift reaction (adsorption coefficients are assumed to remain constant over the temperature range 220 to 270°C)

WGS rate equation fitted:	Adsorption coefficients	Activation energy (Ea - kJ/mol)	Pre-exponential factor (A°)	MARR (%)
Botes-WGS (2008)	k_{H2O} = 1.1 k_{OH} = 6.3	94	1.08E-05	20.2

The MARR value for equation 12 is quite high. This indicates that the kinetic model has difficulty in predicting the experimental data, especially at conditions of high temperature and space velocity.

5.3 Comprehensive Gas Chromatography: analysis of the Fischer – Tropsch product.

Due to the large number of components formed in the Fischer - Tropsch synthesis (i.e. components with different functional groups, carbon numbers and isomers), together with the large range in their respective concentrations (10 to 0.01 mass %). It becomes impossible to directly and accurately quantify all component concentrations with standard 1-dimensional gas chromatography. Presently, when investigating the minor component selectivity of each carbon number for the FT synthesis, methods such as hydrogenation or bromination of the products is used [Shi *et al.*, 2005 and Schulz *et al.* 2005]. These methods have proven to work well but are extremely time intensive and therefore limited to the number of components that can be quantified in an experimental program. On the other hand, comprehensive gas chromatography can analyse the full FT product spectrum in approximately the same time as normal 1-D-GC analysis. Comprehensive GC analysis therefore has the potential to be applied as a routine analytical method in the further study of the Fischer-Tropsch product spectrum.

One-dimensional gas chromatography was compared to comprehensive gas chromatography in chapter 4, (Figures 4.6 and 4.7). There were two main differences, namely: higher selectivity for the comprehensive GC than for the 1-D-GC in the “lighter” carbon number fraction (C_5 to C_9 for 1-olefins and n-paraffin) and a lower selectivity for the comprehensive GC than for the 1-D-GC in the “higher” carbon number fraction (C_{10} to C_{20} for 1-olefins and n-paraffins). The reasons for these differences i.e. better resolution of peaks (more sample per second) and co-elution of compounds was briefly discussed in chapter 4 and will be discussed further at this point.

The observed “higher” selectivity for the comprehensive GC compared to the 1-D-GC in the light carbon number fraction at first appears to be an overestimation of the peak areas of the comprehensive GC, but as aluded to earlier this is actually due to the higher peak resolutions obtained with comprehensive GC analysis i.e. a larger number of data points per peak as compared to the 1-D-GC. Proper peak quantification requires a minimum number of data points per peak. For example, at a data-sampling rate of 10 Hertz, or 10 data points per second, peaks of less than one second wide will have less than 10 data points and therefore may not be quantified accurately. In the case of

samples containing very low concentrations, as in the FT synthesis, some compounds might not be detected. Figure 5.5 below illustrates this concept and importantly shows that when direct comparisons are made between the same components / sample, the components analysed with the higher sampling rate can result in a higher and more correct value for the area counts.

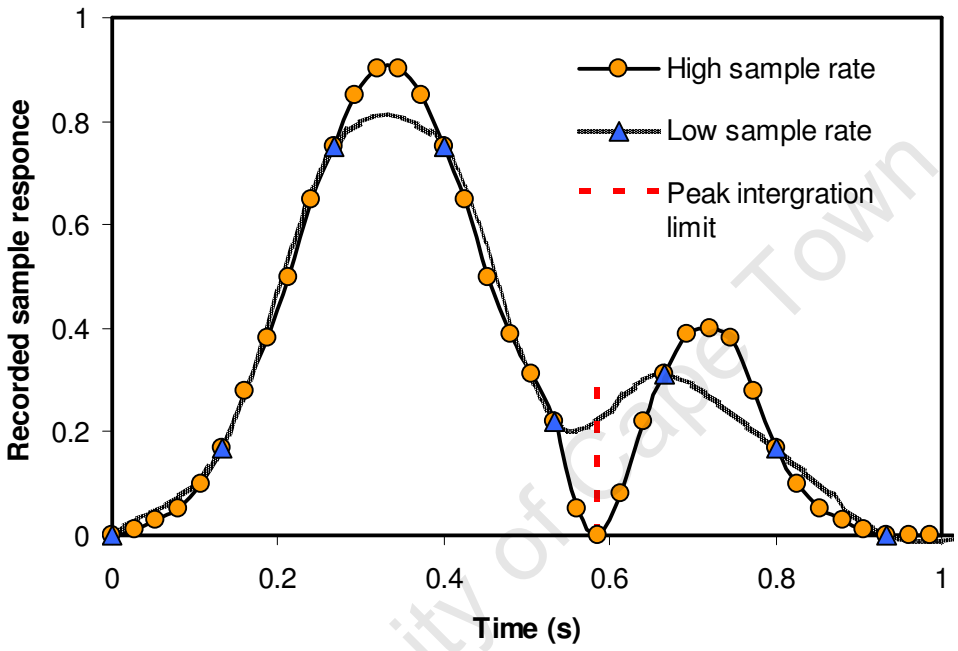

Figure 5.5 Example to illustrate effect of data sampling rate on the value for the area count

Secondly, the observed lower selectivity for the comprehensive GC as compared to the 1-D-GC in the high carbon number fraction can be ascribed to the orthogonal separation of the comprehensive GC. This combined with the increased peak resolution leads to the observed lower selectivity's.

5.4 Modelling the Fischer-Tropsch product spectrum

As discussed in section 5.3 above, the Fischer-Tropsch synthesis leads to a large number of products. It is therefore not feasible to describe the selectivity towards each component separately. Fortunately however, there is a high degree of ordered multiplicity in the different carbon number fractions [Schulz *et al*., 1988], i.e. the Fischer-Tropsch synthesis can be viewed as a polymerisation-type of reaction whereby organic molecules are formed by the stepwise addition of a C_1 monomer species. This high degree of order in the Fischer-Tropsch product is well suited for selectivity modeling [Claeys and van Steen, 2004].

The chain growth probability (p_g) is an example of a parameter, which can be used to characterize the Fischer-Tropsch product spectrum. As discussed in chapter 2 section 2.6.1, if the chain growth probability is independent of the chain length/carbon number the Anderson-Schulz-Flory distribution is obtained.

$$x_N = (1 - p_g) \bullet p_g{}^{n-1} \qquad (5.14)$$

Experimentally observed Fischer-Tropsch product spectra are however known to deviate from the ideal Anderson-Schulz-Flory distribution. The most prominent deviations being: higher than expected molar methane content, lower than expected molar C_2 content, increase in the chain growth probability with increasing carbon number and chain length dependent olefin content, decreasing with increasing carbon number.

Many product characterization models to describe these trends have already been proposed in the literature. Botes (2008) grouped these models into two main sets i.e. double-α and olefin reincorporation models, which he reviews in detail in his thesis.
Chain length dependent desorption model

This model, proposed by Botes (2008) is based on the assumption that the rates of chain growth and hydrogenation are independent of chain length, but that the rate of desorption is a function of carbon number. This assumption can be elucidated from the viewpoint that chain growth and hydrogenation only occur at the active endpoint of the

intermediate, thus the length of the chain connected to the active endpoint has very little or in this case, no influence on either of these reactions. On the other hand, the entire chain connected to the active endpoint may well have an interaction with the catalyst surface. Therefore, the longer the chain, the greater the interaction it will have with the catalyst surface and hence, the longer its residence time will be. This "physisorption" type of effect can explain both the increasing chain growth probability and the decreasing olefin to paraffin ratio with increasing carbon number (C#).

In his thesis, Botes (2008) devotes three entire sections to the mathematical formulation of this model, the application of this model and the fitting of this model, respectively. For this reason the essential elements are summarized here.

Based on the assumptions above, the rate of growth, hydrogenation and desorption can be represented as:

$$r_g = k_g \left[C_n^*\right] \tag{5.15}$$

$$r_h = k_h \left[C_n^*\right] \tag{5.16}$$

And

$$r_d = k_d \left[C_n^*\right] \bullet f(C\#) \tag{5.17}$$

It is known that the enthalpy of adsorption of hydrocarbons on solid surfaces increases linearly with increasing carbon number [van der Laan and Beenackers, 1999]. By analogy, Botes (2008) suggests that there would be a linear relationship between the energy required for desorption and the carbon number of the intermediate. Furthermore, if the energy of desorption is taken as the activation energy of the desorption step, it can be incorporated as an Arrhenius term.

$$r_d = k_d \left[C_n^*\right] \bullet e^{-\frac{Ed}{RT}} \tag{5.18}$$

where:

$Ed = k'\,n$

$\left[C_n^*\right]$ = surface concentration of the growing intermediate

K = k'/RT

Since hydrogenation and desorption are both growth termination steps, the chain growth probability (Pg) or alpha (α_n) as a function of carbon number can be calculated as follows:

$$\alpha_n = \frac{k_g}{k_g + k_h + k_d \bullet e^{-Kn}} \tag{5.19}$$

Botes (2008) defines two parameters, T_P which relates the competition between hydrogenation to form a paraffin vs. further chain growth, and T_O which relates the competition between desorption to form an olefin vs. further chain growth.

$$T_P = \frac{k_h}{k_g} \tag{5.20}$$

$$T_O = \frac{k_d}{k_g} \tag{5.21}$$

Via some re-arrangement and substitution of equations 18, 19 and 20 the following equation for the chain growth probability and olefin to paraffin ratio results:

$$\alpha_n = \frac{1}{1 + T_P + T_O \bullet e^{-Kn}} \tag{5.22}$$

$$(O/P)_n = \frac{T_O}{T_P} \bullet e^{-Kn} \tag{5.23}$$

The distribution of products can now be calculated on a carbon atom basis, for the case where alpha varies as a function of carbon number:

$$\frac{S_{n+1}}{n+1} = \alpha_n \bullet \frac{(1-\alpha_{n+1})}{1-\alpha_n} \bullet \frac{S_n}{n} \tag{5.24}$$

5.5 Evaluation of experimental data with chain length dependent desorption model

5.5.1 Fitting of K, T_O and T_P followed by calculation of C_1 and C_2 fractions

From the discussion above it is clear that the chain length dependent desorption model in its current form can only predict the formation rates of olefin's and paraffins relative to that of a reference component. In this case the carbon atom selectivity of the C_3 hydrocarbon fraction in the gas phase was taken as the reference component.

The chain length dependent desorption model was fitted to the experimental C_3 to C_8 hydrocarbon fraction from experiments at five different reaction temperatures via non-linear regression (fitting of T_O, T_P and K). The results of the fitting procedure are given in appendix C and show K to be independent of temperature i.e. temperature does not seem to have much effect on the observed rate of decrease in olefin to paraffin ratio. The model was therefore, re-fitted with a constant K of 0.07.

Table 5.3 Fitted values for K

Temperature	Fitted value for K
220	0.08
230	0.07
245	0.07
260	0.06
270	0.06

Mean	**0.07**
% deviation from mean	**10.05**

Figure 5.6 shows the optimized parameter fits for T_O and T_P while fixing K at 0.07. In Figure 5.6 the value of T_O decreases with increasing temperature and then levels off around 260℃, while T_P continues to decrease with increasing temperature.

From literature it is generally accepted that the chain growth probability will decrease with increasing temperature [Dry, 2004]. It then follows that T_O and T_P should increase with increasing temperature i.e. T_O and T_P respectively, relate the competition between desorption to form an olefin and hydrogenation to form a paraffin vs. further chain growth. The decreasing nature of T_O and T_P with increasing temperature in Figure 5.6 are therefore opposite to what is expected. Looking back at the results from section 4.5.3, the chain growth probability of the experimentally measured data in Figure 4.14 for the range C_3 to C_7 are also observed to increases with increasing temperature (0.63 at 220℃ to 0.75 at 270℃). Since the chain length dependent desorption model was fitted on the experimental C_3 to C_8 fraction, the trends observed for T_O and T_P can be explained by the experimental data. The reason for the unexpected trend in the experimental data is however, not known. For further discussion on the chain growth probability as a function of temperature see the section below.

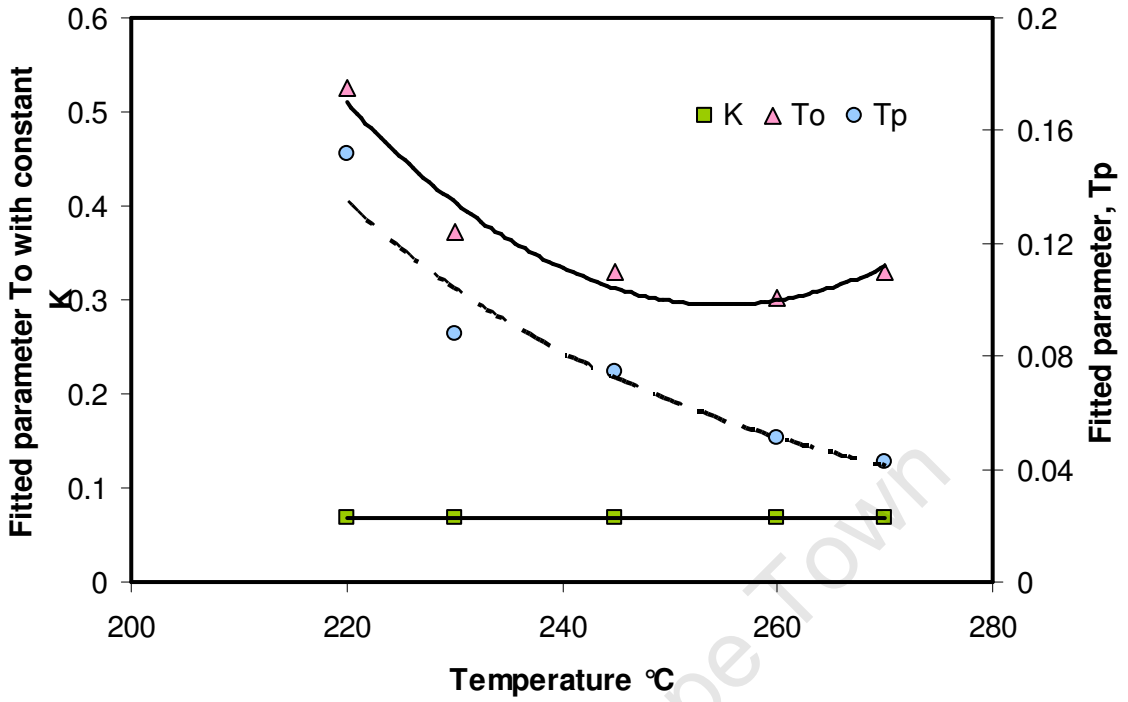

Figure 5.6 Fitted values T_O and T_P by non-linear regression (constant K)

Table 5.4 Results from fitting the chain length dependent desorption model

Temperatures (℃)	K	T_O	T_P	MARR (%)
220	0.07	0.53	0.15	3.5
230	0.07	0.37	0.09	5.1
245	0.07	0.33	0.08	13.6
260	0.07	0.30	0.05	4.9
270	0.07	0.33	0.04	11.7

The fitted parameter values in table 5.4 are in the lower range of those reported by Botes (Table 5.5). An explanation is that the experiments in this thesis were completed at synthesis conditions or with a catalyst, where secondary reactions were less likely to occur vs. the synthesis conditions / catalyst used by van der Laan (1999).

Table 5.5 Fitted values from Botes (2008) based on data of van der Laan (1999)

Experiments	K	T_O	T_P
Run A	0.19	0.36 – 0.86	0.02 – 0.33
Run C	0.2	0.41 – 0.91	0.03 – 0.32

Given that the parameter values have been fitted, the C_1 and C_2 fractions can now be calculated by application of the parameter values from table 5.4. For the C_2 chain growth probability an adapted version of equation 5.21 is used, this is because the C_2 formation rate would be overestimated if equation 21 were directly applied. Botes (2008) accounts for the experimentally observed lower C_2 fraction by assuming that the C_2 intermediate has a growth rate twice as large as that of the C_{3+} species. The resulting equation to calculate the C_2 chain growth probability is:

$$\alpha_2 = \frac{1}{1 + 0.5T_P + 0.5T_O \bullet e^{-2K}} \tag{5.25}$$

The C_1 fraction is calculated directly from equation 5.21, this is however not mechanistically sound as it implies that the C_1 species could terminate via both hydrogenation and desorption. Botes (2008) acknowledges the mechanistic implications of this assumption and assumes that the C_1 surface species will be governed by the same two steps as the longer chain intermediates. Since it cannot exist as a desorbed unsaturated species it will remain near the surface (chemisorbed / physisorbed) until it is fully hydrogenated. Parity plots showing the predicted vs. experimental data for the C_2 olefin to paraffin ratio, total C_2 fraction and the methane selectivity are given in appendix C.

An example of the complete model for the 230℃ experiment is given in Figure 5.7 below; the MARR value of 5.1 indicates that the model fit at 230℃ fits well. The remaining experiments were also fitted using the parameters in Table 5.4, the figures are given in appendix C.

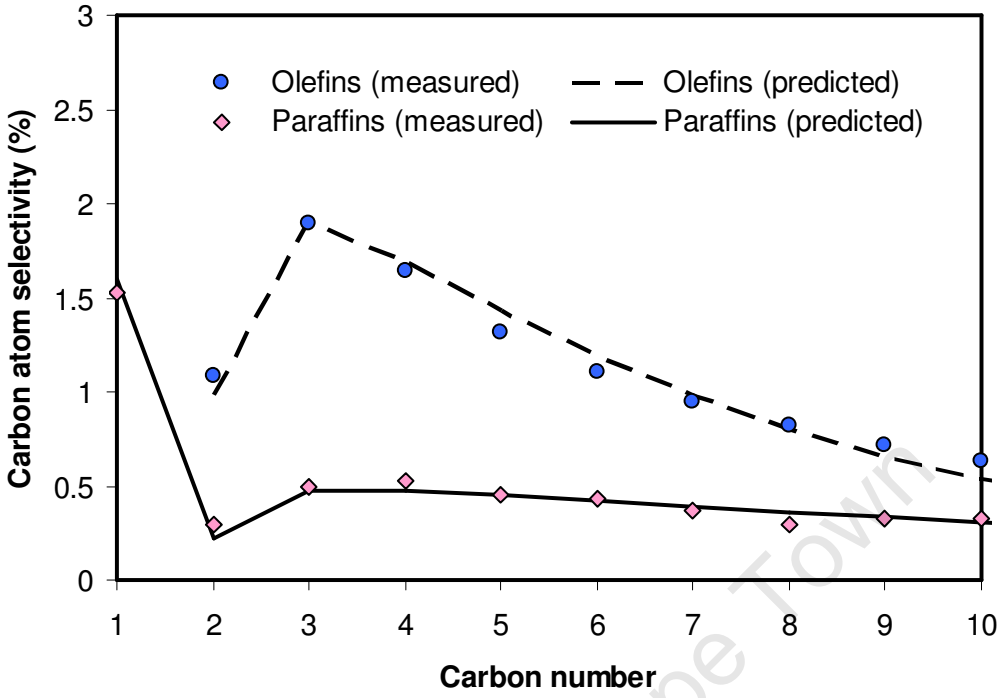

Figure 5.7 Example of the complete model: based on the fitted parameter values from Table 5.4 (data from experiment at 230 °C)

5.6 Chain growth probability as a function of temperature and carbon number

Figures 5.8 and 5.9 give the chain growth probability for the hydrocarbon fraction and the separate olefin and paraffin fractions as a function of temperature, respectively. The trends of these two figures are similar i.e. although the chain growth probability in the C_3 to C_7 hydrocarbon fraction increases with increasing temperature the rate at which they increase by decreases with increasing temperature, (the chain growth probability at 260 and 270℃ being almost identical). It is therefore postulated that at higher temperatures (temperatures > 260℃) the chain growth probability may level out or even decline.

At this point it is not clearly understood why the chain growth probability in the C_3 to C_7 fraction increases with increasing temperature. It is however plausible that the increase in chain growth probability is due to re-incorporation of re-adsorbed olefins [Schulz and Claeys[a, b], 1999] i.e. if primary short chain olefins are increasingly re-adsorbed and

incorporated into growing surface "chains" with increasing temperature, the chain growth probability of the C_3 to C_7 fraction would increase with increasing temperature. Furthermore, if the re-incorporation of re-adsorbed olefins is restricted to the C_2 olefins then the observations of Botes (2007 and 2008) as well as the chain length dependent desorption model still hold.

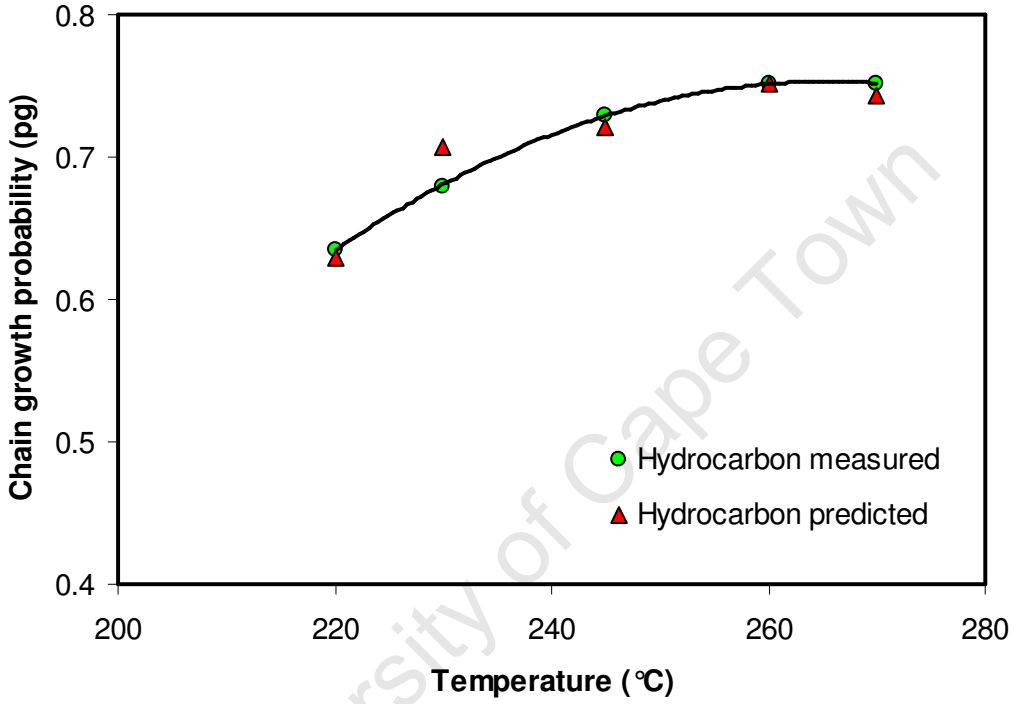

Figure 5.8 Chain growth probability (C_3 to C_7 hydrocarbon fraction) as a function of temperature (chain length dependent desorption model fitted to the C_3 to C_8 hydrocarbon fraction)

On further inspection of Figure 5.9 the chain growth probability of the C_3 to C_7 olefin fraction is lower than that of the paraffin fraction, this is substantiated by the fitted parameter values of T_O and T_P from Figure 5.6. Secondly, the rate of change in the chain growth probability as a function of temperature for the C_3 to C_7 olefin fraction is less than for the paraffin fraction.

These two differences in the chain growth probability of the C_3 to C_7 olefin and paraffin fractions suggest that primary olefin formation will be favoured over primary paraffin

formation and that the ratio of olefins to paraffins of the same carbon number will increase with increasing temperature.

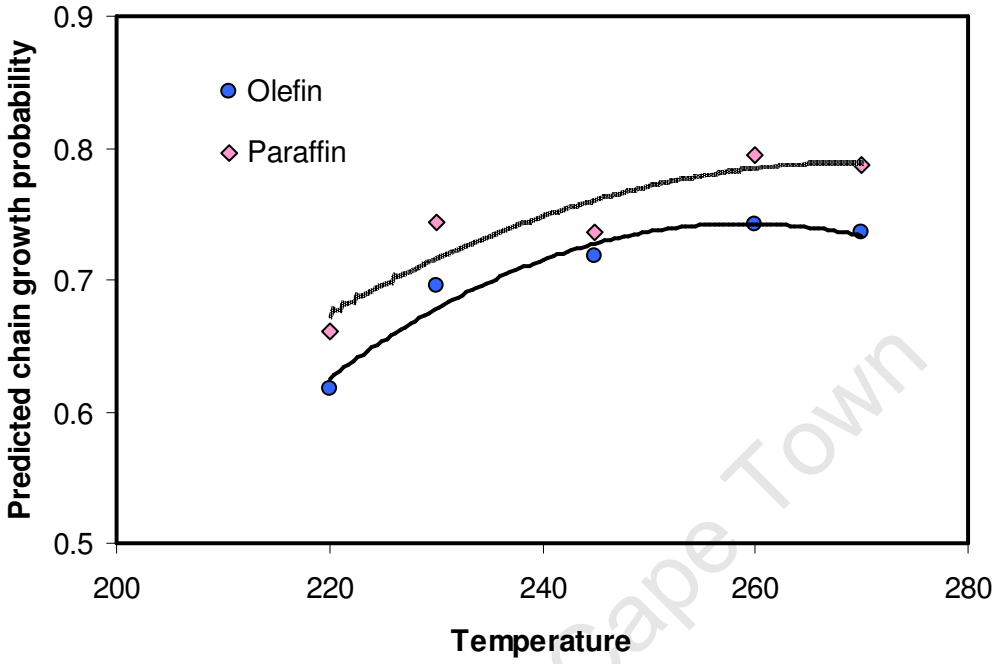

Figure 5.9 Predicted chain growth probability (C_3 to C_7 olefin and paraffin fraction) as a function of temperature (chain length dependent desorption model fitted to the C_3 to C_8 hydrocarbon fraction)

Figure 5.10 gives an example of the predicted and measured Schulz-Flory plots as a function of carbon number.

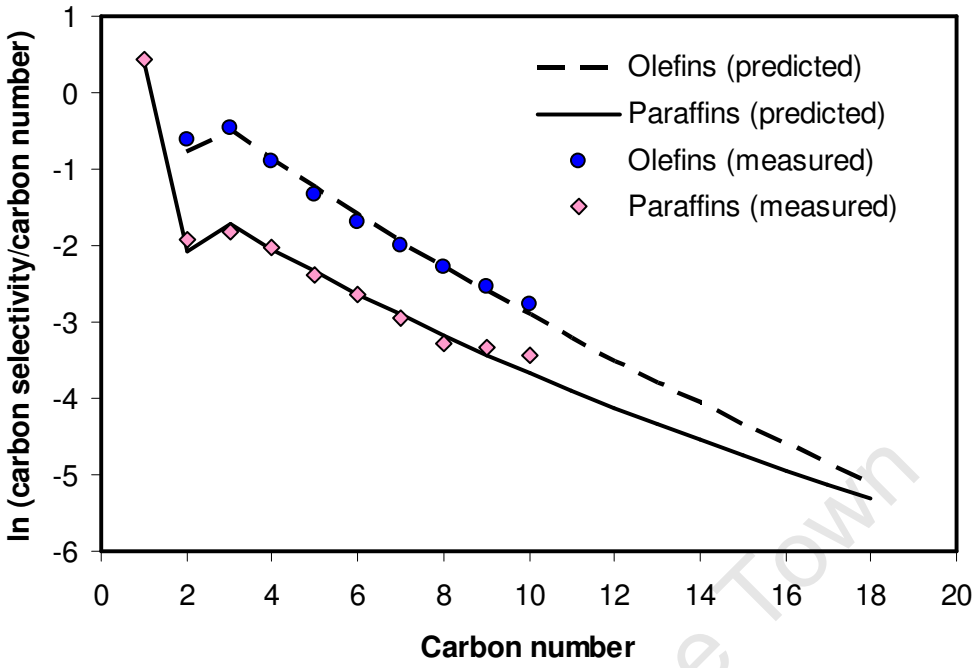

Figure 5.10 Predicted and measured chain growth probability as a function of carbon number

5.7 Linear hydrocarbon formation

The chain length dependent desorption model above describes the experimental data relatively well and the fitted model parameters are within the range of those reported by Botes (2008). Based on the fundamental assumptions of this model the results for the hydrocarbon fraction of chapter 4, section 4.5.4, are discussed in further detail.

5.7.1 Carbon number effects on the linear hydrocarbon selectivity:

In Figure 4.14, a carbon number dependent decrease for the fraction of linear olefins in linear hydrocarbons (C_3 to C_{14} product) is observed. A similar trend is observed in Figure 4.17 where the fraction of α-olefins in linear olefins also decreases with increasing carbon number for the C_8 to C_{16} product. In literature [van der Laan, 1999, Kuipers *et al.* 1995 and Iglesia *et al.* 1993] the decreasing α-olefin fraction, is explained by assuming that primarily formed olefins, can in part undergo re-adsorption followed by secondary

reaction (hydrogenation or isomerisation). An important implication of this explanation is that the tendency for α-olefin re-adsorption and hence secondary reaction will increase with increasing carbon number. To account for the increase in secondary reaction with increasing carbon number, three effects are widely discussed in literature; these have been reviewed in chapter 2 section 2.5.4. They are: 1) carbon number dependent diffusivity of liquid products in catalyst pores, 2) carbon number dependent solubility of products in the liquid phase and 3) carbon number dependent physisorption of products on the catalyst surface.

Recently however there is mounting evidence that the enhanced residence time of olefins with increasing chain length cannot stem from diffusion effects alone and that increasing solubility of olefins with carbon number cannot explain the chain length deviations observed in the Fischer-Tropsch synthesis [Iglesia *et al.,* 1993 and Botes, 2008]. Botes (2007) showed that over a potassium-promoted iron catalyst, ethene can be hydrogenated to ethane, an effect that increases with increasing recycle ratio. The hydrogenation of propene to propane was however shown to be negligible; consequently the ratio of propene to propane remained constant even with increasing recycle ratio.

Therefore, for the case of iron catalysts under realistic Fischer-Tropsch synthesis conditions, it seems unlikely that a C_3+ α-olefin will re-adsorb on the catalyst surface after it has fully desorbed, re-adsorption becoming even more unlikely with increasing carbon number.

Based on similar results for co-fed C_3+ olefins i.e. that at commercially relevant Fischer-Tropsch synthesis conditions the co-fed olefins do not undergo any significant secondary reactions [Hanlon *et al*., 1988 and Huff *et al.,* 1984]. Kuipers *et al.,* (1996) proposed that for an olefin to reinsert into a growing surface chain it is not necessary to first fully desorb. He proposed that after the breaking of the chemical bond between the olefin and the surface remains in the vicinity of the growth site due to physisorption, thereby allowing the olefin the chance to re-adsorb. Botes (2008) extends the model of Kuipers by assuming that the chemical bond of the growing intermediate stays physically and chemically attached to the catalyst surface. Botes hypothesized that the deviations from the ideal product distribution are due to the rates of chain growth and hydrogenation

(formation of a paraffin as the product) being independent of chain length, but that the rate of desorption is a function of carbon number (formation of an olefin as the product).

This approach implies that the observed increase in chain growth probability and decrease in olefin to paraffin ratio as a function of carbon number are not due to secondary reactions but rather, the primary carbon number dependent desorption of the intermediate from the catalyst surface. Since larger carbon number surface species are assumed to desorb at a slower rate, the residence time of the surface species will increase with increasing carbon number, hence the fraction for chain growth, hydrogenation or isomerisation per carbon number will increase with increasing carbon number.

Based on the most recent understanding of secondary olefin reaction over iron Fischer-Tropsch catalysts at commercially relevant synthesis conditions [Botes, 2008] and the relatively good prediction of the experimental results above. The chain length dependent desorption model is viewed to be a plausible explanation for the results of the hydrocarbon fraction given in chapter 4 as opposed to carbon number dependent diffusivity of liquid products in catalyst pores or the carbon number dependent solubility of products in the liquid phase. This however, only holds for the case if the C_2 olefins and not the C_3+ olefins are reactive for re-adsorption leading to re-incorporation and further chain growth.

5.7.2 Temperature effects on the linear hydrocarbon selectivity:

For the fraction of linear olefins in linear hydrocarbons (Figure 4.15), an increase in the C_{3+} fraction with increasing temperature is observed. For the C_2 fraction the ratio of linear olefins in linear hydrocarbons is relatively constant declining slightly as a function of temperature. Interestingly these results can also be described by the chain length dependent desorption model i.e. with increasing reaction temperature the rate of desorption (as an olefin) vs. the rate of hydrogenation (as a paraffin) and the rate of secondary reaction are expected to increase. Since only ethene is known to be active for secondary reaction over iron FT catalysts (predominantly hydrogenation), the C_3+ fraction of linear olefins in linear hydrocarbons is expected to increase with increasing

carbon number. For the C_2 fraction, the ratio of linear olefins in linear hydrocarbons may vary due the differences in activation energy for desorption vs. hydrogenation.

In Figure 4.18, the ratio of α-olefins to total linear (internal + α) olefins goes through a minimum when plotted as a function of temperature. Based on the assumptions of the chain length desorption model, the parabolic shape of Figure 4.18 can indeed be described by two competing effects. The decrease in the ratio of α-olefins to total linear olefins may be due to the increasing thermodynamic stability of the internal olefin vs. α-olefin with increasing temperature. While the increase in the ratio of α-olefins to total linear olefins at even higher temperatures (>245℃) may be due to an increased rate of desorption which in turn leads to a decreased residence time of the surface species and therefore less chance for the formation of the thermodynamically more stable internal olefin.

Based on the results of chapter 4 section 4.5.4 and the discussion above for the olefin selectivity as a function of temperature, it is expected that the ratio of linear olefin selectivity relative to the linear paraffin selectivity of the same carbon number in the C_3+ fraction will increase with increasing temperature due to an increased rate of desorption vs. hydrogenation for the primarily formed surface species. The make - up of the olefin fraction (internal olefin vs. α-olefin) varies due to the differences in residence time of the surface species.

As discussed above, it seems unlikely that a C_3+ α-olefin will re-adsorb on the catalyst surface after it has fully desorbed. The results for the C_3+ olefins can therefore not explain the increase in the chain growth probability for the C_3 to C_7 fraction with increasing temperature (Figures 4.13, 5.8 and 5.9). It has however been shown that the C_2 α-olefin fraction does not follow the trend of the other olefins with increasing temperature (Figure 4.15); the deviation of the C_2's being attributed to the high reactivity of ethene for secondary reactions, particularly secondary hydrogenation [Botes., 2008 and Schulz and Claeys[a]. 1999]. The increase in the chain growth probability for the C_3 to C_7 fraction with increasing temperature may therefore be explained by the increased readsorption of the C_2 α-olefin with increasing temperature to form a surface species capable of further chain growth or re-incorporation, this species being indistinguishable from the other surface species.

Chapter 6

Conclusions

In this thesis, the catalyst activity and product selectivity were determined as a function of reactor temperature while keeping the reactor partial pressures, catalyst and catalyst activation procedure constant.

Mass transport limitations:

The effect of external mass transport limitations were determined by variation of the stirrer speed where the catalyst activity stabilised at stirrer speeds above 400 rpm, consequently stirrer speeds of 450 rpm were utilised for all experiments. The effect of internal mass transport limitations were evaluated; first by calculation of the Weisz-Prater criterion (C_{WP}) and then by estimation of the effectiveness factor (η_{FT}). The results of Weisz-Prater criterion were inconclusive since values of 1.2 were obtained at temperatures of 270°C and only values for C_{WP} »1 are said to cause severe internal mass transport limitations. The estimation of the effectiveness factor however, showed there to be negligible internal mass transport limitations, the rate of reaction varying by less than 5% throughout the catalyst particle. The results for both the external and internal mass transport limitations therefore show that for this catalyst applied under the reaction conditions of this thesis, mass transport limitations do not occur to any significant extent.

Apparent activation energy:

The apparent activation energy and pre-exponential factors for both the water-gas shift (WGS) and low temperature Fischer-Tropsch (LTFT) reactions were calculated by non-linear regression. The resulting apparent activation energy for the Fischer-Tropsch reaction ranged from 62.5 to 66 kJ/mol (differing slightly due to the rate equation used) while the apparent activation energy for the water-gas shift reaction was calculated to be

94 kJ/mol. It must be noted that the adsorption coefficients were assumed to be constant over the temperature range tested and an additional study will be required to decouple these kinetic parameters from the pre-exponential factors.

Formation of CO_2:

The overall trend for CO_2 selectivity is that it increases "slightly" with increasing temperature. At reaction conditions far from the WGS equilibrium the formation of CO_2 does however seem to be sensitive to changes in the gas-hourly space velocity (GHSV) this indicating that a major route for CO_2 formation occurs via the secondary reaction of CO with primarily formed H_2O (water-gas shift reaction). Therefore, at commercial low temperature Fischer-Tropsch reaction conditions the WGS reaction can be regarded as an irreversible, consecutive reaction following the formation of the major product compound water.

Formation of CH_4:

For the case where the partial pressures of carbon monoxide and hydrogen are kept constant and temperature is varied, the methane selectivity is observed to increase with increasing reaction temperature. Based on literature [Claeys and van Steen, 2004] this increase is expected, and has been explained by an increased rate of desorption at higher reaction temperatures. These results however, do not fit with the model results of chapter 5, where T_P (desorption due to hydrogenation vs. further chain growth) decreases with increasing temperature, therefore predicting a decrease in the methane selectivity. The conclusion that can be reached is that the chain length dependent desorption model extrapolated to C_1, does not correctly predict the methane selectivity of these experiments (i.e. experiments with variation in temperature).

Chain growth probability:

Overall the chain growth probability in the range C_8 to C_{14} decreases with increasing temperature from 0.91 at 220°C to 0.87 at 270°C. This is in line with literature [Donnelly *et al.,* 1989], but realistically the decrease in chain growth probability is quite small considering the 50°C variation in temperature. Interestingly, the chain growth probability

in the range C_3 to C_7 is observed to increase from 0.63 at 220℃ to 0.75 at 270℃, with the rate of increase slowing at higher temperatures.

At this point it is not clearly understood why the chain growth probability in the C_3 to C_7 fraction increases with increasing temperature. It is however plausible that the increase in chain growth probability may be due to the re-incorporation ethene in growing chains i.e. if ethene is increasingly re-adsorbed and incorporated into growing surface "chains" as a function of temperature, the chain growth probability of the C_3 to C_7 fraction will increase with increasing temperature. The slowing of the rate of increase in the chain growth probability at higher temperatures can be explained if the activation energy for ethene hydrogenation is larger than for ethene re-incorporation (i.e. the rate of ethene hydrogenation will be larger than for re-incorporation at "high" reaction temperatures).

The predicted chain growth probability of the C_3 to C_7 olefin and paraffin fractions shown in Figure 5.9 (chain length dependent desorption model) suggest that primary olefin formation will be favoured over primary paraffin formation and that the ratio of olefins to paraffins of the same carbon number will increase with increasing temperature.

Hydrocarbon selectivity:

For the fraction of linear olefins in linear hydrocarbons (Figure 4.15), an increase in the C_{3+} fraction with increasing temperature is observed, this is in agreement with the predicted (chain length dependent desorption model) chain growth probability of the C_3 to C_7 olefin and paraffin fractions. For the C_2 fraction the ratio of linear olefins in linear hydrocarbons is relatively constant declining slightly as a function of temperature. The difference in the trend of the C_2 fraction as compared to the C_3+ fraction is due to an increased extent of secondary reaction for the C_2 olefins. The observed trends for both the C_2 and C_3+ linear hydrocarbon fractions are also described by the chain length dependent desorption model.

In Figure 4.18, the ratio of α-olefins to total linear (internal + α) olefins goes through a minimum when plotted as a function of temperature. The decrease in the ratio of α-olefins to total linear olefins may be due to the increasing thermodynamic stability of the internal olefin vs. α-olefin with increasing temperature. While the increase in the ratio of

α-olefins to total linear olefins at even higher temperatures (>245℃) may be due to an increased rate of desorption which in turn leads to a decreased residence time of the surface species and therefore less chance for the formation of the thermodynamically more stable internal olefin.

Based on the results of this thesis, it is therefore expected that the ratio of linear olefin selectivity relative to the linear paraffin selectivity of the same carbon number in the C_3+ fraction will increase with increasing temperature due to an increased rate of desorption (as an olefin) vs. hydrogenation for the primarily formed surface species. The make - up of the olefin fraction (internal olefin vs. α-olefin) varying, due to the differences in the residence time of the surface species.

Branching:

For the C_7 to C_{12} range, the fraction of branched hydrocarbons relative to the total hydrocarbon product increases with increasing temperature, this effect has also been observed by Schulz and Gokcebay, (1982). As with the linear hydrocarbons, the formation of branched olefins relative to the formation of branched hydrocarbons is observed to increase with increasing temperature.

Oxygenate selectivity:

According to literature, [Dry, 2004] the linear alcohols selectivity will decrease due to increasing temperature but will increase due to the decreasing residence time. Therefore, since the increase in temperature for the experiments of this thesis were accompanied by a proportional increase in the space velocity to maintain constant carbon monoxide to Fischer-Tropsch product conversions, the two effects were expected to cancel each other out. The results therefore support literature, since only a small decrease in the linear 1-alcohols was observed with increasing temperature.

The acid number of the water fraction seems to decrease with increasing temperature and implies that with increasing reaction temperature the formation of acids in the Fischer-Tropsch synthesis is reduced.

Cyclic and aromatic selectivity:

There is almost no effect of temperature on the cyclic olefin selectivity in the hydrocarbon fraction (linear hydrocarbons + cyclic olefins). The data at 260℃ (point of highest space velocity) being the exception. Assuming that the decrease in cyclic olefin selectivity in the hydrocarbon fraction is a caused by the high in space velocity of this point, the result indicates that cyclic olefins may be formed via a secondary reaction.

The selectivity data for the aromatic content in the hydrocarbon fraction (linear hydrocarbons + aromatics) at 245℃ is far higher than for the other carbon numbers, (this is especially apparent in Figure 4.27) but no explanation can be given at this point and it is assumed that this is caused by scatter in the data.

References

Aasberg-Peterson K., Christensen I., Dybkjaer I., Sehested M., Ostberg M., Coertzen R., Keyser M.J., Steynberg A.P.
Fischer-Tropsch technology: Chapter 4 Synthesis gas production for FT Synthesis
Studies in surface science and catalysis **152** (2004), 258 – 405

Adahchour M., Beens J., Vreuls R.J.J., Brinkman U.A.Th.
Recent developments in comprehensive two-dimensional gas chromatography (GC x GC) III: Applications for petrochemicals and organohalogens
Trends in analytical chemistry, **25** (2006)

Anderson R.B.
Catalysts for the Fischer-Tropsch synthesis
Van Nostrand Reinhold **4** (1956)

Anderson R.B.
The Fischer-Tropsch synthesis
Academic Press, Inc. (1984)

Anil A. K., Brisk M. L.
Sequential experimental design for precise parameter estimation 1. Use of re-parameterization
Industrial Engineering and Chemical Process Design Development **24** (1985) 203 - 207

Asian Tribune
India, China will drive global energy use increase
http://www.asiantribune.com/show_news.php?id=4059 (2003)

Aspen Technology Inc.
Aspen plus 2006., Estimation of pure component properties

Atwood H.E., Bennet C.O.
Kinetics of the Fischer-Tropsch reaction over iron
Industrial Engineering Chemical Process Des.Dev **18** (1979), 163-170

Biel H.B.
The effect of water partial pressure on low temperature iron Fischer-Tropsch reaction rate, selectivity and catalyst structure
MSc Thesis, University of Cape Town (2004)

Bond G.C.
Metal-Catalysed Reaction of Hydrocarbons
Springer Science + Business Media Inc. (2005)

Botes F.G., Breman B.B.
Development and testing of a new macro kinetic expression for the iron-based low-temperature Fischer–Tropsch reaction
Industrial Engineering Chemical Research **45** (2006), 7415-7426

Botes F.G.
Water–gas-shift kinetics in the iron-based low-temperature Fischer–Tropsch synthesis
Applied Catalysis A: General **328** (2007), 237-242

Botes F.G.
Kinetic and selectivity modelling of the iron-based low-temperature Fischer-Tropsch synthesis
PhD Thesis, Eindhoven University of Engineering (2008)

Claeys M.
Selektivität, Elementarschritte und kinetische modellierung bei der Fischer-Tropsch synthese
PhD Thesis, University of Karlsruhe (1997)

Claeys M., van Steen E.
Fischer-Tropsch technology: Chapter 8 Basic studies
Studies in surface science and catalysis **152** (2004), 601

Conner W.C., Falconer J.L.
Spillover in heterogeneous catalysis
Chemical Reviews **95** (1995), 759-788

Deckwer W.D., Kokuun R., Sanders E., Ledakowicz S
Kinetic studies of Fischer-Tropsch synthesis on suspended Fe/K catalyst. Rate inhibition by CO_2 and H_2O
Industrial Egineering Process Des.Dev. **25** (1986), 643-649

Dictor R.A., Bell A.T.
Fischer-Tropsch synthesis over reduced and unreduced iron oxide catalysts
Journal of Catalysis **97** (1985), 121

van Dijk H.A.J.
The Fischer-Tropsch synthesis: A mechanistic study using transient isotopic tracing
PhD thesis (2001)

Donnelly T.J., Satterfield C.N.
Product distributions of the Fischer-Tropsch synthesis on precipitated iron catalysts
Applied Catalysis **52** (1989), 93-114

Dry M.E., Shingles T., Boshoff L.
Rate of the Fischer-Tropsch reaction over iron catalysts
Journal of Catalysis **25** (1972), 99-104

Dry M.E.
Advances in Fischer-Tropsch chemistry
Industrial and Engineering Chemistry Product Research and Development **15** (1976), 282-286

Dry M.E.
The Fischer-Tropsch Synthesis
Catalysis vol. IV, P. H. Emmett, Reinhold Publishing Corp., New York, **Chap. 4** (1981), 158-253

Dry M.E.
Practical and theoretical aspects of the catalytic Fischer-Tropsch process
Applied Catalysis A: General **138** (1996), 319-344

Dry M.E.
Fischer-Tropsch reactions and the environment
Applied Catalysis A: General **189** (1999), 185-190

Dry M.E.
The Fischer-Tropsch process: 1950-2000
Catalysis Today **71** (2002), 227-241

Dry M.E.
The Fischer-Tropsch process to clean fuels and chemicals
ACS Division of Fuel Chemistry, Preprints **48** (2003), 211

Dry M.E.
Present and future applications of the Fischer-Tropsch process (editorial)
Applied Catalysis A: General **276** (2004), 1-3

Eckert C.A.
Molecular thermodynamics of chemical reactions
Industrial Engineering Chemistry **59** (1967), 20-32

Eisberg N.
Old king coal returns
Chemistry and Industry, Issue No. **7** (2005)

Erkey C., Rodden J.B., Akgerman A.
Diffusivities of synthesis gas and n-alkanes in Fischer-Tropsch wax
Energy and Fuels **4** (1990) 275

ExxonMobil publication to shareholders
Playing to our strengths
The Lamp **87** No.1 (2005)

Fogler H. S.
Elements of chemical reaction engineering 3rd edition
Prentice Hall International (1999)

Froment G.F.
Model discrimination and parameter estimation in hterogeneous catalysis
AIChE Journal **21, no. 26** (1975) 1041

Geerlings J.J.C., Wilson J.H., Kramer G.J., Kuipers H.P., Hoek A., Huisman H.M.
Fischer-Tropsch technology - from active site to commercial process
Applied Catalysis A: General **186** (1999) 27

Govender N.S., Botes F.G., de Croon M.H.J.M., Schouten J.C.
Mechanistic pathway for methane formation over an iron-based catalyst
Journal of Catalysis **260** (2008) 254 - 261

Gray D., Tomlinson G.
A novel configuration for coproducing Fischer-Tropsch fuels and electric power from coal and natural gas
Mitretek Systems, funded by *DOE* under contract number DE-AC22-95PC95054 (1997)

Hanlon R.T., Satterfield C.N.
Reactions of selected 1-olefins and ethanol added during the Fischer-Tropsch synthesis
Energy and Fuels **2** (1988) 196 - 204

Huff G.A., Satterfield C.N.
Evidence for two chain growth probabilities on iron catalysts in the Fischer-Tropsch synthesis
Journal of Catalysis **85** (1984), 370-379

Iglesia E., Reyes S.C., Madon R.J.
Transport enhanced α-olefin readsorption pathways in ruthenium-catalysed hydrocarbon synthesis
Journal of Catalysis **129** (1991), 238

Iglesia E., Reyes S.C., Madon R.J., Soled S.L.
Selectivity control and catalyst design in the Fischer-Tropsch synthesis: sites, pellets and reactors
Advances in Catalysis **39** (1993) 221

Jordan D.S., Bell A.T.
Catalytic reactions of carbon monoxide
Journal of Physical Chemistry **90** (1986), 4797-4805

Komaya T., Bell A.
Estimates of the rate coefficients for elementary process occurring during Fischer-Tropsch synthesis over Ru TiO_2
Journal of Catalysis **146** (1994) 237 - 248

Krishnamoorthy S., Li A., Iglesia E.
Pathways for CO_2 formation and conversion during Fischer-Tropsch synthesis on iron-based catalysts
Catalysis Letters **80** (2002), 77-86

Kuipers E.W., Scheper C., Wilson J.H., Vinkenburg I.H., Oosterbeek H.
Non-ASF product distributions due to secondary reactions during Fischer-Tropsch synthesis
Journal of Catalysis **158** (1996) 288 - 300

Kuipers E.W., Vinkenburg I.H., Oosterbeek H.
Chain length dependence of α-olefin readsorption in Fischer-Tropsch sythesis
Journal of Catalysis **152** (1995) 137

van der Laan G.P., Beenackers A.A.C.M.
Hydrocarbon selectivity model for the gas-solid Fischer-Tropsch synthesis on precipitated iron catalysts
Industrial and engineering chemistry research **38** (1999), 1277-1290

van der Laan G.P.
Kinetics, Selectivity and Scale Up of the Fischer-Tropsch Synthesis
PhD Thesis, University of Groningen (1999)

Ledakowicz S., Nettelhoff H., Kokuun R., Deckwer W.D.
Kinetics of the Fischer-Tropsch synthesis in the slurry phase on a potassium-promoted iron catalyst
Industrial and engineering chemistry **24** (1985), 1043-1049

Ledford E. B., TerMaat J.R., Billesbach C.A.
Technical Note KT030606-1: What is Loop Modulation?
Zoex Corporation, http://www.zoex.com/applications/technical_notes.asp (2005)

Madon R.J., Reyes S.C., Iglesia E.
Primary and secondary reaction pathways in ruthenium-catalyzed hydrocarbon synthesis
Journal of Physical Chemistry **95** (1991), 7795-7804

Maitlis P.M. Long H.,Quyoum R., Turner M.
Heterogeneous catalysis of C-C bond formation: black art or organometallic science?
Chemical Communications **1** (1996), 1-8

Malherbe J.A.
The effect of catalyst pre-treatment on the mechanical integrity and synthesis performance of an iron based Fischer-Tropsch catalyst
Masters Thesis – University of Cape Town 2006

Marano J., Holder G.
Cahracterisation of Fischer-Tropsch liquids for vapour-liquid equilibria calculations
Fluid Phase Equilibria (1997)

Millat J., Dymond J.H., Nieto de Castro C.A. (editors)
Transport properties of fluids: Their correlation, prediction and estimation
Chapter 13: Empirical estimation
Press Syndicate of the University of Cambridge (1996)

Morita Y.
Marketability of GTL from natural gas
The 370th meeting for briefing research reports (2001)

Neathery J., Gray D., Challman D., Derbyshire F.
The pioneer plant concept: co-production of electricity and added-value products from coal
Fuel **78** (1999), 815-823

Novak S., Madon R.J., Suhl H.
Secondary effects in Fischer-Tropsch synthesis
Journal of Catalysis **77** (1982), 141-151

Perry R.H., Green D.W.
Perry's chemical engineers handbook, 7th edition
McGraw-Hill (1997)

Pichler H., Schulz H., Eistner M.
Gesetzmäßigkeiten bei der synthese von kolenwasserstoffen aus kolenoxid und wasserstoff
Breenstoff-Chemie **3** (1967), 78-87

Poling B.E., Prausnitz J.M., O'Connell J.P.,
The properties of gases and liquids fifth edition
McGraw – Hill Book Company (1987)

Puskas I., Hurlbut R.S.
Comments about the causes of deviations from the Anderson-Schulz-Flory distribution of the Fischer-Tropsch reaction products
Catalysis Today **84** (2003) 99

Riedel T., Claeys M., Schulz., Schaub G.
Comparative study of Fischer-Tropsch synthesis with the H2/CO and H2/CO2 syngas using Fe- and Co- based catalysts
Applied Catalysis A **186** (1999) 201-213

Robinson S.
China blossoms with chemical growth
Chemistry and Industry, Issue No. **23** (2003)

Rostrup-Nielsen J.R.
Syngas in perspective
Catalysis Today **71** (2002), 243-247

van Santen R.A., van Leeuwen P.W.N.M., Moulijn J.A., Averill B.A.
Catalysis an integrated approach, second. revised and enlarged version: Chapter 8 Catalytic reaction engineering
Studies in surface science and catalysis **123** (1999), 375 - 433

Sarup B., Wojciechowski B.W.
Studies of the Fischer-Tropsch synthesis on a cobalt catalyst: I Evaluation of product distribution parameters from experimental data
Canadian Journal of Chemical Engineering **66** (1988), 831-842

Schulz H., Beck K., Erich E.
Kinetics of Fischer-Tropsch selectivity
Fuel Processing Technology **18** (1988) 293

Schulz H., Claeys M.[a]
Reactions of α-olefins of different chain length added during Fischer-Tropsch synthesis on a cobalt catalyst in a slurry reactor
Applied Catalysis A: General **186** (1999), 71 – 90

Schulz H., Claeys M.[b]
Kinetic modeling of Fischer-Tropsch product distributions
Applied Catalysis A: General **186** (1-2), (1999) pp. 91-107

Schulz H., Elrich E., Gorre H., van Steen E.
Regularities of selectivity as a key for discriminating FT-surface reactions and formation of the dynamic system
Catalysis Letters **7** (1990) 157

Schulz H., Gokcebay H.
Fischer-Tropsch CO-hydrogenation as a means for linear olefins production
9th Conference on Catalysis of Organic Reactions (1982)

Schulz H., Riedel T., Schaub G.
Fischer-Tropsch principles of CO hydrogenation on iron catalysts
Topics in Catalysis **32** (2005) 117 - 124

Schulz H., van Steen E., Claeys M.
Selectivity and mechanism of Fischer-Tropsch synthesis with iron and cobalt catalysts
Natural Gas Conversion II (1994) 455

Schulz H., Zein El Deen A.
New concepts and results concerning the mechanism of carbon monoxide hydrogenation. II. Evolution of reaction steps on the basis of detailed product composition and other data
Fuel Processing Technology **1(1)** (1977), 45 - 56

Schulz H.
Short history and present trends of Fischer-Tropsch synthesis
Applied Catalysis A: General **186** (1999), 3-12

Shi B., Davis B.H.
Fischer-Tropsch synthesis: The paraffin to olefin ratio as a function of carbon number
*Catalysis Today **106** (2005), 129-131*

Shi B., Keogh R.A., Davis B.H.
Fischer-Tropsch synthesis: The formation of branched hydrocarbons in the Fe and Co catalyzed reaction
*Journal of Molecular Catalysis A: Chemical **234** (2005), 85-97*

Smith W.T., Greenbaum, S., Rutledege G.P.
Correlation of critical temperatures with thermal expansion coefficients of organic liquids
Journal of Physical Chemistry **58** (1954), 443

van Steen E., Schulz H.
Polymerisation kinetics of the Fischer-Tropsch CO hydrogenation using iron and cobalt based catalysts
Applied Catalysis A: General **186** (1999), 309-320

Steynberg A.P.[a]
Fischer-Tropsch technology: Chapter 1 Introduction to Fischer-Tropsch technology
Studies in surface science and catalysis **152** (2004), 1 – 63

Steynberg A.P.[b]
Fischer-Tropsch technology: Chapter 2 Fischer-Tropsch reactors
Studies in surface science and catalysis **152** (2004), 64 – 196

Storch H.H., Golumbic H., Anderson R.B.
The Fischer-Tropsch and related synthesis
John Wiley & Sons, New York (1951)

Sung S., Hoffmann R.
How carbon monoxide bonds to metal surfaces
Journal of the American Chemical Society **107** (1985), 578-584

Tau L., Dabbagh H., Bao S., Davis B.H.
Fischer-Tropsch synthesis. Evidence for two chain growth mechanisms
Catalysis Letters **7** (1990) 127

Tillmetz K.D.
Thermodynamic simultaneous equilibriums in Fischer-Tropsch synthesis
Chemie Ingenieur Technik **48** (1976) 1065

Vannice M.A.
Catalytic synthesis of hydrocarbons from hydrogen-carbon monoxide mixtures over the group VIII metals. I. Specific activities and product distributions of supported metals
Journal of Catalysis **37** (1975), 462

Vosloo A.C., Gibson P. and Van Berge P.J.
21st Annual International Pittsburgh Coal Conference (2004), Osaka, Japan.

Weitkamp A.W., Seelig H.S., Bowman N.J., Cady W.E.
Products of the hydrogenation of carbon monoxide over an iron catalyst – aliphatic and alicyclic hydrocarbons
Industrial and Engineering Chemistry **45** (1953), 343-349

Wilhelm D.J., Simbeck D.R., Karp A.D., Dickenson R.L.
Syngas production for gas-to-liquids applications: technologies, issues and outlook
Fuel Processing Technology, **71** (2001) 139-148

Wojciechowski B.W.
The kinetics of the Fischer-Tropsch synthesis
Catalysis Reviews – Science and Engineering **30** (1988), 629-702

Zimmerman W.H., Bukur D.B.
Reaction kinetics over iron catalysts used for the Fischer-Tropsch synthesis
Canadian Journal of Chemical Engineering **68** (1990), 292-301

Zimmerman W.H.
Kinetic model of Fischer-Tropsch synthesis in the slurry phase
Chemical engineering science **13(1)** (1992), 2707 - 2712

Appendices

Appendix A

Internal mass transport limitations

Estimation of binary liquid diffusion coefficients at infinite dilution [Poling et al., 2001]:

The binary liquid diffusion coefficients at infinite dilution were estimated using the Wilke-Chang method:

$$D_{AB} = \frac{7.4 \bullet 10^{-8} (\Phi M_B)^{0.5} T}{\eta_B V_A^{0.6}} \quad \text{(A.1)}$$

Where:

D_{AB} = mutual diffusion coefficient of solute A at very low concentration in solvent B ($cm^2.s^{-1}$)

Φ = association factor of solvent B

M_B = molecular weight of solvent B ($g.mol^{-1}$)

T = temperature (K)

η_B = viscosity of solvent B (cP)

V_A = molar volume of solute A at its normal boiling temperature ($cm^3.mol^{-1}$)

The liquid/slurry phase was assumed to have an average carbon number of 22 and to only contain n-parrafins (i.e. slurry phase = n-$C_{22}H_{46}$). Furthermore, the liquid viscosity of the solvent was calculated as a function of temperature using Aspen and the Peng - Robinson equation of state.

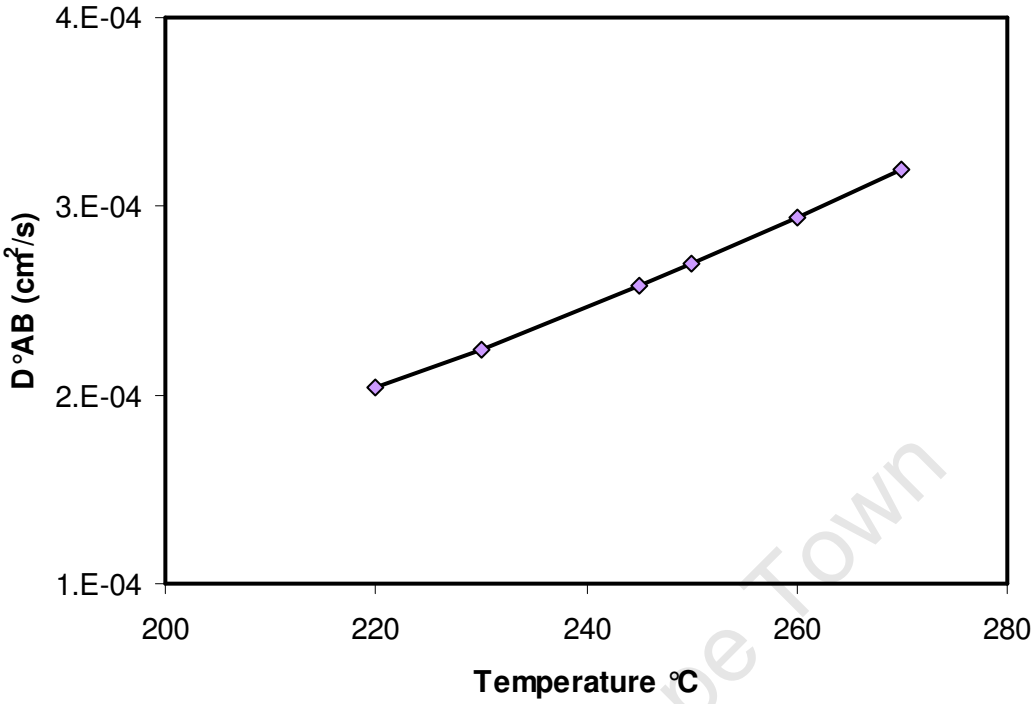

Figure A1 Binary liquid diffusion coefficients at infinite dilution as a function of temperature, estimated using the Wilke-Chang method

Calculation of the Weisz-Prater criterion:

$$C_{WP} = \frac{-r_{A,obs} \bullet \rho_c \bullet R^2}{D_e \bullet C_{CO,liq}} \qquad \text{(A.2)}$$

Where:

C_{WP} = Weisz-Prater criterium

$r_{A,obs}$ = observed reaction rate (mol/g-cat.s)

p_c = catalyst density (g.cm^{-3})

R = particle radius (cm)

D_e = effective diffusivity (cm^2.s^{-1})

$C_{CO,,liq}$ = liquid phase concentration of CO (mol.m^{-3})

In the absence of gas-liquid / external mass transfer limitations, the liquid phase concentrations of H_2 and CO can be calculated using the following gas-liquid solubility relationships:

$$p_{CO} = C_{CO,liq} \bullet H^{\infty}_{CO} \bullet V_{m,liq} \quad \text{(A.3)}$$

$$p_{H_2} = C_{H_2,liq} \bullet H^{\infty}_{H_2} \bullet V_{m,liq} \quad \text{(A.4)}$$

Where:

p_{CO} = partial CO pressure in the gas phase (bar)

p_{H2} = partial H_2 pressure in the gas phase (bar)

$C_{CO,liq}$ = liquid phase concentration of CO ($mol.m^{-3}$)

$C_{H2,liq}$ = liquid phase concentration of H_2 ($mol.m^{-3}$)

H°_{CO} = infinite-dilution Henry coefficient for CO in n-$C_{22}H_{46}$ as a function of temperature (bar)

H°_{H2} = infinite-dilution Henry coefficient for H_2 in n-$C_{22}H_{46}$ as a function of temperature (bar)

$V_{m,liq}$ = molar liquid volume of the liquid phase ($m^3.mol^{-1}$)

The infinite-dilute Henry coefficients (H°_i) for CO and H_2 in n-$C_{22}H_{46}$ were calculated using correlations by Marano and Holder, (1997):

$$H_{i,0} = A + \frac{B}{T} + C \bullet \ln T + DT^2 + \frac{E}{T^2} \quad \text{(A.5)}$$

$$\ln H^{\infty}_i = H_{i,0} - n \bullet \Delta H_i \quad \text{(A.6)}$$

Where:

n = carbon number of paraffin solvent (i.e. 22)

Table A1 gives the constants (i.e. A, B, C, D, E and $DeltaH_i$) used to calculate the infinite-dilution Henry coefficients

Table A1 Constants for calculation of infinite-dilution Henry coefficients, Marano and Holder, (1997) (valid for C_{16}-C_{36} paraffin in temperature range of 300 – 553 K)

Species	**A**	**B**	**C**	**D** (x 10^{-6})	**E**	Δ**H$_i$**
H_2	12.9353	22.9058	-0.974709	-1.20408	2244.61	0.0200959
CO	5.79833	19.5937	0.152199	-1.89733	2031.63	0.0173238

Table A2 Infinite-dilution Henry coefficients, Marano and Holder, (1997) (valid for C_{16}-C_{36} paraffin in temperature range of 300 – 553 K)

Temperature (°C)	**H_{CO} inf (bar)**	**H_{H2} (bar)**
220	383	499
230	376	483
245	367	460
250	363	452
260	357	438
270	350	424

Values for the liquid phase concentrations ($C_{i,liq}$) of CO and H_2 as a function of temperature can now be calculated. The effective diffusivity (D_e) is determined assuming a tortuocity (t) of 1.414 [Fogler, 1999].

Table A3 Liquid phase concentrations of CO and H_2 as well as effective diffusivity vs. temperature

Temperature (°C)	**Cco,liq (mol/m^3)**	**C_{H2}, liq (mol/m^3)**	**De (m^2/s)**
220	20.54	31.89	7.20E-09
230	21.58	33.68	7.94E-09
245	21.75	35.53	9.11E-09
250	22.29	35.60	9.53E-09
260	20.26	38.18	1.04E-08
270	19.52	36.68	1.13E-08

Estimation of the influence of internal mass transport limitations

The influence of internal mass transport limitations as a function of temperature was estimated using the Thiele modulus and effectiveness factors.

For arbitrary kinetics, the Fischer-Tropsch effectiveness factor (n_{FT}) can be calculated by solving the single particle differential equations [Froment *et al.*, 1990; Fogler, 1999]. It is however possible to approximate n_{FT} analytically with reasonable accuracy [Botes, 2008; Steyberg *et al.*, 2004]. To achieve this, the kinetic equation must be simplified to pseudo-first order in one of the reactants [Fogler, 2006]. Since the FT kinetic model of Botes (2008) was selected to estimate the internal mass transfer limitations it will be applied here again where CO is considered the key reactant [Botes, 2008]:

Writing the rate equation of Botes (2008) in terms of liquid phase concentrations:

$$r_{FT} = A'' \bullet \frac{C_{CO,liq} C_{H2,liq}^{0.5}}{\left(1 + k_{CO}^{''} C_{CO,liq}\right)^2} \tag{A.7}$$

Accounting for the case where intra-particle mass transfer limitations are significant, the observed reaction rate can be represented by:

$$r_{FT,obs} = \eta_{FT} \bullet A'' \bullet \frac{C_{CO,liq} C_{H2,liq}^{0.5}}{\left(1 + k_{CO}^{''} C_{CO,liq}\right)^2} \tag{A.7.1}$$

Applying the assumption that the kinetic equation can be simplified to pseudo-first order in CO:

$$r_{FT} = k_{pfo,FT} \bullet C_{CO,liq} \quad \text{with} \quad k_{pfo,FT} = \frac{\frac{A}{\rho_c} \bullet H_{CO} H_{H_2}^{0.5} V_{m,liq}^{1.5} C_{H_2,liq}^{0.5}}{\left(1 + k_{CO} H_{CO} V_{m,liq} C_{CO,liq}\right)^2} \tag{A.8}$$

Where the observed reaction rate is also simplified to first order kinetics:

$$r_{FT,obs} = \eta_{FT} \bullet k_{pfo,FT} \bullet C_{CO,liq} \qquad \text{(A.8.1)}$$

The Thiele modulus and effectiveness factor for the simplified pseudo-first order kinetics of equation A.7 are given by the following equations:

$$M_T = \frac{R}{3}\sqrt{\frac{k_{pfo,FT}}{D_e}} \qquad \text{with} \quad D_e = \frac{\varepsilon_P}{\tau} D_{CO,liq} \qquad \text{(A.9)}$$

$$\eta_{FT} = \frac{\tanh(M_T)}{M_T} \qquad \text{(A.10)}$$

Where:

r_{FT} = reaction rate (mol.s^{-1}.m$^{-3}_{\text{pore-vol}}$)

$r_{FT,obs}$ = observed reaction rate (mol.s^{-1}.m$^{-3}_{\text{pore-vol}}$)

$k_{pfo,FT}$ = pseudo-first order Fischer-Tropsch reaction rate constant (s^{-1})

A" = Activity coefficient in terms of liquid phase concentrations

A = Activity coefficient

p_c = catalyst density (g.m^{-3})

n_{FT} = estimated Fischer-Tropsch effectiveness factor

R = catalyst particle radius (m)

D_e = effective diffusivity (m^2.s^{-1})

M_T = estimated Thiele modulus

Appendix B

Normalised comprehensive GC oil analysis

Table B1 Normalised oil selectivity data for experiment at 230℃ from comprehensive GC analysis

C#	n-Paraffins	Branched Paraffins	α-Olefins	Internal Olefins	Branched Olefins	Cyclic Olefins	Aromatics	1-Alcohols	Internal Alcohols	Branched Alcohols	Ketones	Acids	Total
1													
2													
3													
4			0.04					0.16			0.02	0.07	0.31
5	0.05		0.20	0.01	0.00			0.47		0.05	0.06	0.13	1.02
6	0.29	0.02	0.64	0.02	0.03	0.01		0.74	0.01	0.12	0.10	0.16	2.27
7	0.83	0.07	1.76	0.09	0.10	0.03	0.01	0.89	0.01	0.15	0.15	0.15	4.29
8	1.62	0.12	3.44	0.17	0.19	0.04	0.02	0.85	0.02	0.13	0.13	0.13	6.92
9	2.31	0.16	4.78	0.28	0.27	0.05	0.03	0.80	0.03	0.13	0.12	0.11	9.12
10	2.73	0.18	5.34	0.40	0.31	0.05	0.03	0.72	0.04	0.12	0.08	0.08	10.14
11	2.96	0.18	5.32	0.53	0.31	0.04	0.04	0.64	0.03	0.11	0.07		10.29
12	3.08	0.17	4.95	0.66	0.29		0.02	0.64	0.03	0.10	0.06		10.10
13	3.11	0.17	4.38	0.78	0.26			0.55		0.10	0.06		9.49
14	3.04	0.16	3.67	0.90	0.24			0.40		0.09			8.57
15	2.82		2.89	0.91				0.31					7.02
16	2.44		2.11	0.87				0.22					5.64
17	1.96		1.42	0.73									4.10
18	1.45		0.90	0.56									2.91
19	0.98		0.56	0.41									1.94
20	0.70		0.31	0.32									1.33
21	0.47		0.19	0.21									0.88
22	0.28		0.09	0.13									0.50
23	0.17			0.11									0.28
24	0.09												0.09

Appendix C

Results from fitting chain length dependent desorption model

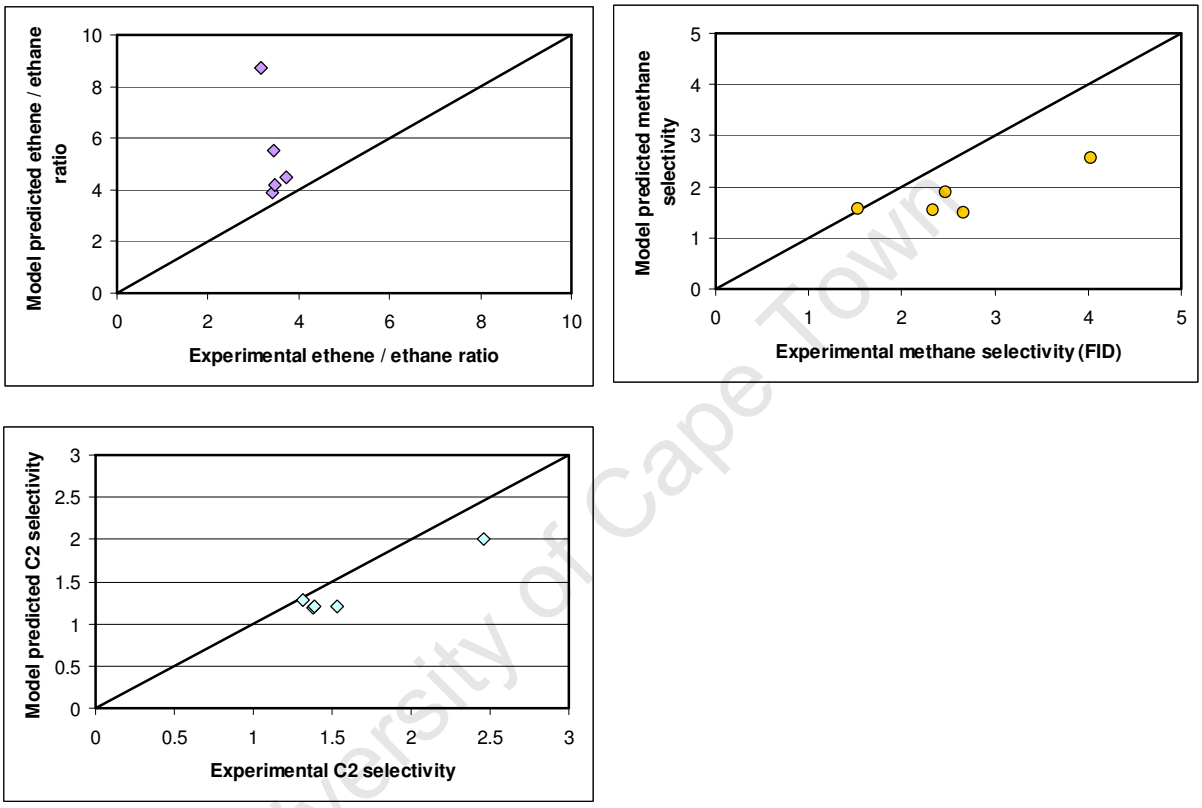

Figure C1 Parity plots for experiments at varying reaction temperatures

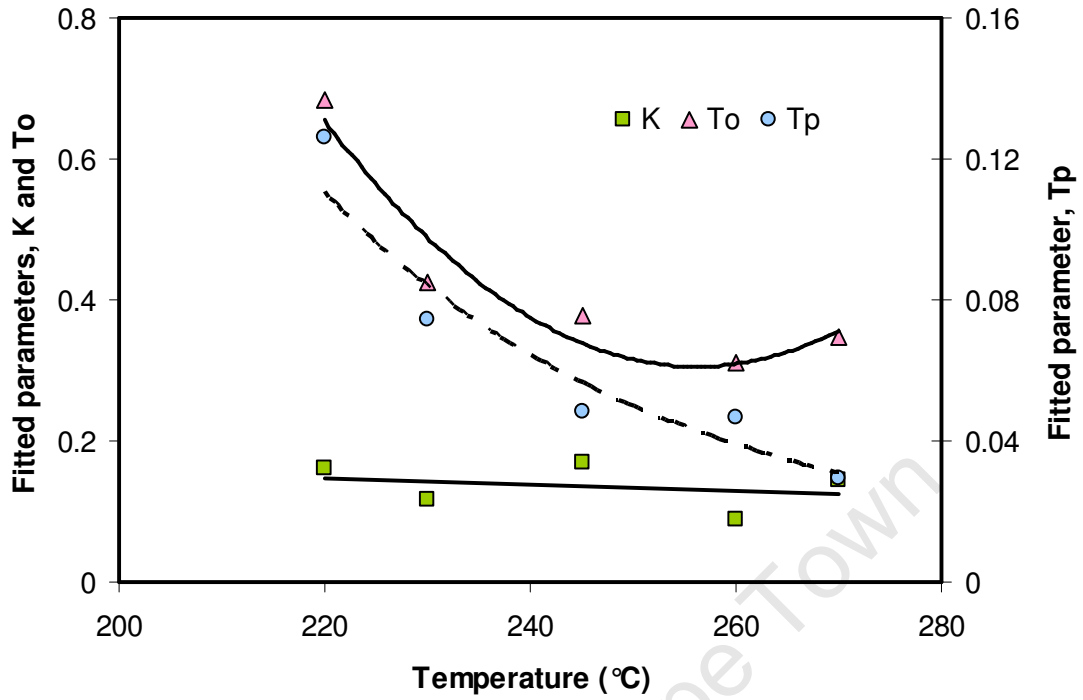

Figure C2 Fitted values T_O and T_P and K by non-linear regression

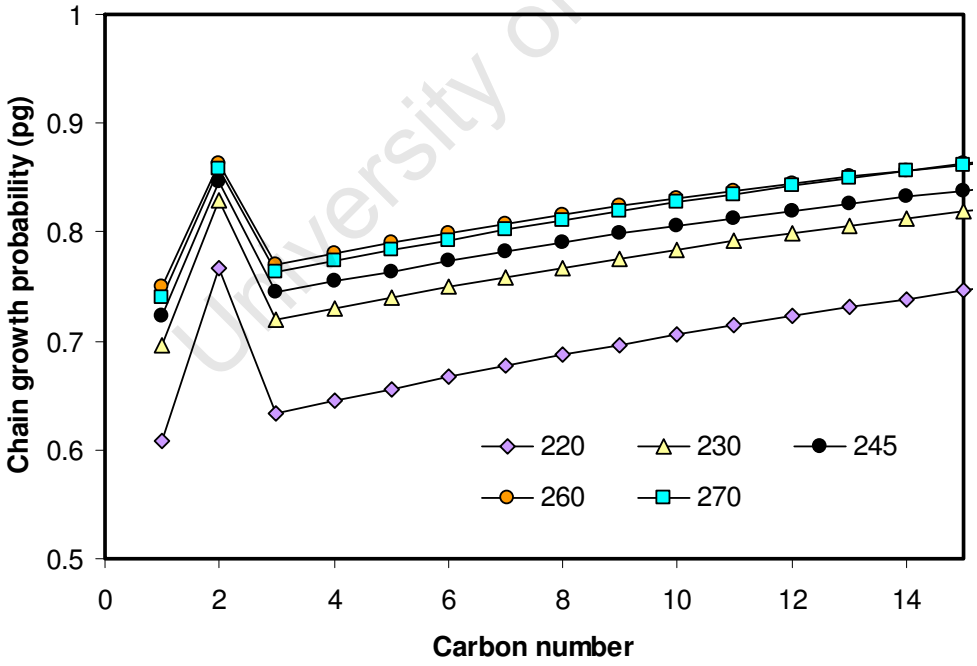

Figure C3 Predicted chain growth probability as a function of temperature (based on values of T_O and T_P and K for the chain length dependent desorption model fitted to the C_3 to C_8 hydrocarbon fraction)

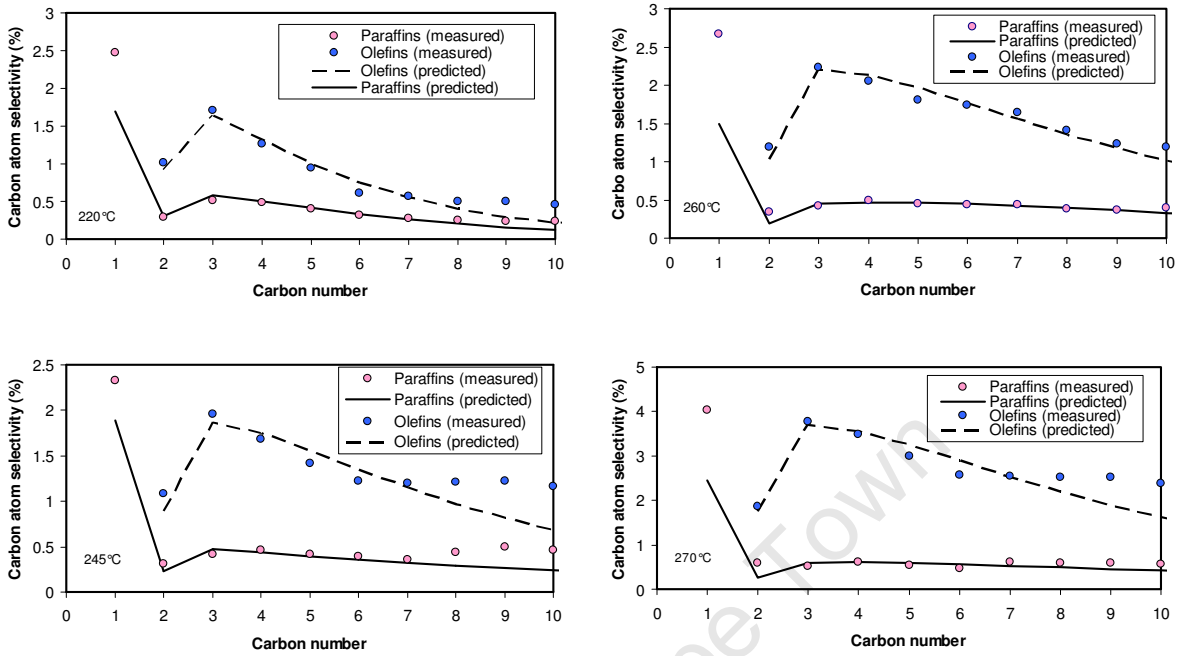

Figure C4 Example of the complete model: based on the fitted parameter values from Table 5.4 (data from experiments at 220, 245, 260 and 270 °C)